University of Wollongong

Research Online

University of Wollongong Thesis Collection 2017+

University of Wollongong Thesis Collections

2019

Dual Drug-eluting Collagen Matrix for Epilepsy Treatment

Marius Berthel

Follow this and additional works at: https://ro.uow.edu.au/theses1

University of Wollongong

Copyright Warning

You may print or download ONE copy of this document for the purpose of your own research or study. The University does not authorise you to copy, communicate or otherwise make available electronically to any other person any copyright material contained on this site.

You are reminded of the following: This work is copyright. Apart from any use permitted under the Copyright Act 1968, no part of this work may be reproduced by any process, nor may any other exclusive right be exercised, without the permission of the author. Copyright owners are entitled to take legal action against persons who infringe their copyright. A reproduction of material that is protected by copyright may be a copyright infringement. A court may impose penalties and award damages in relation to offences and infringements relating to copyright material. Higher penalties may apply, and higher damages may be awarded, for offences and infringements involving the conversion of material into digital or electronic form.

Unless otherwise indicated, the views expressed in this thesis are those of the author and do not necessarily represent the views of the University of Wollongong.

Research Online is the open access institutional repository for the University of Wollongong. For further information contact the UOW Library: research-pubs@uow.edu.au

Dual Drug-eluting Collagen Matrix for Epilepsy Treatment

Marius Berthel

BSc (Chemistry)

The thesis is presented as part of the requirements for the conferral of the degree:

Master of Philosophy (M. Phil)

from

The University of Wollongong

Intelligent Polymer Research Institute (IPRI)

Australian Institute of Innovative Materials (AIIM)

February 2019

Abstract

Epilepsy is the most prevalent chronic brain disease affecting approximately 1% of the worldwide population. Systemic treatment with anti-epileptic drugs are reported to only control seizures in up to 70% of the patients, while the remaining patients report insufficient seizure alleviation. Due to drug resistance, an increasing concentration of the drug is required for systemic administration, resulting in pronounced side effects. Localized drug delivery in the form of an implant enabling sustained drug-release is regarded as a promising strategy to challenge refractory epilepsy.

Collagen, a naturally derived polymer, is one of the most useful biomaterials which has been widely used in medical applications. Recently, an electrochemical technique has been developed to generate oriented and highly clustered collagen fibres with increased mechanical stiffness. The objective of this study was to investigate the potential to incorporate drug-loaded microspheres into electrochemical compacted collagen (ECC) with a view to achieve a sustained dual drug-release profile. Dexamethasone (DEX), commonly used to prevent acute inflammatory reactions after implantation, and phenytoin (PHT), an anti-epileptic drug, were encapsulated into poly (lactic-co-glycolic) acid microspheres via emulsification solvent evaporation technique. Sphere-loaded ECC membranes were successfully prepared by suspension of the microspheres into the collagen solution prior to the electrochemical compaction process. Tensile tests revealed that the incorporation of microspheres decreases the tensile strength of ECC membranes by 25% from 1.11 ± 0.36 MPa to 0.73 ± 0.24 MPa. Finally, the drug-release behaviour of sphere-loaded ECC membranes were investigated in an *in-vitro* experiment. *In-vitro* release studies of DEX-MP/PHT-MP loaded ECC matrices showed DEX-elution to reduce from 86% to 60% of completion at day 11, whereas PHT-elution was characterized by a high burst release resulting in PHT-elution increased from 4% to 82% of completion at day 1.

In conclusion, the incorporation of drug-loaded microspheres into ECC membranes demonstrates a promising approach for the development of novel collagen-based drug delivery systems with increased mechanical properties. The data indicates that sustained drug release from ECC matrices highly depends on the ability of the targeted drug to undergo the electrochemical fabrication process and thus further studies need to be performed in order to receive an in-depth understanding of the procedure.

Acknowledgements

Firstly, I would like to thank my co-supervisors Dr. Zhilian Yue and Dr. Xiao Liu for their assistance during the entire project. Your patient guidance and valuable advice supported me to focus on my study and fulfil this investigation. I highly appreciate your great help with my publication and thesis writing.

Special thanks to my clinical mentor, Prof. Dr. Mark J. Cook, for his constructive comments and his clinical perspective throughout the year.

I would like to extend my thanks to Prof. Dr. Gordon Wallace for his guidance during the past year and giving me the opportunity to work within IPRI. At last, but not least, I want to thank Prof. Dr. Paul Dalton for his endless support during the whole master's program.

Certification

I, Marius Berthel, declare that this thesis submitted in fulfilment of the requirements for the conferral of the degree Master of Philosophy, within the AIIM Faculty at the Intelligent Polymer Research Institute, University of Wollongong, is wholly my own work unless otherwise referenced or acknowledged. This document has not been submitted for qualifications at any other academic institution.

Marius Berthel

February 14th, 2019

Biofabrication Double Degree Statement

Appended to this document is an additional annex that represents the entirety of a six months thesis undertaken at the Julius-Maximilians-Universität and submitted as part of the fulfilment of the Double Degree Masters of Biofabrication between the UOW and the Julius-Maximilians-Universität Würzburg.

According to the Memorandum of Agreement between: Queensland University of Technology, University of Wollongong, Julius-Maximilians-Universität Würzburg and Utrecht University, the Biofabrication Double degree master's programme was started.

Students in the programme will be expected to obtain a master's degree from one European and one Australian institution. The student initiates the Biofabrication Mobility Programme in a master's degree at the home institution for two semesters (60 EC in Europe), prior to taking up enrolment in another master's degree at the overseas participating institution, hereinafter referred to host institution for a period of two semesters (60 EC in Europe) over one year.

Students shall enrol in a master's degree at the home institution in accordance with the Biofabrication Mobility Programme specifications approved jointly by the institutions. Students will undertake a research project at the host institution in accordance with the project descriptions provided by each institution (supervisory and infrastructure capacity).

List of Abbreviations

A	Ampere
ACN	Acetonitrile
aCSF	artificial cerebrospinal fluid
AED	Anti-epileptic drug
BBB	Blood-Brain-Barrier
CNS	Central Nervous System
CP	Continuous phase
CSF	Cerebrospinal fluid
DCM	Dichloromethane
DEX	Dexamethasone
DP	Dispersed phase
EA	Ethyl acetate
ECC	Electrochemical compacted collagen
ESE	Emulsification solvent evaporation
GABA	gamma-Aminobutyric acid
HPLC	High Pressure Liquid Chromatography
LEV	Levetiracetam
MP	Microparticle
PBS	Phosphate-buffered saline
PHT	Phenytoin
PLGA	Poly (lactic-*co*-glycolic) acid
rpm	Revolutions per minute
s	Second
SEM	Scanning Electron Microscopy
VGC	Voltage-gated channel
v	Volume
w	weight
µL	Microliter
µm	Micrometre
µg	Microgram

Table of Contents

Abstract ..... - 1 -

Acknowledgements ..... - 2 -

Certification ..... - 3 -

Biofabrication Double Degree Statement ..... - 4 -

List of Abbreviations ..... - 5 -

Table of Contents ..... - 6 -

List of Figures ..... - 8 -

List of Tables ..... - 9 -

1. Introduction ..... - 10 -

1.1 Collagen ..... - 10 -

1.1.1 Biological background ..... - 10 -

1.1.2 Collagen matrices for dural repair in neurosurgery ..... - 11 -

1.1.3 Electrochemical compaction of collagen ..... - 12 -

1.2 Epilepsy ..... - 13 -

1.3 Pharmacologic mechanism of anti-epileptic drug action ..... - 16 -

1.4 Drug delivery for epilepsy ..... - 17 -

1.4.1 Limitation of oral dosage forms ..... - 17 -

1.4.2 Local drug delivery ..... - 18 -

1.4.3 Encapsulation of drugs ..... - 20 -

1.5 Aims and objectives ..... - 22 -

2. Materials and Methods ..... - 23 -

2.1 Microsphere preparation ..... - 23 -

2.1.1 Encapsulation of DEX ..... - 23 -

2.1.2 Encapsulation of rhodamine B isothiocyanate-dextran ..... - 23 -

2.1.3 Encapsulation of LEV ..... - 23 -

2.1.4 Encapsulation of PHT ..... - 25 -

2.2 Characterization of microspheres ..... - 25 -

2.3 Loading efficiency ..... - 25 -

2.4 *In-vitro* drug release study of microspheres ..... - 26 -

2.5 Fabrication of particle-loaded ECC matrices ..... - 26 -

2.6 Tensile mechanical properties ..... - 26 -
2.7 *In-vitro* drug release study of ECC matrices ..... - 26 -
2.8 Scanning Electron Microscopy (SEM) ..... - 27 -
3. Results and Discussion ..... - 28 -
3.1 Fabrication of drug-loaded microspheres ..... - 28 -
3.1.1 Characterization of DEX-loaded microspheres ..... - 28 -
3.1.2 Encapsulation of anti-epileptic LEV ..... - 30 -
3.1.3 Characterization of PHT-loaded microspheres ..... - 35 -
3.2 Electrocompaction of collagen matrices ..... - 38 -
3.3 Incorporation of microspheres into ECC matrices ..... - 40 -
3.4 Mechanical properties of drug-loaded ECC matrices ..... - 41 -
3.5 Characterization of ECC morphology by SEM-Imaging ..... - 42 -
3.6 Drug-release from sphere-loaded ECC matrices ..... - 43 -
4. Future Perspectives ..... - 47 -
5. Conclusion ..... - 49 -
6. References ..... - 50 -
Poster: 9th World Congress of Biomimetics, Artificial Muscles and Nano-Biotechnology ..... - 55 -
Poster: International Conference on Nanoscience and Nanotechnology 2017 ..... - 56 -
Review Article ..... - 57 -
Annex: Master thesis at the University of Wuerzburg ..... - 58 -

List of Figures

Figure 1. Assembly of collagen molecules to fibres. Formation of the triple-helical structure consisting of three polypeptides subunits, followed by the removal of the terminal peptides of procollagen by procollagen peptidase. Helices are assembled to collagen fibrils after secretion from the cell followed by the assembly of fibrils to collagen bundles [5]. ..... - 10 -
Figure 2. Collagen-based resorbable membrane Cova™ for post-operative adhesion [9]. ..... - 11 -
Figure 3. Electrochemical compaction of collagen molecules during the electrolysis of water. Monomeric collagen between the electrodes assumes different net charges due to its amphoteric nature. Repulsion from the same charged electrodes causes compaction of the collagen chains at the isoelectric point [18]..... - 12 -
Figure 4. Electrical transmission in brain neurons. Depolarization of the neuron occurs due to opening of sodium channels during the span of a spike. Following a spike, repolarization occurs due to closing of the sodium channels which leads to hyperpolarization of the neuron. The resting potential of the neuron is restored by ion pumps [35]. ..... - 15 -
Figure 5. Action sites of common AEDs. Reduction of the electrical signal transmission due to either suppression of voltage-dependent ion channels, up-regulation of GABA-mediated inhibitory neurotransmission or reduction of Glutamate-mediated excitatory neurotransmission [41].. ..... - 16 -
Figure 6. Low penetration of neurotrophic factors (radiolabeled) into the brain parenchyma at 20 h after intracerebroventricular injection [68]. ..... - 18 -
Figure 7. Double-emulsion technique for hydrophilic MP. An aqueous drug-loaded phase (W) is emulsified into a polymer containing oil phase (O). The primary emulsion W/O is further emulsified into an outer aqueous phase(W) to fabricate drug-loaded oil droplets. Evaporation of the volatile organic solvent causes solidification of the microspheres [84]. ..... - 20 -
Figure 8. Influence of the precipitation on MP morphology. Fabrication of porous microspheres due to the delayed polymer precipitation results in low encapsulation efficiency. Fast polymer precipitation provides high encapsulation efficiency due to the formation of a uniform shell of the microsphere [88]. ..... - 21 -
Figure 9. Concept of the fabrication process of drug-loaded collagen sheets. Drug-loaded microspheres are mixed to the monomeric collagen solution and injected between the electrodes. Application of an electrical field triggers the compaction of collagen molecules at the isoelectric point and causes entrapment of the microspheres within the collagen sheet. ..... - 22 -
Figure 10. Photomicrographs of the microspheres prepared using an O/W emulsion from (A) 5%, (B) 10%, (C) 15% and (D) 20% PLGA. ..... - 28 -
Figure 11. SEM micrographs of the DEX-loaded MPs prepared from 20% w/v PLGA using an O/W emulsion method taken at x600 (A) and x2500 (B) magnification. ..... - 29 -
Figure 12. Cumulative DEX released from the 20% PLGA microspheres during an in-vitro release study in aCSF (pH 7.4) at 37 °C (n = 3) for 11 days. (A) Quantitative release of DEX per mg microspheres. (B) Total amount of DEX released as a percentage of the total amount of drug encapsulated into the 20% PLGA microspheres. ..... - 30 -
Figure 13. Fluorescent micrograph of the PLGA microspheres loaded with rhodamine B isothiocyanate-dextran. ..... - 31 -
Figure 14. Teas graph representation of the solubility characteristics for organic solvents of PLGA. (1: tetrahydrofuran, 2: DCM, 3: chloroform, 4: dimethylformamide,5: EA, 6: ACN, and 7: acetone). Water and Ethanol are illustrated by asterisk. The solubility range of LEV is illustrated by the dark area [95]. - 32 -

Figure 15. PLGA microspheres prepared by W/O/W double emulsion using EA. (A) Fluorescent micrograph of the PLGA microspheres loaded with rhodamine B isothiocyanate-dextran from 8% (w/v) PLGA solution. (B) Increasing the polymer concentration to 15% (w/v) and 20% (w/v), respectively, resulted in polymer precipitation (red arrow). ..... - 33 -
Figure 16. Photomicrograph of the 10% PLGA formulation prepared by W/O/O double emulsion reveals agglomeration of the MPs. ..... - 34 -
Figure 17. Photomicrographs of the PHT-spheres prepared using an O/W emulsion from (A) 10%, (B) 15% and (C) 20% PLGA. ..... - 36 -
Figure 18. Cumulative PHT released from the PLGA microspheres during an in-vitro release study in aCSF (pH 7.4) at 37 °C (n = 3) for 30 days. (A) and (C) Quantitative release of PHT from 1 mg of 10% and 15% PLGA-microspheres, respectively. (B) and (D) Total amount of PHT released as a percentage of the total amount of drug encapsulated into the 10% and 15% PLGA- microspheres, respectively. ... - 37 -
Figure 19. Fabrication of ECC matrices. (A) Image of the electrochemical cell for the compaction of collagen. (B) Highly transparent ECC matrix recovered from the electrode after the electrochemical process. (C) Representative current-time-curve of the compaction process of collagen matrices. (D) Bubble entrapment (red arrow) into ECC matrices prepared at 7 V. ..... - 39 -
Figure 20. Photo-crosslinking of ECC matrices. (A) Representative results of rheological testing of riboflavin induced crosslinking of ECC matrices. Increase of the storage modulus after exposure to UV-light for 30 s at 60 s.(B) Collected ECC matrices after photo-crosslinking. ..... - 40 -
Figure 21. Incorporation of microspheres into ECC matrices. (A) Fluorescent microscopy of particle-loaded ECC matrix. (B) Photomicrograph of particle-loaded ECC matrix. ..... - 41 -
Figure 22. Tensile properties of ECC with and without microspheres (n=3). (A) Stress-Strain curve and (B) Tensile modulus. ..... - 41 -
Figure 23. SEM micrographs of ECC matrices at x23000, x600, 8500 and 23000 magnifications. (A) cross-section of ECC matrices without microspheres, (B) surface of sphere-loaded ECC matrices, (C) cross-section of sphere-loaded ECC matrices and (D) high-resolution of the cross-section of sphere-loaded ECC matrices. ..... - 42 -
Figure 24. In-vitro release profile from single and dual drug-loaded ECC matrices (n=3) in aCSF (pH 7.4) at 37 ^{o}C for 12 and 14 days, respectively. (A) Quantitative single-release of DEX from ECC matrices. (B) Total amount of DEX released as a percentage of the total amount of drug encapsulated into ECC matrices. (C) Quantitative amount of PHT and DEX released from dual-drug loaded ECC matrices. (D) Total amount of PHT and DEX released as a percentage of the total amount of drug encapsulated into ECC matrices. ..... - 44 -
Figure 25. *Schematic illustration of the electrospraying setup for fabrication of microspheres with core-shell morphology [103].* ..... - 47 -
Figure 26. Layer-by-layer electrocompaction of collagen sheets (modified) [20]. ..... - 48 -

List of Tables

Table 1. Summary of microsphere characterization at different PLGA concentrations. ..... - 29 -
Table 2. Summary of microsphere characterization at different PLGA concentrations using EA. ... - 33 -
Table 3. Summary of PHT-microsphere characterization at different PLGA concentrations. ..... - 35 -
Table 4. Drug-loading efficiency of microsphere-loaded ECC matrices ..... - 43 -

1. Introduction

The focus of this work is the fabrication of durable collagen films for a neurosurgery application with the capacity and capability of dual drug release. Anti-inflammatory dexamethasone (DEX) and anti-epileptic levetiracteam (LEV) or phenytoin (PHT) are the drugs considered for this study. The objective of this chapter was to give the reader a clear picture of the surgical application of collagen devices, the need for novel treatment strategies for refractory epilepsy, specifically regarding the fabrication aspects.

1.1 Collagen

1.1.1 Biological background

Collagen typifies the primary structural protein representing about 30% of the body proteins in humans [1]. To fulfil various biological features collagen can present itself in 13 different configurations [2]. All subtypes of collagen represent a particular triple-helix arrangement of three polypeptide subunits, also known as α-chains. Type I collagen is the basic configuration of collagen responsible for the mechanical integrity of tendons and ligaments. It consists of two α1 and one α2 chains, in which a high quantity of glycine is present. Due to its small side group and its frequent appearance within the α-chain, the polypeptide chains are able to form a close arrangement into a helix [3]. To fulfil its characteristic physiological and biological properties, the triple-helical collagen molecules are assembled longitudinally and bilaterally into fibrils. Larger constructs of collagen are formed through the organization of fibrils into greater fibre bundles (Fig. 1) [4].

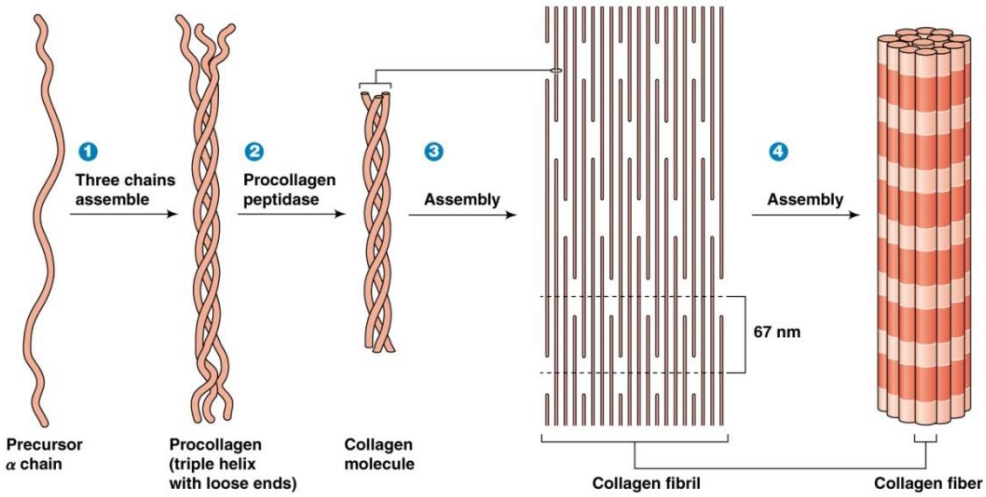

Figure 1. Assembly of collagen molecules to fibres. Formation of the triple-helical structure consisting of three polypeptides subunits, followed by the removal of the terminal peptides of procollagen by procollagen peptidase. Helices are assembled to collagen fibrils after secretion from the cell followed by the assembly of fibrils to collagen bundles [5].

Along with the physiological assembly of fibrils, cross-linking of the collagen structure is essential for the mechanical and chemical stabilization of collagen fibrils. Intra- and intermolecular crosslinking of fibres is catalyzed by lysyl-oxidase during fibril formation. Lysyl-oxidase generates highly reactive aldehyds from lysin sidechains of the triple-helix. These activated side chains can easily undergo spontaneous chemical reactions like Schiffs' base type or aldol condensation type crosslinking [6].

1.1.2 Collagen matrices for dural repair in neurosurgery

Collagen is regarded as one of the most beneficial biomaterials which has been adopted in several medical applications. The advantage of collagen-derived products is mostly based on its excellent biological compatibility and safety due to biodegradability and weak antigenicity properties [7]. Due to its superior properties, the use of collagen in biomedical application has been rapidly expanded, including its use in drug delivery systems, tissue-engineering and surgical devices. One of the most promising applications of collagen, regarding its use in surgeries, is to support the post-operative dura mater regeneration (Fig. 2) [8].

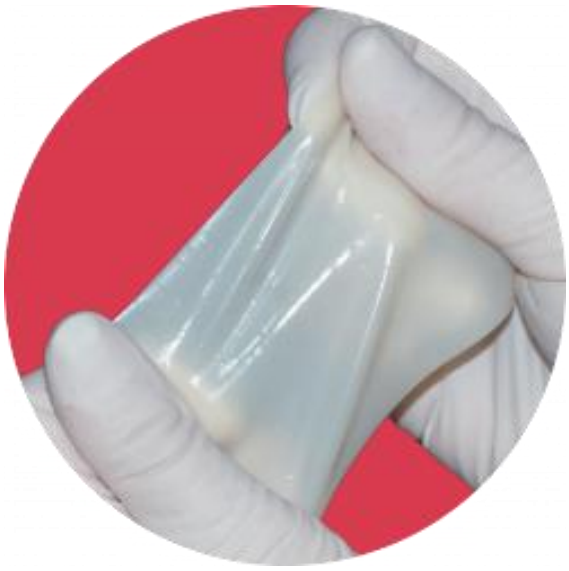

Figure 2. Collagen-based resorbable membrane Cova™ for post-operative adhesion [9].

The dura mater is a thick membrane and the outermost of three layers surrounding the brain and the spinal cord. Because it almost completely surrounds the brain tissue, neurosurgeons often must perforate this dural layer to perform a procedure. This process can lead to dural defects including retraction, shrinkage or excision [8]. To minimize the development of such defects, dural grafts, made of either metallic or synthetic material are used to prevent post-operative adhesions. These layers of scar tissue often occur after surgical invasive operations [10]. Excess of scar tissue is a severe condition

for patients who depend on multiple surgeries as it is difficult to penetrate during medical interventions [11].

In contrast to the low biological performance of metal or synthetic polymeric grafts, collagen fleeces promote the vascularization and the reconstitution with host cells, while minimizing the immunological body response [12]. *Tacho-Comb*, a commercialized fibrinogen-based collagen fleece mostly used in vascular surgery, was firstly evaluated by M. Reddy *et al*. to demonstrate its superior suitability as a dural substitute in neurosurgery application [8].

1.1.3 Electrochemical compaction of collagen

For the application of collagen in surgeries, a significant challenge is the ability to provide suitable mechanical properties to ensure safety and facilitate handling of the devices. In the native tissue, the density and high orientation of collagen provides the mechanical and structural strength of load-bearing extracellular matrices [13]. An assembly process of collagen which enables the fabrication of dense, oriented, tissue-like constructs would thus highly increase the application range of collagen. In the last decades a variety of techniques including dehydration processes, electrospinning or anisotropic chemical nanopatterns, were developed to synthesize collagen structures with increasing degree of orientation [14-16]. However, all these techniques have different limitations regarding cost-effectiveness, toxicity of solvents or time frame. Recently an electrochemical alignment procedure, referred to as electrochemical compaction, was developed by X. Cheng *et al.* to generate extraordinarily oriented and highly compressed collagen bundles from aqueous monomeric collagen solution (Fig. 3) [17].

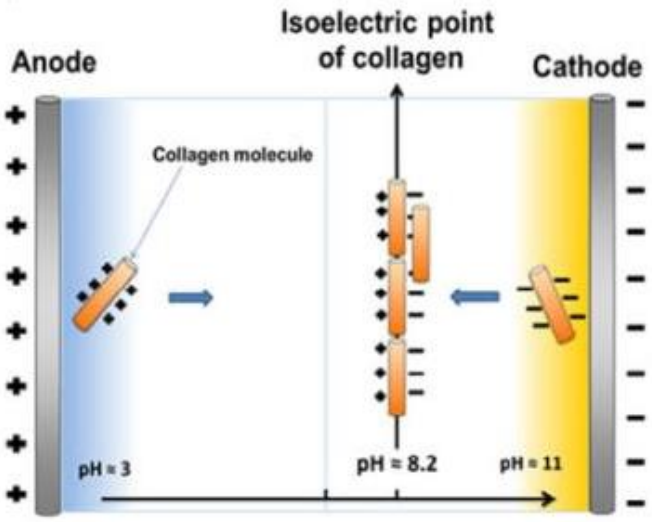

Figure 3. Electrochemical compaction of collagen molecules during the electrolysis of water. Monomeric collagen between the electrodes assumes different net charges due to its amphoteric nature. Repulsion from the same charged electrodes causes compaction of the collagen chains at the isoelectric point [18].

In general, the electrochemical reaction used in this process is based on the electrolysis of water. At the anode, oxygen and oxonium ions are formed due to the reduction of water leading to an acidic environment. In contrast, oxidation of water to hydroxide ion and hydrogen at the cathode forms a basic milieu [17]. The induced pH gradient causes different net charges of the collagen molecules. Next to the anode collagen gets a positive charge and those molecules close to the cathode assume a negative charge. The similar charge of collagen as compared to the electrodes triggers repulsion of the molecules towards the isoelectric point of collagen, where the total charge is zero and a compaction of molecules occurs [19]. Studies on the cell migration through 3D bundles of collagen fabricated using this process have shown that these collagen structures are conductive to cell proliferation [17]. Apart from collagen bundles, further investigation into this electrochemical fabrication process could provide a solution to collagen device fabrication, representing differences in architectural complexity and composition [20-22]. This technique could also be a promising method to prepare collagen membranes with increased mechanical strength, making it suitable for applications such as an adhesion barrier in neurosurgery.

1.2 Epilepsy

Epilepsy is the most prevalent chronic brain disease affecting approximately 1% of the worldwide population, it is associated with significant morbidity and mortality rates [23-25]. Even if it is regarded more than a diverse group of dysfunctions underlying abnormal electrical transmission of brain neurons, all forms of epilepsy reveal the hallmark characteristic of periodic irrepressible seizures [26]. Epilepsy is versatile, demonstrating around 15 specifiable types of seizures and about 30 epilepsy syndromes [27, 28]. In general, these seizures are classified into focal seizures, in which the epilepsy focus appears at a cortical site, and generalized seizures, in which the neuronal disorder is distributed in both hemispheres of the cortex. The impact of seizure to the patients' wellbeing can be motor, like brief shock-like jerks of muscles (myoclonic), sudden stiffness of bodyparts (tonic) or loss of muscle tone (atonic). Tonic-clonic seizures, the most common type associated with epilepsy patients, appear as a loss of consciousness and muscle stiffness which is followed by rhythmical jerking of the extremities. Aside from these physiological symptoms, there are also known non-motor symptoms like lapses in awareness which is present in absence seizures. The classification of epilepsy seizures is still a field of research and undergoes dynamic change [29]. Despite research efforts over the last decades, the exact mechanism causing neurochemical irregularities present in epilepsy are still not completely understood [30]. In the normal brain, signal transmission is organised non-synchronously and is regulated by a highly clocked mechanism (Box 1). In Epilepsy patients this regulation breaks down due to either, the reduction of inhibitory neurotransmission or through an increase in excitatory

transmission resulting in a state of uncontrolled hypersynchronous and excitatory firing of brain neurons [31]. The instance by which the intact brain is degenerating towards this electrical abnormality is termed epileptogenesis. As Goldberg *et al.* declares this process is basically classified in three stages: the incident of a procuring event, continued by an inactive period of time during which changes happen in motion and third, chronic established epilepsy. Factors which can trigger epileptogenesis vary greatly and can include; acquired brain pathology, like tumours, infections and injuries as well as mutations in single genes or neurodevelopmental disorders which can influence the formation of an epileptic brain [24].

Box 1: Neuronal communication pathway in the normal brain

Neurons are the key structure in the nervous system responsible for receiving and sending signals. Due to the expression of ligand- and voltage-gated membrane-channels neurons are capable to create potential variations between the inside of the cell and the outside membrane [32]. The resting membrane potential relays mostly to the difference between positively charged ions inside and outside the cell at rest and is approximately -70 mV [33]. Binding of neurotransmitters at the membrane receptor causes opening of ion channels which enables positive ions to enter the neuron. This process causes a change of potential and leads to firing of so-called action potentials. Creation of an action potential is an "all-or nothing" event what means that the neuron starts to depolarize completely when threshold potential is reached (Fig. 4) [34].

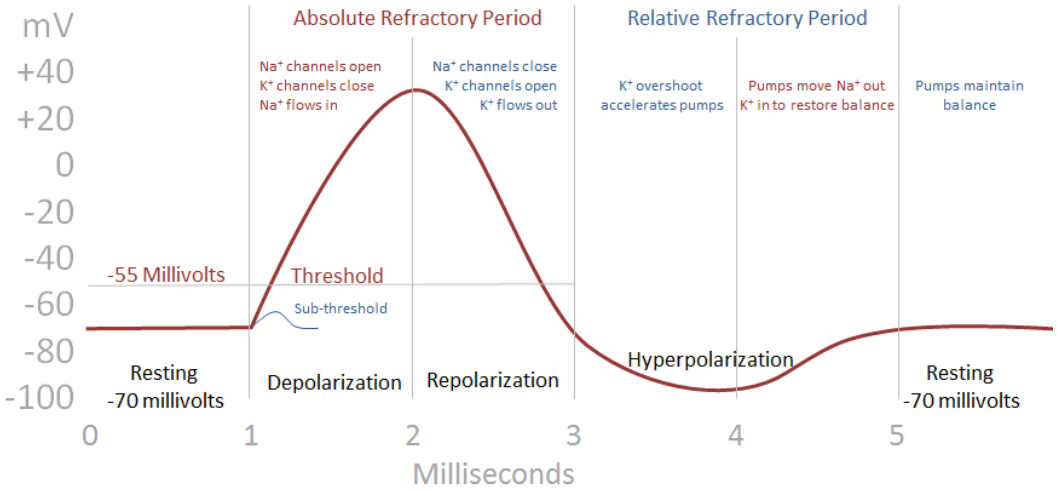

Figure 4. Electrical transmission in brain neurons. Depolarization of the neuron occurs due to opening of sodium channels during the span of a spike. Following a spike, repolarization occurs due to closing of the sodium channels which leads to hyperpolarization of the neuron. The resting potential of the neuron is restored by ion pumps [35].

Repolarization of the cell begins due to closing of Na^+ channels to reset the resting potential of the cell. In this period the cell is unable to form further action potentials. While closing the sodium gateway potassium ions rapidly leaving the cell through voltage-gated K^+-channels and causes a strong negatively potential called hyperpolarization. Once the hyperpolarized potential is achieved sodium channels will be opened again for adjusting the cells' resting potential [34-36].

1.3 Pharmacologic mechanism of anti-epileptic drug action

Therapies with anti-epileptic drugs (AEDs) still remain the mainstay in epilepsy treatment, even though the prescription of these drugs is only used to symptomatically supress seizure once they occur [37, 38]. So far, there is no AED known that has been demonstrated to inhibit the occurrence of epilepsy in patients prior to the first seizure event [39]. Application of AEDs aims to reduce the passing of electrical or chemicals signals in the neuronal network to return electrical transmission to a normal level. Transmission of stimuli in the brain takes place at synapses, the structure of neurons in which the action potential of the excitatory cell is propagating. Even if in the last decades a broad spectrum of new AEDs has been developed, their mechanisms of action is still classified into three basic mechanism on the cellular level: adjustment of voltage-dependent ion channels (Na^+, Ca^{2+}, K^+), augmentation of y-aminobutyric acid (GABA)-related inhibitory activity and reduction of excitatory (glutamate-related) transmission (Fig. 5) [31, 40].

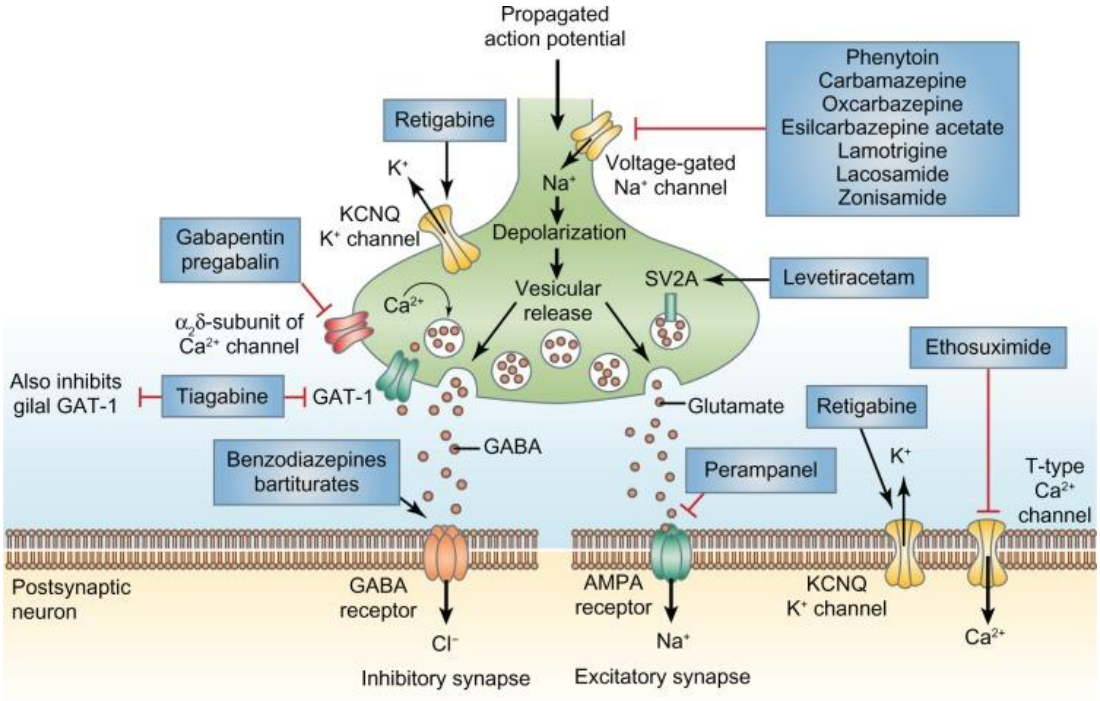

Figure 5. Action sites of common AEDs. Reduction of the electrical signal transmission due to either suppression of voltage-dependent ion channels, up-regulation of GABA-mediated inhibitory neurotransmission or reduction of Glutamate-mediated excitatory neurotransmission [41]..

A large range of drugs act by modulation of voltage-gated ion channels (VGCs) through binding at specific subunits at the membrane receptors [42, 43]. Through blocking of subunits, for example the Na^+ channel by AEDs, sodium can't enter the neuron and depolarize the cell which is necessary for the neurotransmitter release. Due to this action common AEDs like phenytoin (PHT) and carbamazepine hinder rapid bursts of action potentials in an effective manner [44]. Potassium-channels are another well-known target for anti-convulsant drug action. On the cellular level K^+ channels are responsible for

the repolarization of the plasma membrane after sodium influxes [45]. Thus, activation of these channels would immediately hyperpolarize the neuronal cell and limits action potential firing [46]. Retigabine is a novel AED that exerts its anti-convulsive effect by initialization of the KCNQ K^+ channels [47]. The GABA system demonstrates one of the most favoured action target for the development of novel AEDs [48]. GABA is a major inhibitory neurotransmitter in the mammalian central nervous system (CNS) [49]. Through binding of specific GABA-receptors at the inhibitory synapses Cl^- conductance is increased which leads to neuronal hyperpolarization [50]. Increased GABA release and synthesis [51], allosteric receptor facilitation [52], and minimized deactivation [53] are targets which have all been applied in the pharmacologic mechanism of clinically used AEDs [54]. The antagonist of GABA is the excitatory glutamate. Glutamate represents the most important excitatory neurotransmitter in the human nervous system and is stored in the so called vesicles at chemical synapses [55]. Following synaptic release, it can bind at ionotropic glutamate receptors. These receptors are principally classified into AMPA, Kainate and NMDA subtypes, forming ligand-gated ion channels for sodium or calcium influxes [56]. Even though none of the AEDs provides its anti-convulsive activity solely by interacting with the glutamate system, blockade of glutamate receptors is regarded to assist in the anti-epileptic action of many drugs like, perampanel [56-58].

1.4 Drug delivery for epilepsy

The development of pharmacological active components alone is not sufficient for the successful therapy of CNS-diseases, like Alzheimer, Parkinson or epilepsy. The development of adequate drug delivery strategies that are able to tackle the biological barriers and release the drug to a targeted area is a major challenge in pharmacology [28, 59].

1.4.1 Limitation of oral dosage forms

For the therapy of epilepsy, the common approach is to use AEDs via oral route. However, this method only achieves a satisfactory result in 70% of the patients while the remaining patients are unable to achieve sufficient seizure alleviation [60, 61]. The phenomenon of unresponsiveness to oral applied AEDs seems to be multifactorial, but there is evidence that suggest that the blood-brain barrier (BBB) plays an important role [62]. The BBB segregates blood and brain interstitial fluid and protects the brain from harmful compounds. This unique biological function is provided by brain vascular endothelial cells which form highly resistant tight junctions. Crossing this cerebral microvasculature barrier is only possible for lipid-mediated or carrier/receptor-mediated transporters [63]. Additionally, another key structure of the BBB are molecular efflux pumps, which can effectively restrict the penetration of commonly AEDs into the brain by pumping them into the vessel lumen [64].

Overexpression of some multidrug resistance proteins has been proved in patients with refractory epilepsy [65]. Due to the drug resistance, an increasing concentration of the AED accumulates in the circulation instead of the brain as the desired target. A high level of AEDs in the circulation leads to intolerable systemic side effects which massively decrease the patients' wellbeing [66]. Furthermore, oral consumption of AEDs is an unspecific way for penetrating the seizure focus. As a result of the delivery through the BBB the anti-epileptic active compounds interfere with the function of all neuronal cells in the CNS which can provoke cerebral side effects (e.g. ataxia, sedation and mood change) [67].

1.4.2 Local drug delivery

As mentioned before, the BBB is the chief factor restricting the anti-convulsive effect of oral dosage forms, which resulted in the development of new strategies to enhance the concentration of AEDs in the brain, including drug delivery systems [68], prodrugs [69], inhibition of molecular efflux pumps [70], disruption of the BBB [71], direct injection behind the BBB [72] as well as gene and cell therapies [28]. Under all these strategies the most promising approach emerged in the field of localized drug delivery. As mentioned before, a delivery system that could release its pharmacological payload specifically to the epileptic focus would be unfavorable for two reasons. First, a high concentration of the drug would be realized and second, it minimizes the toxic effect on the intact neuronal network. Application of the drug into the cerebrospinal fluid (CSF) can be an alternative to common treatment of epilepsy because of the direct delivery of the drug bypassing the BBB [73, 74]. The main advantage of this method is the decreased systemic toxicity. However, intracerebroventricular injection of AEDs has some limits regarding the transport to the epileptic seizure area. As drug movement is controlled by diffusion the brain penetration of AEDs is limited to ependymal cells which line the ventricles (Fig. 6) [75]. Furthermore, a fast exit of the drug from the brain is caused by flushing into the circulation [76].

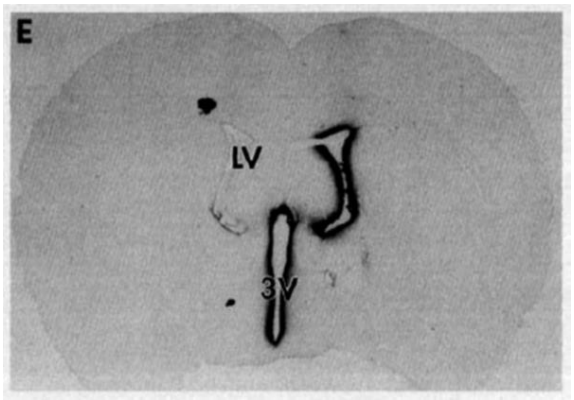

Figure 6. Low penetration of neurotrophic factors (radiolabeled) into the brain parenchyma at 20 h after intracerebroventricular injection [68].

To overcome many of the drawbacks of the intracerebroventricular administration direct transport of anti-convulsant drugs into the brain parenchyma seems like a suitable alternative. Clinically useful local drug delivery systems for epilepsy have been developed over the past decade. One of the most promising methods is the construction of polymer-based implants that serve as a drug reservoir for long term release of AEDs [77]. In general, polymeric devices are classified as biodegradable and non-biodegradable polymers. In the case of biodegradable polymers, the body's own degradation processes, e.g. hydrolysis or enzymatic degradation, breaks down the medical device, leading to a slow gradual drug release near the target area over time. An advantage of biodegradable implantable devices is the elimination of surgeries required to replace the implant, compared with non-biodegradable devices. However, for an effective clinical use these implants have to fulfil a range of important properties. First of all, the degradation time of the biomaterial must be aligned with the regeneration time for the surgical intervention. In addition, the body's inflammatory response incurred by implantation must be prevented [67]. Furthermore, the medical device should have mechanical properties similar to the target area of the body without compromising permeability and processability [78].

Initial studies of polymer-based implants performed by M. Kokaia *et al.* have shown a sustained release of anti-convulsant drug. In an animal model, the implantation of a GABA-eluting polymeric device into the hippocampus of a rat, showed the ability to ameliorate seizure strength for up to 2 days [72]. In the past few years research has focussed on improving the long-time drug-release properties of polymer-based implants. To achieve a sustained long-term drug release, several studies have investigated the combination of microparticles (MP) and monolithic devices to provide slow release of the drug [79-81]. As an example of such a device, Szybala *et al.* demonstrated drug release for 21 days from an implant containing drug-loaded silk microspheres embedded in multiple layers of silk. Investigations into the potential of such a device to prevent seizures were carried out in a rodent model of temporal lobe epilepsy, which demonstrated 10 days of seizure suppression after implantation. Despite progress over the last few decades to extend the drug-release properties of implantable devices, an appropriate implant for refractory epilepsy treatment has still not been achieved. Due to the high risk of intracranial infection or neurological deficits related to neurosurgical implantation of the device, Hallidays *et al.* mentioned, that the main challenge for an clinical application of the implant is to create a device, which is able to provide seizure alleviation for at least 12 months [67].

1.4.3 Encapsulation of drugs

Over the last few decades several methods have been progressed to encapsulate core materials into polymeric microspheres. In general, these techniques are grouped into chemical procedures (e. g. *In situ* polymerization, polycondensation), physio-chemical procedures (e. g. Sol – gel encapsulation, coacervation and phase separation) and physico-mechanical procedures (e. g. Spray drying and congealing, solvent evaporation) [82, 83]. Among these techniques, emulsification solvent evaporation (ESE) is a well-defined technique commonly used for encapsulation of pharmaceutical compounds. The ESE process is divided in two steps (Fig. 7).

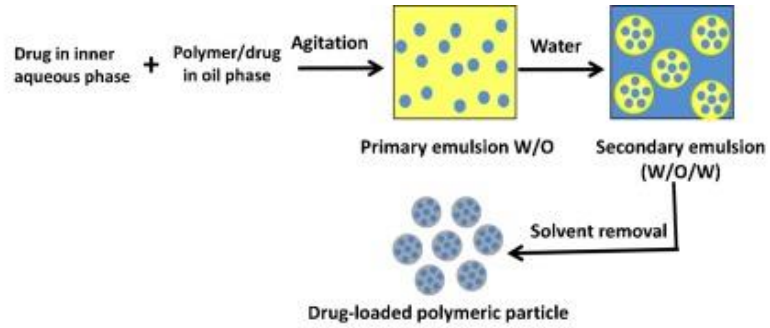

Figure 7. Double-emulsion technique for hydrophilic MP. An aqueous drug-loaded phase (W) is emulsified into a polymer containing oil phase (O). The primary emulsion W/O is further emulsified into an outer aqueous phase(W) to fabricate drug-loaded oil droplets. Evaporation of the volatile organic solvent causes solidification of the microspheres [84].

For hydrophobic drugs, like DEX, the first step includes emulsification of the polymer- and drug-loaded oil phase into an aqueous phase. Due to the high shear stress produced during the emulsification, the polymer-containing oil phase is highly dispersed in microdroplets. The MP size is the main parameter influenced by this primary step [85]. Encapsulation of a hydrophilic drug, like LEV, requires two emulsification steps. An aqueous phase of the compound is mixed into a polymer containing oil phase, forming a primary emulsion (W/O). Addition to a second water phase results in the formation of oil droplets including a drug-loaded aqueous phase (W/O/W) [86]. In the second step, the solvent is removed by evaporation of the volatile compounds and the final polymer precipitation takes place, leading to the formation of microspheres. The parameters determined by the second step of the ESE are the morphology of generated MPs which have crucial influence on the encapsulation efficiency and release behaviour (Fig. 8) [87].

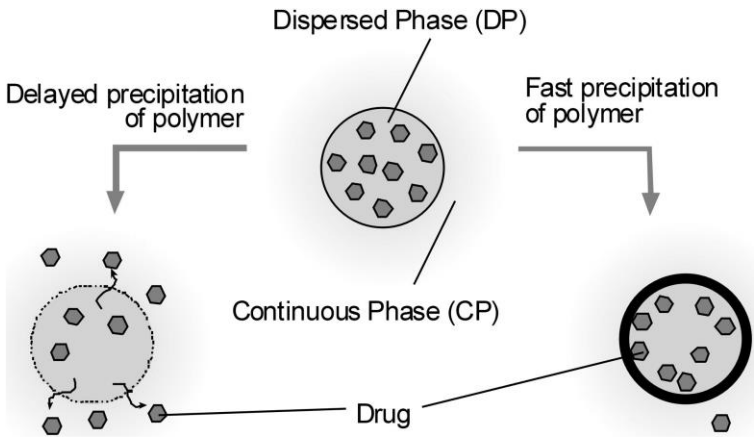

Figure 8. Influence of the precipitation on MP morphology. Fabrication of porous microspheres due to the delayed polymer precipitation results in low encapsulation efficiency. Fast polymer precipitation provides high encapsulation efficiency due to the formation of a uniform shell of the microsphere [88].

In principle high encapsulation efficiency of drugs are obtained by a fast solidification of MPs which is influenced by several parameters [89]. As Mehta *et al.* mentioned, a low solubility of the polymer in the oil phase decreases solidification time of the microspheres [90]. In addition, high solubility of the organic liquid in water benefits the encapsulation procedure leading to rapid precipitation of the polymer, based on a fast mass-transfer between the dispersed (DP) and the continuous phase (CP) [89]. Increasing the polymer concentration is another crucial parameter resulting in high encapsulation efficiency. This relationship can be interpreted in two ways, on the one hand that the polymer has a faster precipitation on the surface of the DP, and on the other hand it prevents drug diffusion across the phase boundary [91, 92]. Additionally, a high concentration of polymers results in an increase in viscosity and thus causes a delay in drug diffusion. The ratio between the DP and the CP also has an important influence on the solidification of microdroplets. A large volume of the CP leads to a high concentration gradient resulting in an enhanced solidification rate of the MPs [90, 92].

1.5 Aims and objectives

As can be seen from the preceding literature investigation the need for novel treatment strategies for refractory epilepsy is indubitable and several different materials and fabrication methods are available to achieve this aim. Nevertheless, there are also some boundary conditions mostly related to the regulatory guidelines to guarantee patients safety.

The ultimate goal of this thesis is the development of a novel implantable medical device hallmarked by sustained dual-release of an anti-convulsive drug for the treatment of pharmaco-resistant epilepsy and an anti-inflammatory agent to support post-operative wound-healing. To realize this aim, the project investigates the possibility of incorporating microspheres, loaded with anti-inflammatory DEX and AEDs (LEV or PHT), into the electrochemical compaction process of collagen to form a unique collagen-based drug delivery system (Fig. 9). To achieve encapsulation of hydrophobic DEX, the single ESE technique (O/W) is investigated and for the hydrophilic LEV the double ESE technique (W/O/W) is used.

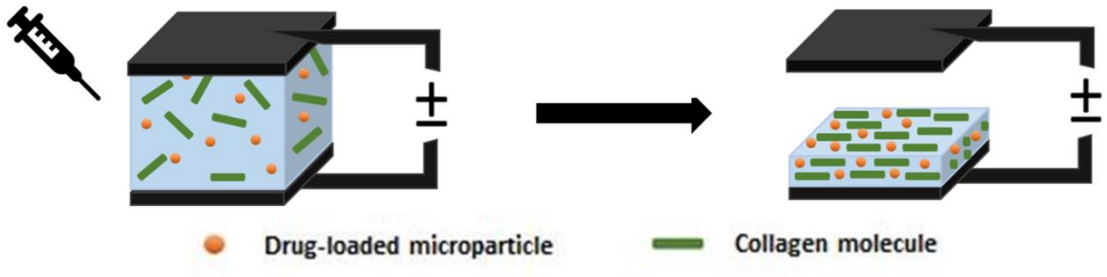

Figure 9. Concept of the fabrication process of drug-loaded collagen sheets. Drug-loaded microspheres are mixed to the monomeric collagen solution and injected between the electrodes. Application of an electrical field triggers the compaction of collagen molecules at the isoelectric point and causes entrapment of the microspheres within the collagen sheet.

The success of the concept for a clinical application, as illustrated above, is dependent on three factors:

I, drug-loaded collagen matrices have to meet the criteria for an application in neurosurgery regarding a sufficient mechanical stiffness of the device.

II, the target fabrication process has to provide a sufficient drug-loading efficiency

III, the release kinetics of the implant must be in consistent with the therapeutic window of inserted drug to guarantee patients safety.

2. Materials and Methods

2.1 Microsphere preparation

2.1.1 Encapsulation of DEX

For the encapsulation of hydrophobic DEX, the single ESE technique (O/W) was used. Poly (lactic-*co*-glycolic) acid (PLGA) with a lactide:glycolide ratio of 50:50 (Purasorb® PDLG 5010, Mw =153 kDa) was utilized for all microsphere formulations. In general, PLGA was dissolved in 6 mL dichloromethane (DCM). The concentration of PLGA varied from 5% w/v, 10% w/v, 15% w/v and 20% w/v. Each oil phase was then emulsified into 60 mL of 2% w/v poly-vinyl alcohol (PVA) aqueous solution at 8000 rpm for 3 min using an IKA® T25 digital ULTRA-TURRAX® homogenizer. The emulsion was then added to 60 mL of deionized water and stirred at 800 rpm at room temperature. After 3 h, the microspheres were isolated by centrifugation at 3000 rpm for 4 min, washed 3 times with distilled water to get rid of any residual PVA and lyophilized for 2 days. MPs were stored under dry conditions at -20 °C and protected from light.

2.1.2 Encapsulation of rhodamine B isothiocyanate-dextran

PLGA microspheres were prepared by a W/O/W emulsion technique previously reported by Freytag *et al.*. 0.5 mg of rhodamine B isothiocyanate-dextran was dissolved into 500 µL of distilled water (forming internal aqueous phase, W). Afterwards the aqueous solution was added to 5 mL of DCM containing 1 g PLGA (O). The primary emulsion was vortexed at 2500 pm for 30 s followed by 5 min of sonification. The W/O emlusion was then added to 10 mL of 4% PVA solution (re-emulsification solution, W) and vortexed at 2500 pm for 30 s. The resulting W/O/W double emulsion was poured into 250 mL of 0.4% PVA solution and stirred at 1000 rpm. After 2 h, the MPs were isolated by centrifugation at 3000 rpm for 4 min, washed 5 times with distilled water to get rid of any residual PVA and lyophilized for 2 days. MPs were stored under dry conditions at -20 ^{o}C and protected from light.

2.1.3 Encapsulation of LEV

For the encapsulation of hydrophilic LEV various batches of microsphere formulations were developed using various methods like water-in-oil-in-oil (W/O/O) double emulsion solvent diffusion (ESD) and W/O/W double ESE techniques. PLGA with a lactide:glycolide ration of 50:50 (Purasorb® PDLG 5010) and 75:25 (Purasorb® PDLG 7507, Mw = 95 kDa) were used as the controlled release polymers.

W/O/W Double ESE method using DCM

Briefly, 100 mg of LEV was dissolved into 500 µL of distilled water (forming internal aqueous phase). Next, the aqueous solution was added to 5 mL of DCM containing 1 g PLGA (oil phase). The primary emulsion was vortexed at 2500 rpm for 30 s followed by 5 min of sonification. The mixture was then added to 10 mL of 4% PVA solution (re-emulsification solution) and vortexed at 2500 rpm for 30 s. The resulting W/O/W double emulsion was poured into 250 mL of 0.4% PVA solution and stirred at 1000 rpm. After 2 h, the MPs were obtained by centrifugation at 3000 rpm for 4 min, washed 5 times with distilled water to remove any residual PVA and lyophilized for 2 days. MPs were stored under dry conditions at -20 °C and protected from light.

W/O/W Double ESE method using ethyl acetate

PLGA microspheres were prepared by a modified W/O/W ESE technique previously reported by F. Meng *et al.* [86]. 40 mg of LEV was dissolved into 200 µL of distilled water and then added to 2 mL of ethyl acetate (EA) containing 200 mg of PLGA with a lactide:glycolide ratio of 75:25. The primary emulsion was vortexed at 2500 rpm for 30 s and re-emulsified at 2500 rpm for 60 s with the external aqueous phase containing 2% PVA. Next, the W/O/W double emulsion was poured into 20 mL of another aqueous phase containing 2% PVA and stirred at 100 rpm for 2 min to pre-solidify the microdroplets. Subsequently, the W/OW emulsion was poured into 200 mL 1% PVA solution and stirred at 400 rpm to solidify the embryonic microdroplets. After 4 min, the microspheres were obtained by centrifugation at 3000 rpm for 4 min, washed 3 times with distilled water to get rid of any residual PVA and lyophilized for 2 days. MPs were stored under dry conditions at -20 °C and protected from light.

W/O/O Double ESD using paraffin oil

PLGA microspheres were prepared by a W/O/O ESD technique previously described by Wu *et al.* with some modifications [93]. Briefly, 200 mg of PLGA (50:50) was dissolved in 2 mL of a mixed solvent system comprising of acetonitrile (ACN) and DCM in equal volumes (1:1). 20 mg of LEV was dissolved in 200 µL of distilled water. The aqueous phase was mixed in the above organic phase and vortexed at 2500 rpm for 60 s to form the W/O emulsion. Afterwards, the W/O emulsion was emulsified into 50 mL of liquid paraffin containing 0.5% Span80. The W/O/O emulsion was stirred at 750 rpm for 4 h at room temperature to evaporate the organic solvents. The MPs were obtained by centrifugation at 3000 rpm

for 4 min, washed 3 times with 20 mL of n-hexane to remove any residual surfactant and lyophilized for 2 days. MPs were stored under dry conditions at -20 °C and protected from light.

2.1.4 Encapsulation of PHT

PHT-loaded microspheres were prepared by a modified O/W ESE procedure [94]. PLGA with a lactide:glycolide ratio of 50:50 (Purasorb® PDLG 5010) was utilized for all microsphere formulations. PLGA and PHT were dissolved in 5 mL of DCM and acetone (4:1) at a weight ratio of 10:1. The concentration of the polymer varied from 10% w/v, 15% w/v and 20% w/v. The organic phase was then emulsified into 50 mL of 2% PVA aqueous solution at 8000 rpm for 3 min using an IKA® T25 digital ULTRA-TURRAX® homogenizer. Afterwards, 50 mL of distilled water was added to the O/W emulsion and stirred at 1000 rpm at room temperature for 4 h. The MPs were obtained by centrifugation at 3000 rpm for 4 min, washed 3 times with 0.2% w/v PVA solution to remove any residual surfactant and lyophilized for 2 days. MPs were stored under dry conditions at -20 °C and protected from light.

2.2 Characterization of microspheres

The volume-mean diameter of the drug-loaded microspheres was quantified using photomicrographs taken on a Zeiss Axiovert 40 CFC microscope. Images of PLGA microspheres were analyzed using NIH ImageJ software. At least 400 particles were evaluated to generate the distribution of particle diameter.

2.3 Loading efficiency

The amount of drug per weight of microspheres was determined by a solvent extraction method. Briefly, 5 mg of MPs was weighed and extracted with ethanol overnight. Samples were then centrifuged at 1000 rpm for 5 min and the supernatant was collected. The amount of the drug was quantified by HPLC analysis. An Agilent 1260 Infinity HPLC system was utilized, equipped with a ZORBAX® Eclipse Plus C18 column (4.6 mm x 100 mm, 5 µm). The temperature of the column was adjusted at 40 °C, the injection volume was 10 µL, the flow rate 1.0 mL/min, and UV detection wavelength at 242 nm. The amounts of DEX and PHT were analyzed using an isocratic mobile phase consisting of water and ACN (70:30, v/v). A standard curve of DEX and PHT prepared in 1 x PBS aqueous solution was established by plotting the peak areas against respective concentrations of standard solutions, respectively.

2.4 *In-vitro* drug release study of microspheres

10 mg of drug-loaded microspheres were suspended in 1 mL of artificial cerebrospinal fluid (aCSF, 0.866 wt% NaCl, 0.224 wt% KCl, 0.0164 wt% $MgCl \cdot 6H_2O$ and 0.0206 $CaCl_2 \cdot 6H_2O$ in 0.001 M PBS), and the release experiment was conducted at 37 °C in a shaker water bath. For each sample, the release medium was obtained by centrifugation at 4000 rpm for 3 min and replenished with fresh aCSF at various time points and stored at -18 °C prior to HPLC analysis being undertaken.

2.5 Fabrication of particle-loaded ECC matrices

Acid soluble type-I bovine collagen solution (Advanced BioMatrix, 6.1 mg/mL) was diluted 1-fold in 20 mM acetic acid and dialyzed ($Mw_{cut\ off}$ = 12-14 kDa) against ultrapure water for 18 h. 5 mg of drug-loaded PLGA MPs were added to 1 mL of freshly dialyzed collagen (3 mg/mL) solution and vortexed at 2500 rpm for 30 s. This emulsion was injected between two plate electrodes and a voltage of 6 V was applied for 20 minutes. At the end of the electrochemical process, the ECC matrices were recovered from the cathode using a pair of tweezers. To promote fibril formation, the fabricated ECC matrices were incubated in 10 times phosphate-buffered saline (PBS) containing 0.5 mM riboflavin at 37 °C for 2h. After incubation, collagen matrices were exposure to an UV light source (400 nm) for 120 seconds to initiate crosslinking. Crosslinked ECC matrices were then washed thoroughly 3 times prior to the *in-vitro* drug release study.

2.6 Tensile mechanical properties

The influence of microsphere entrapment on the mechanical properties of ECC matrices was analyzed by using a Shimadzu EZ mechanical tester. In-plane tensile tests were performed on ECC sheets (12.5 mm x 8 mm x 0.2 mm) with and without microspheres (N=3/group). Samples were fixed on paper tabs and rehydrated with 1x PBS. The thickness of the ECC matrices were determined using an optical microscope (Zeiss Axiovert 40 CFC). Afterwards, the samples were mounted onto the tensile clamps with 10 mm gauge length and subjected to uniaxial tensile loading until failure at a strain rate of 1 mm/min. The load-displacement data were used to calculate the Young´s modulus of ECC matrices.

2.7 *In-vitro* drug release study of ECC matrices

Drug-loaded ECC matrices (N=3) were suspended in 1 mL of aCSF and the release experiment was conducted at 37 °C in a shaker water bath. For each sample, the release medium was collected and

replenished with fresh aCSF at various time points and stored at -18 °C prior to HPLC analysis being undertaken.

2.8 Scanning Electron Microscopy (SEM)

To assess the microscopic morphology of the ECC matrices, SEM was undertaken on the compacted collagen matrices and MP-loaded collagen matrices. An analogue sample preparation method was utilized, as recently described by Kishore *et al.* [19]. First, collagen matrices were fixed in 3.7 % paraformaldehyde for 3 h. Next, the samples were dehydrated in ethanol: water solutions (20%, 50%, 75%, 90% and 100% ethanol) for 5 minutes each. The matrices were then allowed to dry at room temperature overnight followed by Pt sputter coating. The surface and cross-section of the prepared collagen samples were observed under high resolution SEM (JEOL JSM-7500 field emission SEM).

Additionally, the morphology of the microspheres was analyzed using a field emission scanning electron microscope (JEOL JSM-7500). The MPs were sputter-coated with Pt to avoid sample charging.

3. Results and Discussion

3.1 Fabrication of drug-loaded microspheres

3.1.1 Characterization of DEX-loaded microspheres

DEX-loaded PLGA microspheres were successfully prepared by an O/W ESE technique (Fig. 10). To investigate the optimized PLGA concentration regarding its encapsulation efficiency of the drug samples were prepared using 5%, 10%, 15% and 20% PLGA.

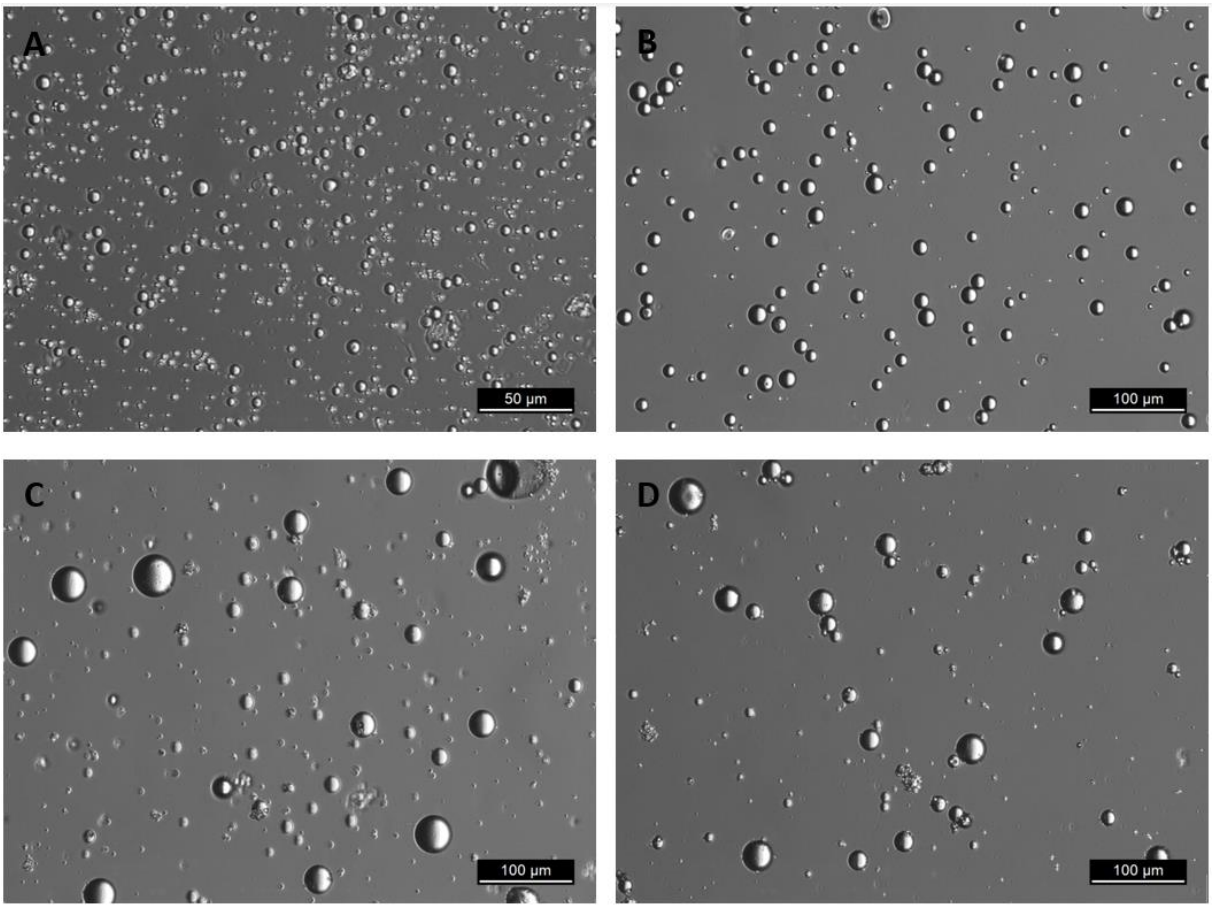

Figure 10. Photomicrographs of the microspheres prepared using an O/W emulsion from (A) 5%, (B) 10%, (C) 15% and (D) 20% PLGA.

An increase of the PLGA concentration correlated with an increase of the particle size of the spheres with a broader distribution (Table 1). Analysis of the drug-loading efficiency showed low encapsulation of DEX for microsphere formulations with low PLGA concentrations. Due to an increase of the polymer concentration up to 20% an acceptable drug-loading of 51% could be obtained.

Table 1. Summary of microsphere characterization at different PLGA concentrations.

Concentration of PLGA	Average particle size (µm)	Drug loading efficiency (%)
5% PLGA	6.1 ± 1.1	11.9 ± 0.9
10% PLGA	15.5 ± 2.9	12.5 ± 0.8
15% PLGA	20.3 ± 8.5	13.4 ± 1.3
20% PLGA	21.9 ± 5.7	51.4 ± 4.9

As previously mentioned, this phenomenon is mostly related to the fast solidification of the microspheres during the O/W emulsion which leads to an enhanced encapsulation efficiency of the hydrophobic drug into the particles. Moreover, SEM-Imaging of 20% PLGA microspheres demonstrated a spherical structure with smooth surface morphology (Fig. 11).

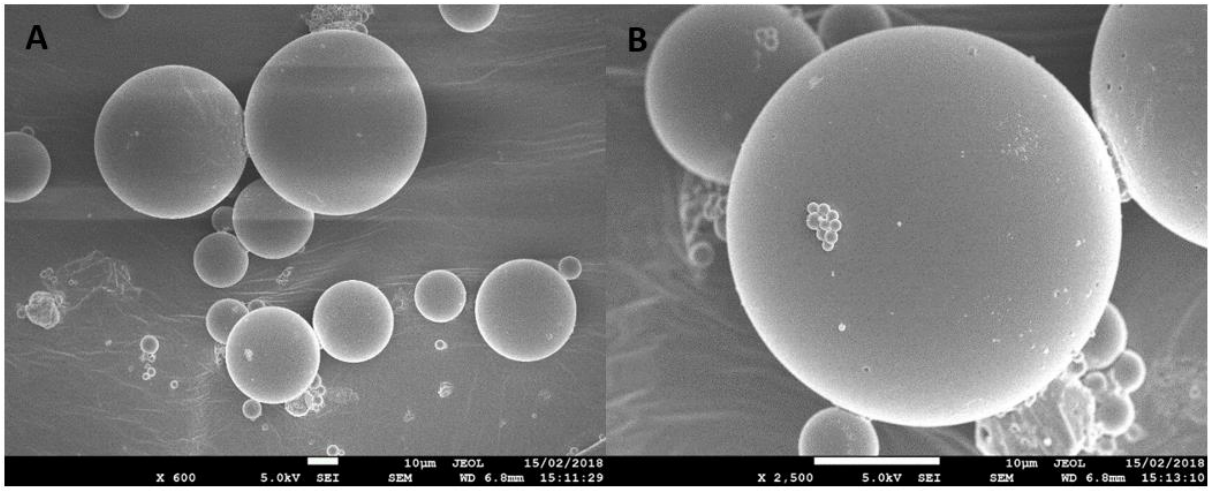

Figure 11. SEM micrographs of the DEX-loaded MPs prepared from 20% w/v PLGA using an O/W emulsion method taken at x600 (A) and x2500 (B) magnification.

To characterize the DEX-release profile from the 20% PLGA microspheres, an *in-vitro* release study was investigated in an aCSF (pH 7.4) solution at 37 °C for 11 days. The DEX-release profile from the PLGA microsphere samples showed multi-stage eluting behavior (Fig. 12).

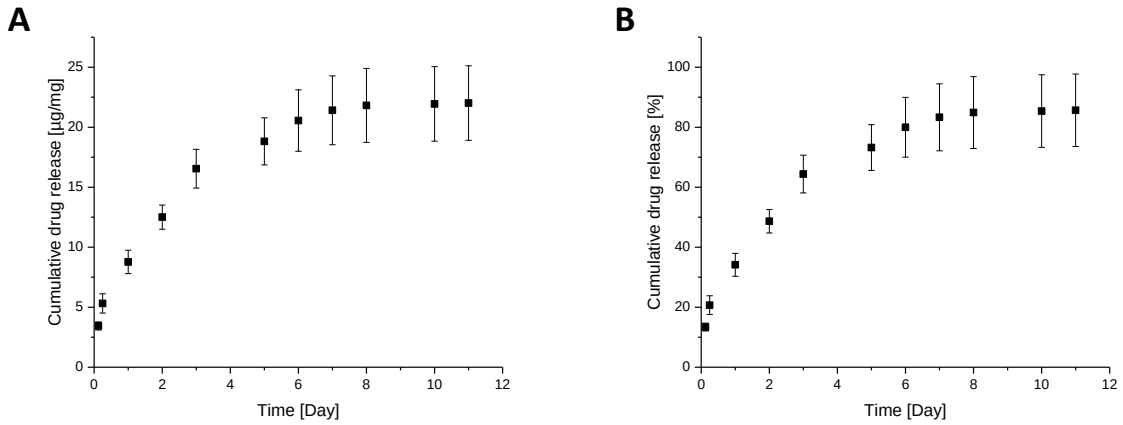

Figure 12. Cumulative DEX released from the 20% PLGA microspheres during an in-vitro release study in aCSF (pH 7.4) at 37 °C (n = 3) for 11 days. (A) Quantitative release of DEX per mg microspheres. (B) Total amount of DEX released as a percentage of the total amount of drug encapsulated into the 20% PLGA microspheres.

DEX-release from the PLGA microspheres followed a multi-stage pattern. An initial burst release of the anti-inflammatory drug has been observed with approximately 20% of the payload released during the first 6h. The phenomenon of this initial burst release can be explained by the release of DEX localized on the surface of the microspheres. Furthermore, as a general observation, it is noteworthy that the obtained PLGA microspheres, as for most particle formulations prepared by ESE, indicate a high variability (Fig. 11). As described by Berchane *et al.*, a high polydispersity in size correlates with a high initial burst release, since a significant amount of drug is entrapped into smaller particles, which demonstrate brief elution times [95].

The subsequent days (1 to 8) showed a decreasing release rate of DEX, associated with the slight diffusion of the drug from the core of the microspheres into the medium. The third stage was characterized by a steady state, reaching 86% of completion until conclusion of the *in-vitro* release study after 11 days.

Summarizing the above, ESE provided drug-loaded microspheres which showed sustained release of DEX for 11 days. As for the anti-inflammatory drug, a controlled release profile for the crucial initial 2 weeks of post-implantation was desired, the 20% PLGA microsphere formulation showed promising results for the incorporation into ECC matrices.

3.1.2 Encapsulation of anti-epileptic LEV

As previously discussed, a great variety of methods, mostly based on single-emulsions, have been utilized to fabricate drug-loaded microspheres but are mainly limited to hydrophobic drugs. To ensure the encapsulation of hydrophilic drugs, which show rather low solubility in most organic solvent

systems, the first approach is a W/O/W ESE method in which the water-soluble drug is dissolved in an inner aqueous phase prior to emulsion in an oil phase.

In a pilot study, fluorescently labelled dextran was used as a hydrophilic model drug to investigate the W/O/W ESE technique to provide drug-loaded PLGA microspheres. For this aim an oil phase comprising of DCM was chosen, due to its fast volatility. Furthermore, a high polymer concentration (20% PLGA) was investigated to induce a rapid solidification to prevent diffusion of the aqueous dextran solution into the external phase. The total amount of particles achieved by this method was 630 mg (63 %) with the particles between 57 µm and 186 µm. The mean-diameter of particles resulted in 107 µm (Fig. 13).

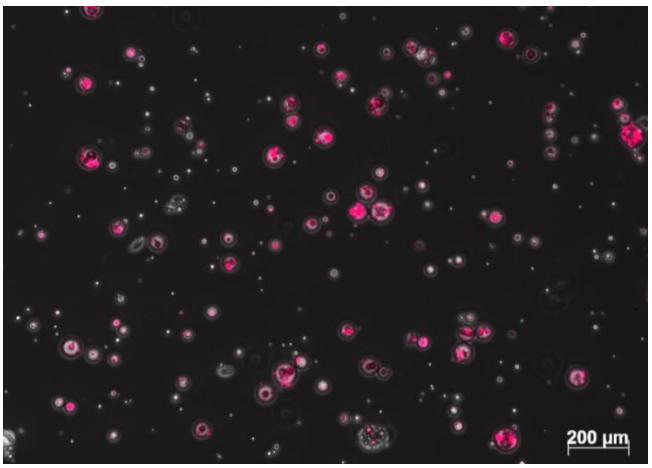

Figure 13. Fluorescent micrograph of the PLGA microspheres loaded with rhodamine B isothiocyanate-dextran.

Fluorescent microscopy could confirm the incorporation of rhodamine B isothiocyanate-dextran into the PLGA microspheres. Taken the result of this pilot experiment into account, further studies were investigated to prepare LEV-loaded microspheres using the double emulsion method. The W/O/W emulsion of LEV provided PLGA microspheres with a mean diameter around 20 µm. However, the analysis of the drug loading efficiency revealed no entrapment of the hydrophilic drug into the PLGA microspheres. As described by Viry *et al.*, the high range of solubility of LEV in common organic solvents used as the oil phase in the emulsion process could complicate encapsulation of the drug into the polymeric system (Fig. 14) [96]. During the emulsification of the inner water phase into the oil phase, the drug can easily pass into the organic phase and finally diffuse into the outer aqueous phase. Furthermore, LEV has a low molecular weight which additionally supports a rapid diffusion of the drug into the medium.

To improve the encapsulation of LEV into PLGA microspheres, we further investigated some modifications of the emulsion process by either decreasing the solubility of the drug into the oil phase or preventing diffusion of the drug into the outer aqueous phase. To reduce drug-diffusion into the oil phase, EA was investigated. In addition to the lower solubility of LEV in EA compared to DCM, the use of EA as the oil phase has also benefits regarding the product approval by regulatory agencies. As

previously described by Sah *et al*., EA is regarded as one of the most beneficial organic solvents with respect to patient safety [97]. However, the high solubility in water as well as the high boiling point are the main drawbacks of EA for its use in the W/O/W ESE process. As mentioned by Meng *et al.*, the high solubility of EA in the aqueous phase leads to a rapid diffusion of EA from embryonic microdroplets into the external water phase during re-emulsification which can cause the precipitation of the polymer instead of the formation of microspheres [86].

Taken the above-mentioned considerations into account, it was chosen to investigate a modified W/O/W ESE procedure, which was previously described by Meng *et al.* and includes an additional preliminary partially solidification step. Due to the addition of a small amount of another external aqueous phase (W_3), a slow extraction of EA from the embryonic microdroplets can be realized. In this study Meng *et al.* were able to effectively restrict the coagulation of oil droplets and thus a high yield of microspheres could be achieved [86].

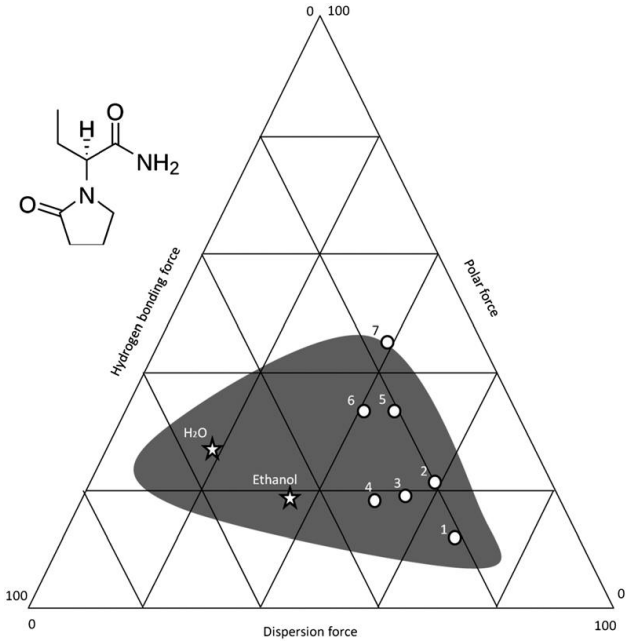

Figure 14. Teas graph representation of the solubility characteristics for organic solvents of PLGA. (1: tetrahydrofuran, 2: DCM, 3: chloroform, 4: dimethylformamide,5: EA, 6: ACN, and 7: acetone). Water and Ethanol are illustrated by asterisk. The solubility range of LEV is illustrated by the dark area [96].

As a proof-of-concept experiment, the encapsulation efficiency of fluorescently labelled dextran into PLGA microspheres prepared by the above-mentioned double emulsion process has been investigated. A relatively low concentration of 8% (w/v) PLGA (75:25) was chosen to minimize polymer precipitation. The double emulsion technique using EA provided spherical MPs without agglomeration or precipitation of PLGA. Furthermore, fluorescent microscopy could confirm the incorporation of rhodamine B isothiocyanate-dextran into the PLGA microspheres (Fig. 15 A).

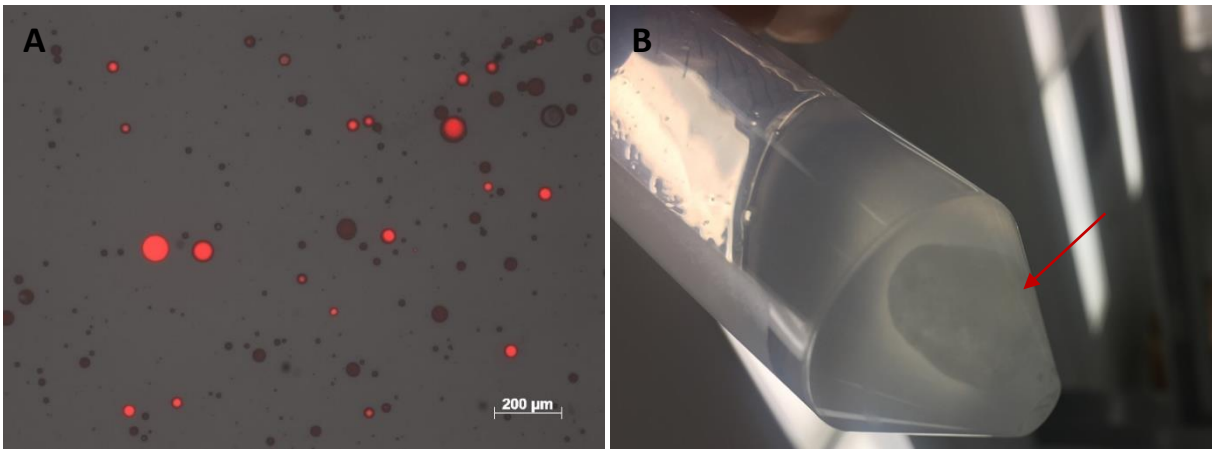

Figure 15. PLGA microspheres prepared by W/O/W double emulsion using EA. (A) Fluorescent micrograph of the PLGA microspheres loaded with rhodamine B isothiocyanate-dextran from 8% (w/v) PLGA solution. (B) Increasing the polymer concentration to 15% (w/v) and 20% (w/v), respectively, resulted in polymer precipitation (red arrow).

The pilot experiment revealed that the W/O/W double emulsion technique using EA and a slow extraction rate provides spherical MPs and is able to successfully encapsulate the hydrophilic model drug even though no quantitative analysis of the fluorescent dextran entrapment was undertaken. Taken the result of this pilot experiment into account, further studies were investigated to encapsulate LEV into the polymeric microspheres. First experiments using a PLGA concentration of 8 % and a drug/polymer ratio of 1:10 resulted in a low encapsulation efficiency about 0.5 % of LEV into the polymer microspheres (Table 2). Another approach investigated the increase of the polymer concentration which should correlate with a higher drug entrapment into the microspheres. For this aim samples were prepared with 15% and 20% PLGA concentration. The increase of the polymer concentration resulted in a fast EA extraction which caused a rapid precipitation of PLGA prior to the formation of microdroplets (Fig. 15 B).

Table 2. Summary of microsphere characterization at different PLGA concentrations using EA.

Concentration of PLGA	Morphology	Drug loading efficiency (%)
8% PLGA	microspheres	0.5 ± 0.1
15% PLGA	precipitation	-
20% PLGA	precipitation	-

As illustrated in Table 2., the investigation of the modified double ESE technique using EA was unsuccessful to provide an acceptable encapsulation efficiency of LEV into the microspheres. Despite

the reduced solubility of LEV in the oil phase by using EA instead of DCM, the diffusion of LEV into the outer aqueous phase was still high and significantly decreased the encapsulation efficiency of the drug. The low drug-loading efficiency of the microspheres is unsuitable for a drug delivery system, especially in terms of a long-term release. For this reason, another approach using a modified W/O/O double ESD technique was investigated. This technique is mostly based on the replacement of the outer water phase by another hydrophobic phase (O_2) to reduce diffusion of the hydrophilic compound. Under all W/O/O emulsion techniques, a mixed solvent system comprising of ACN/DCM (O_1) and liquid paraffin (O_2) is well described in the literature [93, 98, 99]. By choosing an oil as the processing medium, the solvent for the polymer needs to be immiscible with the oil (O_2) while providing suitable solubility for the polymer. Compared to most other polar organic solvents, ACN is oil-immiscible but water-miscible, which would cause precipitation of the water/ACN phase (W/O_1). Thus, to guarantee microsphere formation, DCM is added to the polymer solution (DCM/ACN, 50:50) to reduce the polarity and to provide a stable emulsion of the polymer solution into the paraffin oil [98].

First experiments using the above described method aimed to proof the ability to entrap fluorescently labelled dextran into PLGA microspheres. Samples prepared with 10% PLGA concentration resulted in the formation of agglomerated microspheres and clusters (Fig. 16).

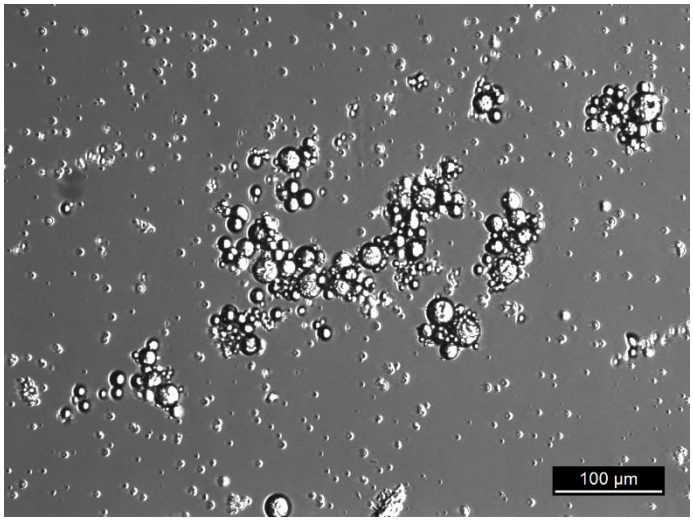

Figure 16. Photomicrograph of the 10% PLGA formulation prepared by W/O/O double emulsion reveals agglomeration of the MPs.

Investigations of the encapsulation efficacy of rhodamine B isothiocyanate-dextran by fluorescent micrographs revealed no compound entrapment into the microspheres. A possible reason for that could be the formation of porous microspheres due to the low evaporation of ACN during emulsification. Longer solvent evaporation time correlates with decreased particle solidification and thus can lead to porous microspheres in which the encapsulated drug can be easily washed out of the system [82].

Given that the pilot experiment of the W/O/O emulsion resulted in no encapsulation efficiency of fluorescent dextran, no further experiments were undertaken to encapsulate LEV. Summarizing the encapsulation efforts for hydrophilic LEV using the W/O/O double ESD and the W/O/W double ESE techniques, all experiments failed to provide microspheres with an acceptable drug loading efficiency.

3.1.3 Characterization of PHT-loaded microspheres

As may be evident from the above, the encapsulation process of very hydrophilic LEV still needs further investigations in order to establish a procedure which provides microspheres with suitable drug loading. Additionally, the pilot experiments revealed that it is uncertain to obtain a sustained drug release of LEV from microspheres using ESD or ESE due to the excellent solubility in both organic and aqueous solvent. As previously mentioned, the neurosurgical implantation of such a device is related to the high risk of intracranial infections or neurological deficits [67]. Thus, a long-term release of the AED is one of the crucial features for an implantable collagen membrane for the treatment of epilepsy. In pursuit of this goal we further centred our investigations on the preparation of PLGA microspheres loaded with anti-convulsive PHT. The advantage of this drug is the low water solubility with around 32 mg/L which enables encapsulation of PHT in a single O/W emulsion as previously described by Jiang *et al.* [94, 100]. To investigate the optimized PLGA concentration regarding its encapsulation efficiency of the drug, samples were prepared using 10%, 15% and 20% PLGA (Fig. 17). PHT-PLGA microspheres prepared by the ESE method showed acceptable PHT content in almost all particle formulations (40.6% - 51.2%) (Table 3). Compared to the preparation of DEX-microspheres, PHT-microspheres showed a smaller mean diameter (7.8 µm – 15.4 µm).

Table 3. Summary of PHT-microsphere characterization at different PLGA concentrations.

Concentration of PLGA	Average particle size (µm)	Drug loading efficiency (%)	Yield (%)
10% PLGA	15.4 ± 4.0	40.6 ± 3.6	71.2
15% PLGA	7.8 ± 1.7	48.6 ± 6.2	62.5
20% PLGA	12.7 ± 3.7	51.2 ± 7.9	14.7

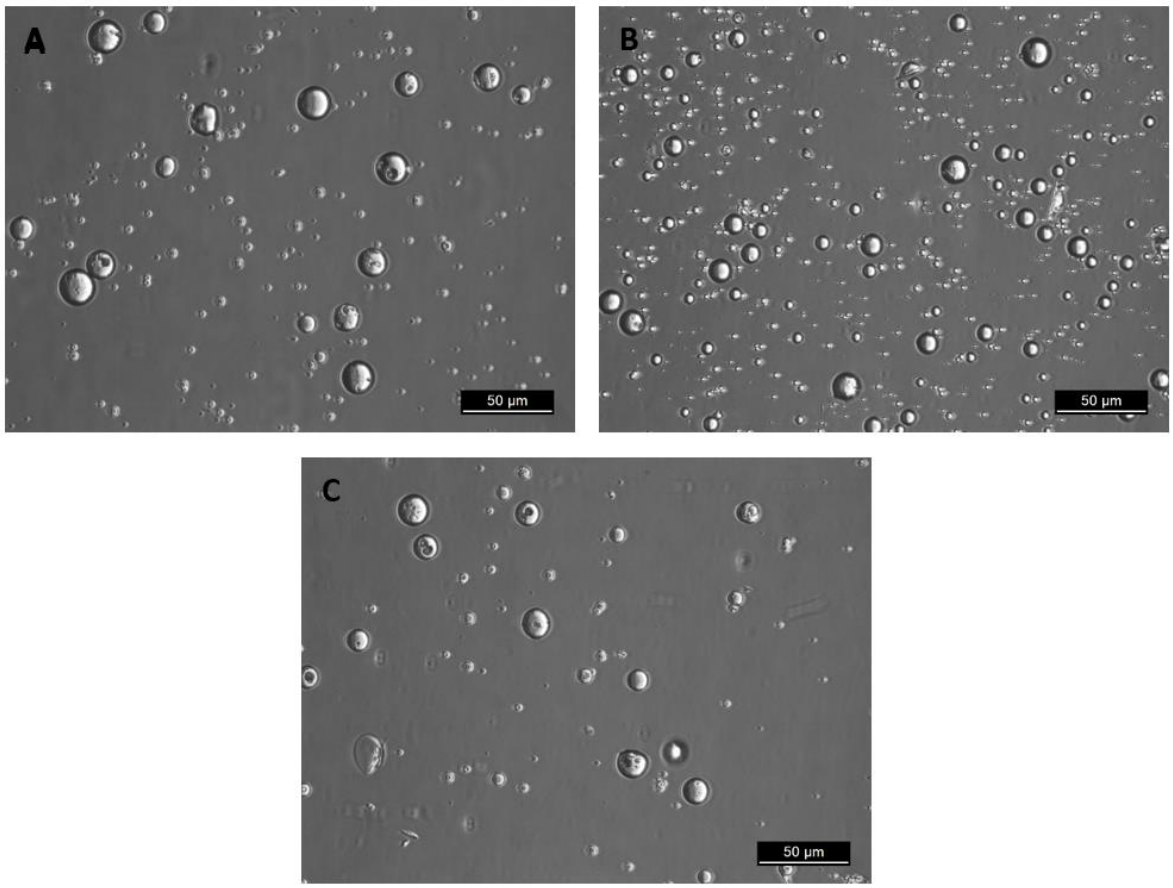

Figure 17. Photomicrographs of the PHT-spheres prepared using an O/W emulsion from (A) 10%, (B) 15% and (C) 20% PLGA.

To assess the drug release behavior of these particle formulations, an *in-vitro* release study was investigated in an aCSF (pH 7.4) solution at 37 °C for 30 days (Fig. 18). For these studies samples from the 10% and 15% PLGA formulations were chosen as the microsphere yield from the 20% PLGA was significantly low due to the concurrent precipitation of a high amount of polymer during emulsification.

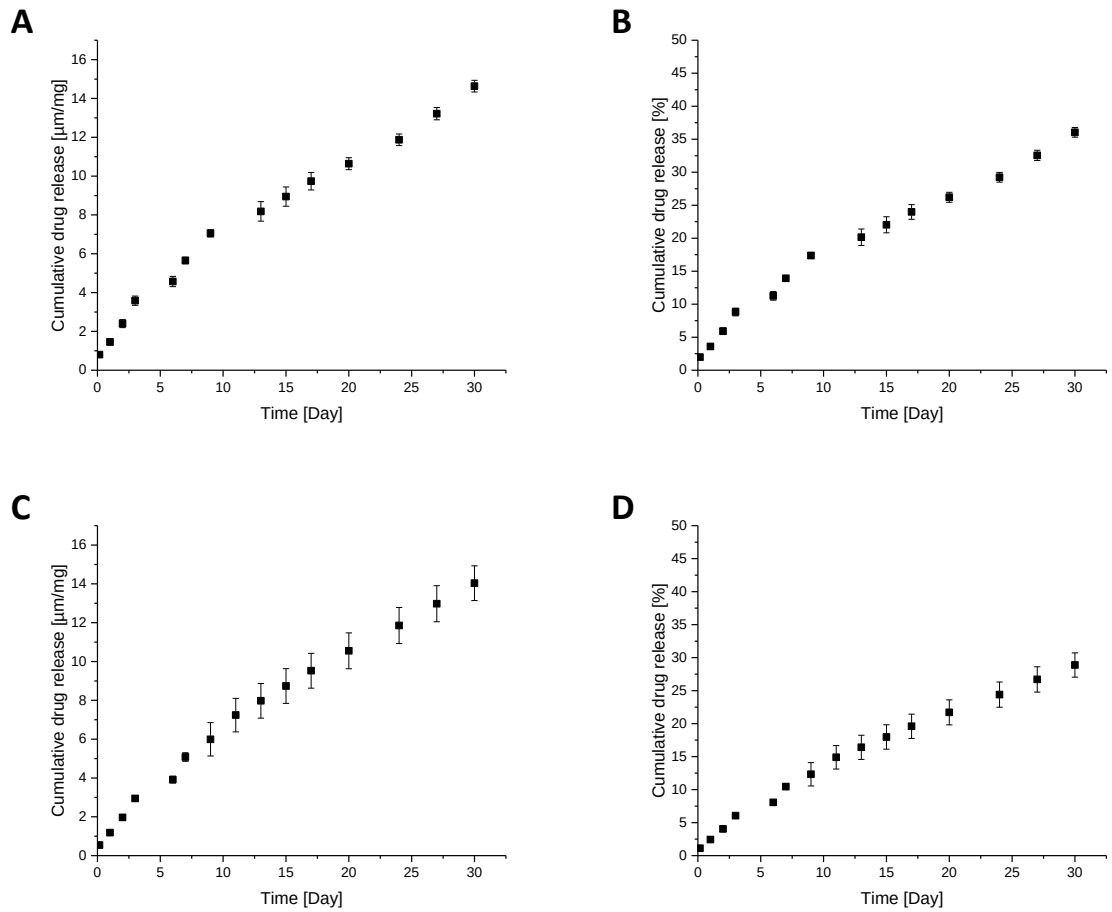

Figure 18 Cumulative PHT released from the PLGA microspheres during an in-vitro release study in aCSF (pH 7.4) at 37 °C (n = 3) for 30 days. (A) and (C) Quantitative release of PHT from 1 mg of 10% and 15% PLGA-microspheres, respectively. (B) and (D) Total amount of PHT released as a percentage of the total amount of drug encapsulated into the 10% and 15% PLGA-microspheres, respectively.

Fig. 18 represents the cumulative release of PHT from 10% and 15% PLGA microspheres about 30 days. Both formulations demonstrated sustained release of PHT following a triphasic release pattern and were characterized by a slight burst release. For the initial 3 days, the early stage of drug release was dominant by dissolution of surface drug and reached 9% (10% PLGA) and 6% elution (15% PLGA) of the total drug-loading. Between 3 and 10 days the release of PHT slowed down due to the dissolution and diffusion of the drug from the core of the spheres into the medium. After 10 days the release of PHT represented an almost linear release pattern for the following 20 days. This phenomenon indicates a change from a diffusion-controlled release pattern to a combined diffusion/erosion-coupled release mechanism due to the degradation of the PLGA microspheres [101, 102]. Another possible reason accounting for the release profile might be the formation of open channels as a result of progressive dissolution of the drug, which may facilitate further release of drug.

Compared to the 10% PLGA formulation which showed 36% drug release at day 30, the microspheres obtained from the 15% PLGA showed a reduced release rate with only 28% of PHT-elution at day 30. With regard to the time frame available, drug release analysis was stopped after 30 days. Nevertheless, the previous discussed results indicated a promising sustained release of anti-convulsive drug from the microspheres. For the drug-release studies of ECC matrices, the 15% PLGA formulation was chosen due to its more sustained drug release profile.

3.2 Electrocompaction of collagen matrices

In order to achieve a good reproducibility and suitable mechanical stiffness of the collagen matrices, the process parameters of the ECC matrices were investigated prior to the incorporation of drug-loaded microspheres.

For the electrochemical compaction of collagen, it is necessary to adjust the strength of the electrical field applied to the monomeric collagen solution. In order to measure the current during electrochemical compaction of collagen, an amperometric three electrodes topology was utilized (Figure 19 A). This measurement is defined by a working electrode (Stainless-steel), where the electrochemical reaction takes place, the reference electrode, which tracks the potential solution and a counter electrode (Indium-tin-oxide-glass, ITO-glass), which supplies the required voltage for the electrochemical reaction at the working electrode. Freshly dialyzed collagen solution was injected between the stainless-steel electrode (cathode) and the counter electrode (anode) in circular silicon rubber washers and an electrical field was applied in the range of 5 – 8 volts. Application of voltages up to 6 V resulted in transparent films free of noticeable air bubbles which could be recovered from the working electrode after the electrochemical process (Figure 19 B). Fig. 19 C represents a representative current-time curve of the electrochemical compaction process of collagen. Within the first 20 seconds a rapid decrease of the current can be observed which indicates the formation of a high resistance within the aqueous solution due to the deposition of collagen. The initial decrease of the current is followed by a slight increase and a final constant current assuming that no further collagen deposition takes place (Fig. 19 C). Application of higher voltages (7 V) showed the appearance of bubbles into the collagen matrices (Fig. 19 D). These phenomena can be explained with a strong hydrolysis taking place in the electrochemical cell, causing an increased hydrogen formation.

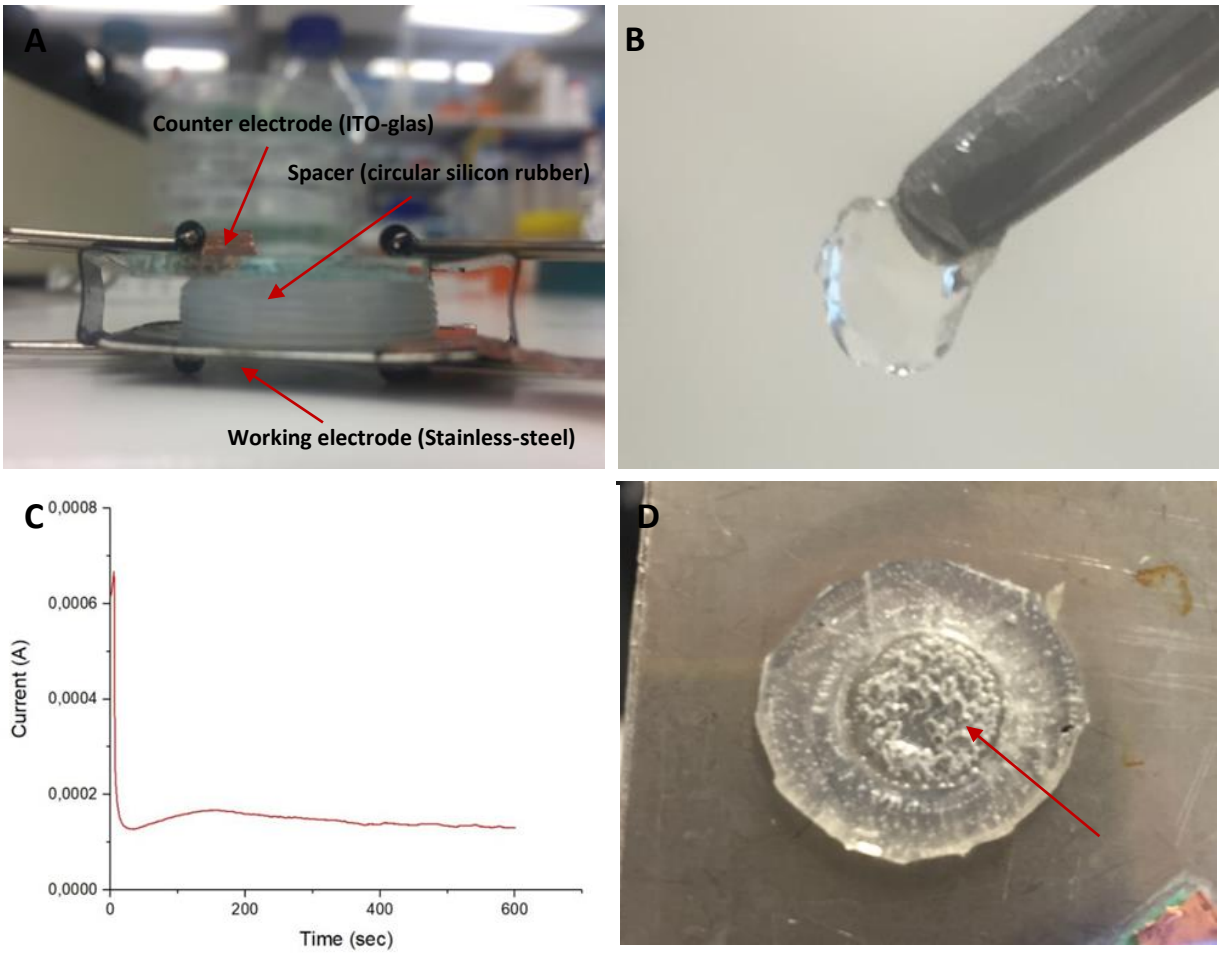

Figure 19. Fabrication of ECC matrices. (A) Image of the electrochemical cell for the compaction of collagen. (B) Highly transparent ECC matrix recovered from the electrode after the electrochemical process. (C) Representative current-time-curve of the compaction process of collagen matrices. (D) Bubble entrapment (red arrow) into ECC matrices prepared at 7 V.

Summarizing the results indicates that the applied voltage shouldn't be chosen higher than 6 V to prevent a strong hydrolysis and to avoid significant air bubble formation within the ECC matrices.

To further increase the mechanical stability of ECC matrices, riboflavin was investigated as a well-known photo-crosslinker. ECC matrices were incubated in 10 times PBS containing 0.5 mM riboflavin for 2h and exposed to UV-light. The rheological investigation of the collagen sheets incubated with riboflavin provided three phases in the curve progression (Fig. 20 A).

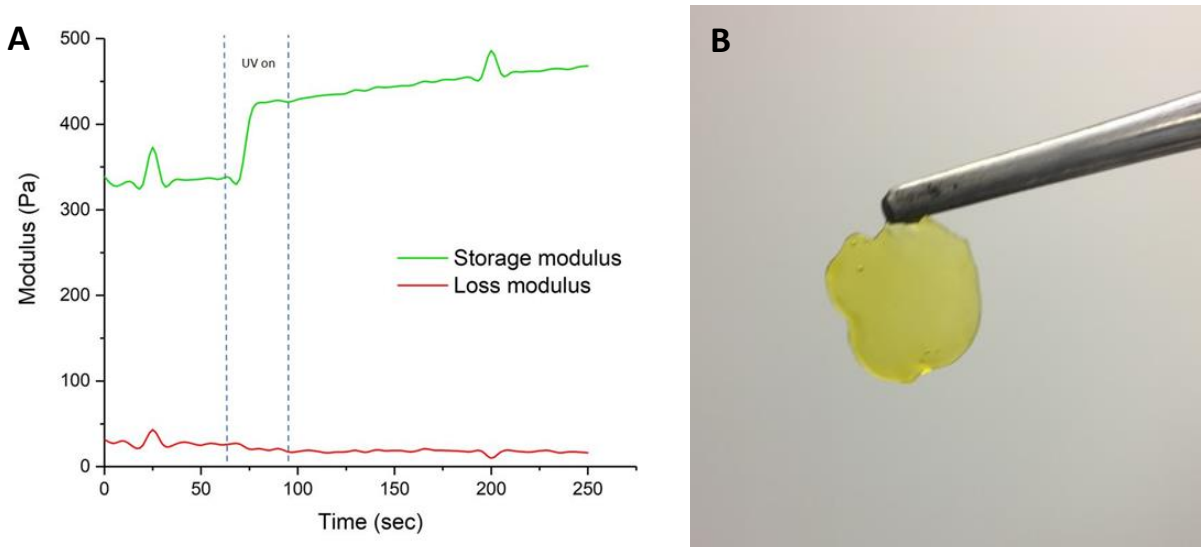

Figure 20. Photo-crosslinking of ECC matrices. (A) Representative results of rheological testing of riboflavin induced crosslinking of ECC matrices. Increase of the storage modulus after exposure to UV-light for 30 s at 60 s.(B) Collected ECC matrices after photo-crosslinking.

For the first phase a constant plateau of uncrosslinked collagen was present, which established the linear viscoelastic properties of the gel. UV-light was applied at 60 s for 30 s. During this time a definite increase of the storage modulus was observed. This is due to crosslinking activity of riboflavin. After UV-light exposure, a small increase of the storage module was still noticeable which might be due to continued crosslinking or continued fibrillogenesis and physical crosslinking of collagen. Furthermore, a slow dehydration might be occurred during UV crosslinking of the ECC matrices. However, further experiments are required to analyze this phenomenon of ECC crosslinking.

3.3 Incorporation of microspheres into ECC matrices

The potential of the electrochemically compaction process of collagen to entrap microspheres was investigated in a proof of principle study. 10 mg of PLGA microspheres loaded with the fluorescent Rhodamine B isothiocyanate-dextran were added to 1 mL of the monomeric collagen solution prior to injection between the plate electrodes and electrochemically compacted. Fluorescent microscopy was performed to evaluate the incorporation capability of fabricated collagen matrices and could demonstrate the existence of fluorescent microspheres entrapped into the ECC matrices (21 A). Compared to ECC matrices prepared without the addition of microspheres, particle-loaded microspheres demonstrated a slight turbidity of the ECC matrices (21 B).

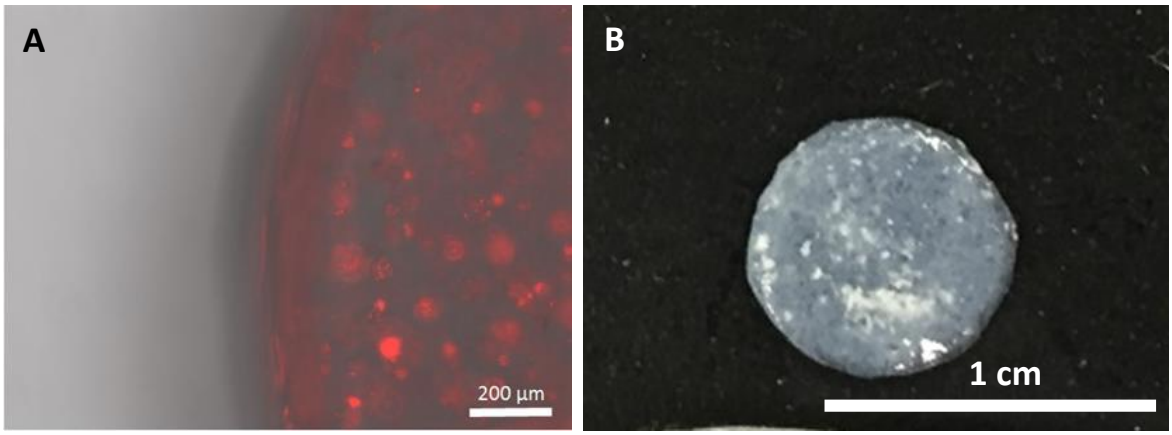

Figure 21. Incorporation of microspheres into ECC matrices. (A) Fluorescent microscopy of particle-loaded ECC matrix. (B) Photomicrograph of particle-loaded ECC matrix.

3.4 Mechanical properties of drug-loaded ECC matrices

To analyze the influence of microsphere entrapment into ECC matrices regarding their mechanical properties, tensile tests were undertaken on ECC matrices and particle-loaded (5mg/mL) ECC matrices. The Young's modulus of ECC matrices were calculated from the Stress-Strain curves (Fig. 22).

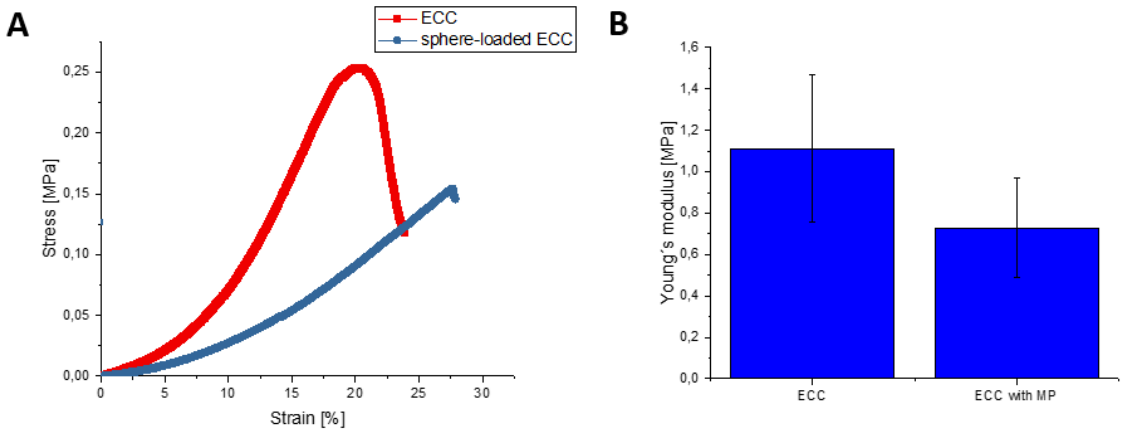

Figure 22. Tensile properties of ECC with and without microspheres (n=3). (A) Stress-Strain curve and (B) Tensile modulus.

The Young's modulus of photo-crosslinked ECC matrices and particle-loaded ECC matrices was 1.11 ± 0.36 MPa and 0.73 ± 0.24 MPa, respectively. Compared to the Youngs modulus of traditional collagen gels, which was investigated by Lopez-Garcia *et al*. and ranged from 1 to 28 kPa., the electrocompacted and crosslinked collagen matrices had a 50-fold greater Youngs modulus [103]. Therefore, these results suggested that electrocompaction and photo-crosslinking significantly improved the tensile strength and stiffness of the collagen matrices. Furthermore, the experiment revealed that the incorporation of microspheres into ECC matrices resulted in a significant decrease of the tensile modulus up to 25%.

This result supported the theory that the incorporation of microspheres inhibits the self-assembly of collagen fibres and thus results in decreased mechanical properties of particle-loaded ECC matrices.

3.5 Characterization of ECC morphology by SEM-Imaging

The microstructure of particle-loaded ECC matrices and ECC matrices without particles were investigated by SEM to achieve an in-depth understanding of the influence of microspheres on the assembly of collagen fibrils. The SEM micrograph of the cross-section of ECC matrices without spheres showed a dense aligned assembly of collagen fibers (Fig. 23 A). Surface analysis of particle-loaded ECC matrices demonstrated the microsphere exposure on the surface of the collagen sheet (Fig. 23 B).

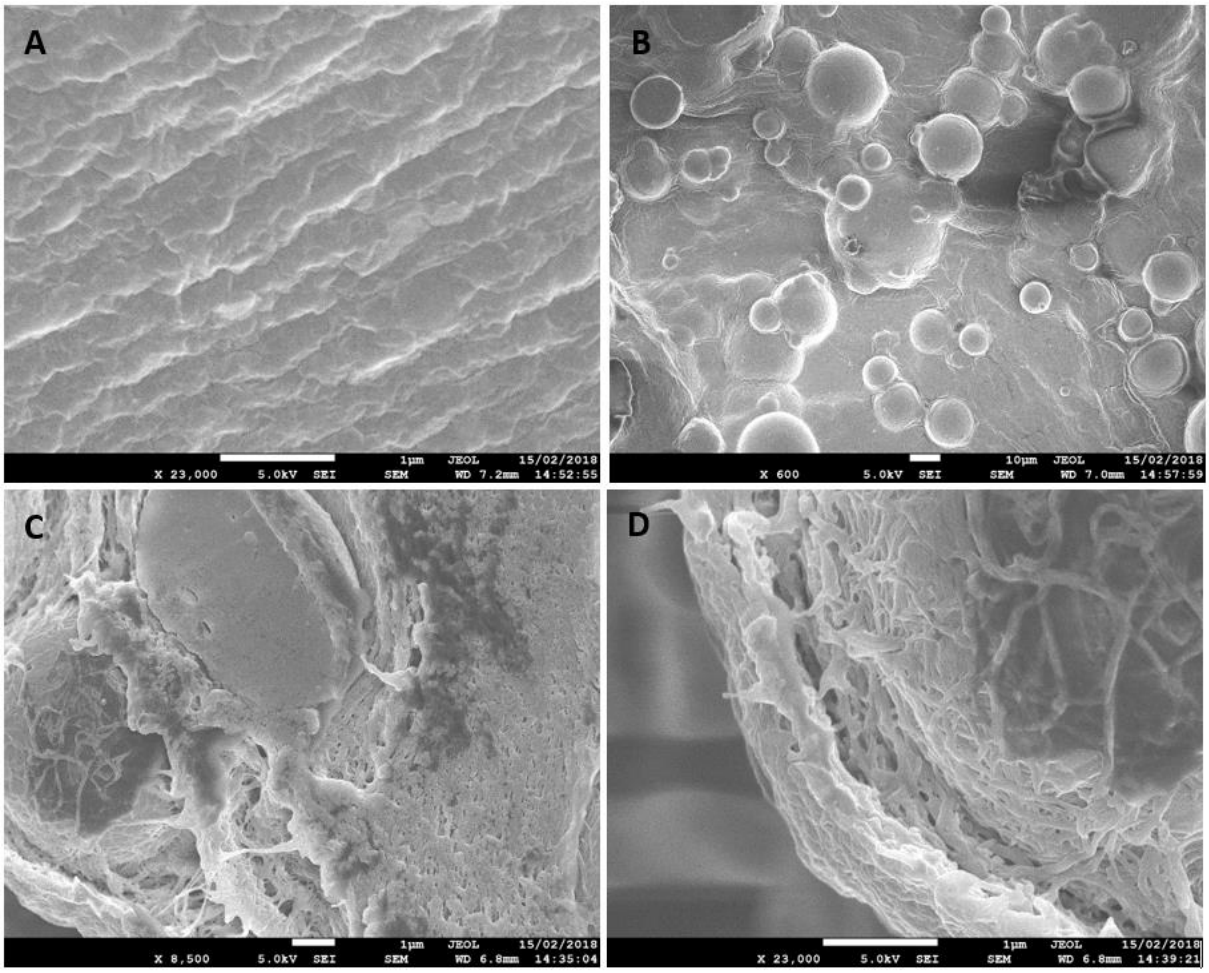

Figure 23. SEM micrographs of ECC matrices at x23000, x600, 8500 and 23000 magnifications. (A) cross-section of ECC matrices without microspheres, (B) surface of sphere-loaded ECC matrices, (C) cross-section of sphere-loaded ECC matrices and (D) high-resolution of the cross-section of sphere-loaded ECC matrices.

In contrast to the cross-section of ECC matrices without microspheres, cross-section of microsphere-incorporated ECC matrices revealed a more irregular microstructure (Fig. 23 C). Next to the microspheres, the density of the collagen fibres is significantly decreased compared to the collagen

assembly in which no spheres are present. Furthermore, Fig. 23 D demonstrates that the collagen molecules located on the surface of the microspheres show significant loss of orientation. Given that the strong mechanical properties of ECC matrices is based on the formation of dense and aligned collagen fibres, SEM-images provided evidence that the microsphere entrapment interrupts the collagen assembly and thus significantly decreases the mechanical stiffnesses of ECC matrices as demonstrated in chapter 3.4.

3.6 Drug-release from sphere-loaded ECC matrices

Adoption of drug-loaded ECC matrices for a controlled drug delivery system greatly relies on the release profile of the targeted drug from the collagen membrane. Depending on the medical application either short-time or sustained long-term release is required. When looking at the drugs of interest in this study, for anti-inflammatory DEX we aimed for 14 days drug release and for anti-convulsive PHT we focussed on sustained drug release for at least 3 months.

The first crucial step in this study was to quantify the microspheres which can be entrapped into the collagen membrane from the aqueous solution by the electrocompaction process. To analyze drug-loading efficiency of ECC matrices, samples were fabricated using 5 mg DEX-microspheres and a ratio of DEX- and PHT-microspheres (1:1) and extracted immediately after the electrocompaction process (Table 4).

Table 4. Drug-loading efficiency of microsphere-loaded ECC matrices

Samples	Drug-loading (µg/matrix)	Theoretical drug-loading (µg/matrix)	Drug-loading efficiency (%)
ECC matrices with DEX-microspheres (1.6 w/w)	11.6 ± 0.9	32.6 ± 1.2	35.5 ± 2.7
ECC matrices with DEX- and PHT-microspheres (1:1) (0.8 w/w)	8.1 ± 0.3 (DEX)	16.3 ± 0.6	49.9 ± 1.8
	6.5 ± 0.4 (PHT)	30.9 ± 0.8	21.0 ± 1.3

As illustrated in Table 4, electrocompaction provides the possibility to fabricate drug-loaded ECC matrices with variable drug-loading efficiency. DEX-loaded samples demonstrated a total drug-loading about 35 %. Whereas the dual-drug-loaded ECC matrices provided 49.9 % and 21.0 % drug-loading for

DEX and PHT, respectively. As can been appreciated from the above, DEX-microspheres seem to be more susceptible for the entrapment into ECC matrices compared to the PHT-loaded spheres. A possible explanation for these findings could be the size of the drug-loaded microspheres. As the mean-diameter of DEX-microspheres was suspected to be 2-fold higher than the diameter of PHT-microspheres, the higher surface area could facilitate the attachment of collagen fibers and thus could increase the particle-entrapment into the ECC membrane.

To assess the drug-release behavior of ECC matrices, an *in-vitro* release study of single- and dual drug-loaded samples were investigated in an aCSF (pH 7.4) solution at 37 °C for 12 and 14 days, respectively (Fig. 24).

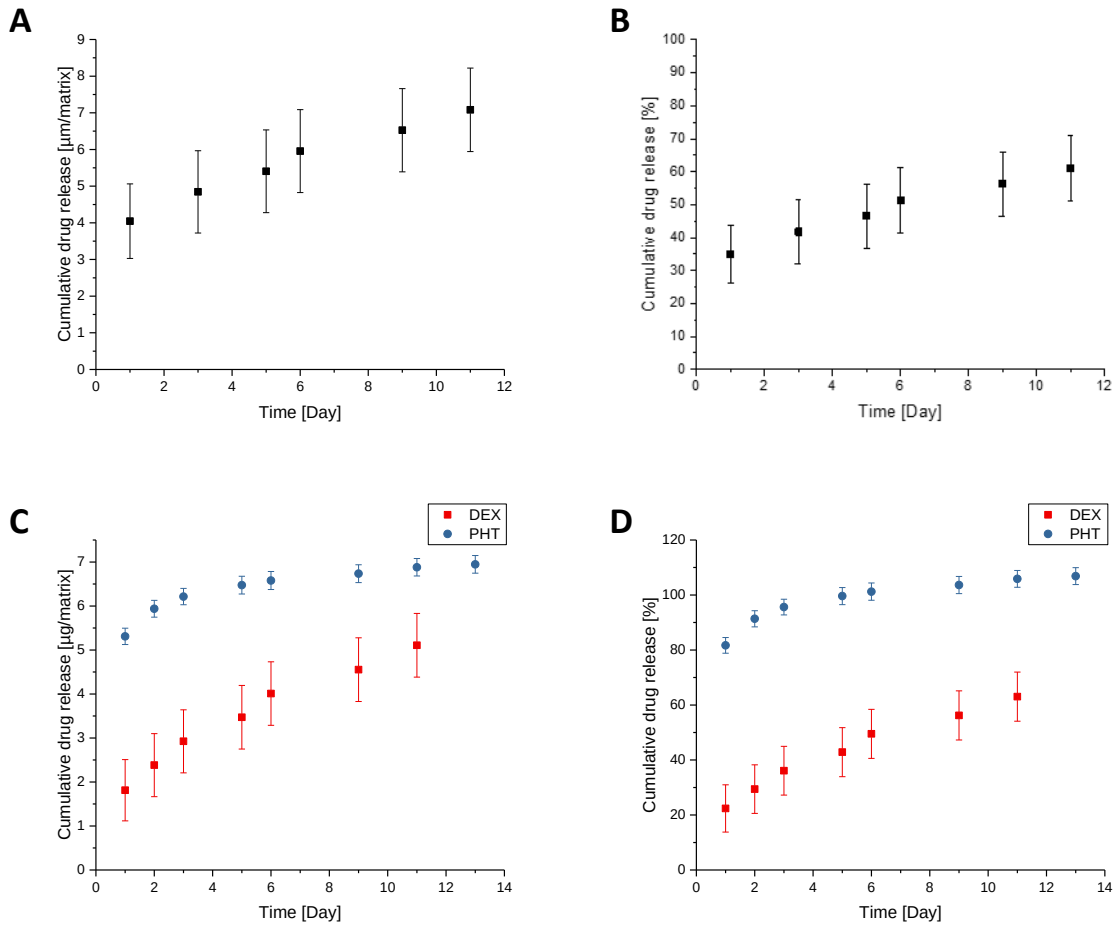

Figure 24. In-vitro release profile from single and dual drug-loaded ECC matrices (n=3) in aCSF (pH 7.4) at 37 °C for 12 and 14 days, respectively. (A) Quantitative single-release of DEX from ECC matrices. (B) Total amount of DEX released as a percentage of the total amount of drug encapsulated into ECC matrices. (C) Quantitative amount of PHT and DEX released from dual-drug loaded ECC matrices. (D) Total amount of PHT and DEX released as a percentage of the total amount of drug encapsulated into ECC matrices.

DEX-MP loaded ECC (Fig. 24 A and B) demonstrated a sustained release for 11 days following a biphasic release pattern. After a burst release of approximately 35% on the first day, DEX-MP loaded ECC showed a more linear release with about 550 ng released per day for the next 10 days reaching 63% of completion. These observations demonstrate a significant change in the release pattern compared to the single DEX-microsphere formulation, which has shown a triphasic release, reaching a steady state at day 8 (chapter 3.1.1). Hence, it appears that the incorporation of DEX-MP into ECC matrices can cause a more prolonged release of DEX. As shown in figure 24 C and D, DEX-release from DEX-MP/PHT-MP loaded ECC matrices is hallmarked by a reduced burst release of approximately 22% on day 1 compared to mono-DEX-MP loaded ECC matrices. However, the biphasic release pattern is similar to the mono-DEX-MP loaded ECC matrices, reaching around 60% of completion at day 11.

PHT-release from DEX-MP/PHT-MP loaded ECC matrices revealed a high burst release with approximately 82% drug-elution at day 1, followed by a decreased release rate for the next 8 days (Fig. 24 C and D). After 9 days of incubation, a plateau was reached without significant drug release. These observations reveal a dramatic change in the release pattern compared to the single PHT-microsphere formulation, which was hallmarked by a sustained PHT-release over 30 days and a slight burst release. Whereas for anti-inflammatory DEX, such an initial burst may be beneficial to ensure immediate relief after implantation of the device, for local release of anticonvulsants it is associated with several negative effects. On one hand, the release of an unnecessary large amount of anticonvulsants leads to a shortening of the implant's life, which is particularly critical given the risks of neurosurgical procedures. On the other hand, an initial burst release is difficult to control, and thus high concentrations of the drug might pose a toxicological risk to the patient [104]. Adjusting a zero-order controlled release of PHT is therefore essential for the clinical success of the device, as a consistent level of anticonvulsant must be present at the seizure focus to consistently inhibit abnormal electrical transmissions once they occur.

As has been demonstrated by Lee *et al*., hydrogel matrices with a sigmoidal drug distribution were able to achieve an almost zero-order sustained release pattern [105]. Taken this into consideration, it would be worthwhile to investigate a non-uniform distribution of anticonvulsant PHT within ECC matrices, which could be easily achieved by electrocompaction of multiple layers of collagen with heterogeneous particle-loading.

Summarizing these results, it appears that the electrochemical fabrication process might have a crucial influence on the release pattern depending on the investigated drug. Whereas, DEX-release from ECC matrices demonstrated slower release compared to the single microsphere formulation, PHT-release from ECC revealed shorter elution times and was hallmarked by a high burst release. To confirm these findings, the initial experiments require further study, for example, the influence of the electrical field

on the drug release. A good experiment is to load the microspheres in the electrical field, using the same condition as for electrocompaction, to analyze the influence of the voltage on the drug release profile.

4. Future Perspectives

Overall, the initial experiments performed in the last 10 months showed potential of electrocompacted collagen as an implantable device for local drug delivery. As may be evident from the above, currently the project is still in its infancy and must be followed up with more detailed characterization as well as process optimization.

a, Preparation of drug-loaded microspheres

As mentioned in section 3.1, all trials with the aim to encapsulate anti-convulsive LEV via ESE or ESD failed to provide PLGA microspheres with suitable drug-loading. However, the advantage of LEV e.g. the low dermatological hypersensitivity or the non-hepatoxicity, makes it worth to investigate further experiments on its encapsulation ability. Electrospraying is a novel powerful method for the encapsulation of hydrophilic drugs into polymer particles (Fig. 25). It is an electrohydrodynamic process, in which a liquid polymer solution is injected onto a collecting plate.

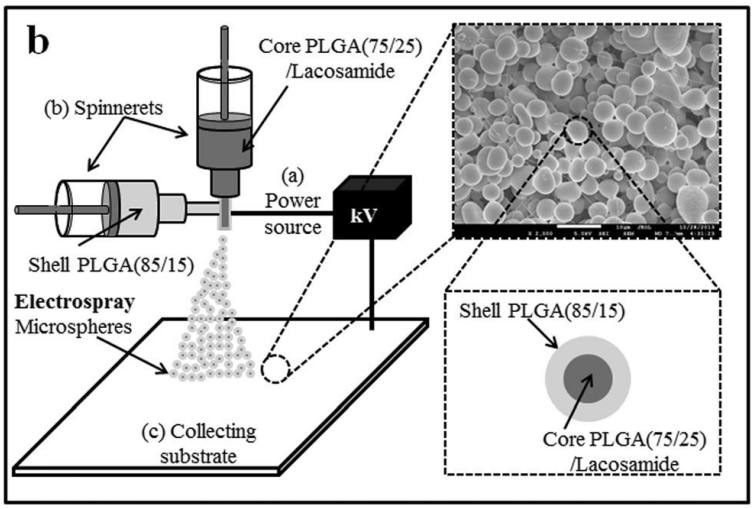

Figure 25. Schematic illustration of the electrospraying setup for fabrication of microspheres with core-shell morphology [106].

Due to the high voltage applied, the polymer solution gets stretched and forms particle droplets. Recently, Chen *et al.* demonstrated the encapsulation of hydrophilic Lacosamide into PLGA microspheres prepared by electrospraying which showed sustained drug-release over 2 weeks [106].

b, Optimization of drug-loaded ECC matrices

Given that the electrochemical fabrication process of drug-loaded ECC matrices caused a dramatic change of the drug-release kinetics compared to the single microsphere formulations, further experiments should focus on the minimization of the burst release. To assess a controlled long-term release, experiments need to be performed to obtain a deep-understanding of the influence of the applied voltage on the drug-release characteristics. Another approach to reduce drug diffusion could be a layer-by-layer electrocompaction of collagen sheets, as recently described by Younesi *et al.* (Fig. 26) [20]. Due to the addition of outer layers of compacted collagen without microspheres, the drug diffusion from the microsphere-loaded inner collagen layer could be slowed.

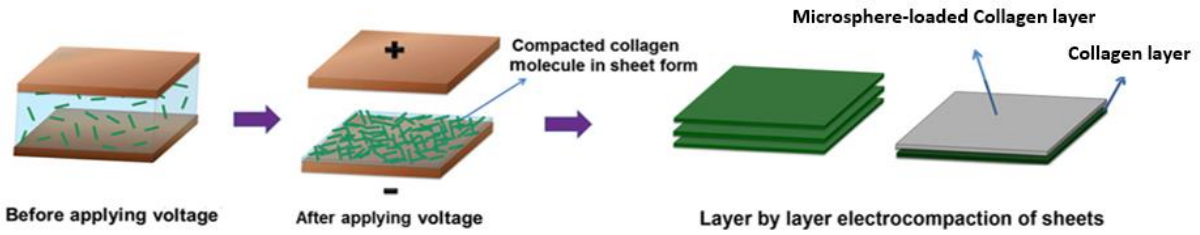

Figure 26. Layer-by-layer electrocompaction of collagen sheets (modified) [20].

c, In-vivo study

Given the nature of the drug-release experiments, in which the release profile was determined by a highly simplified *in-vitro* study, it is essential to take into account *in-vivo* studies. *In-vivo* experiments would give the opportunity to evaluate ECC matrices in terms of its biocompatibility. A rat tetanus toxin model of temporal lobe epilepsy could be investigated on the efficacy of drug-loaded ECC matrices to successfully suppress seizure activity.

5. Conclusion

In this research project, electrochemical compaction of collagen was evaluated as a potential drug delivery system for local therapy of refractory epilepsy. Anti-inflammatory DEX and anti-epileptic PHT were successfully encapsulated into PLGA microspheres using ESE and demonstrated sustained drug release in an *in-vitro* experiment. Initial experiments have demonstrated the ability of the electrocompaction process to incorporate drug-loaded microspheres into the ECC membranes. Tensile tests were performed to ensure an in-depth understanding of the influence of particle-entrapment into the ECC matrices in regards of their mechanical properties. The *in-vitro* release study of DEX-loaded ECC matrices demonstrated a more sustained release behaviour compared to the single microsphere formulation. The *in-vitro* release study of the dual drug-loaded ECC matrices revealed a dramatic change in the release behaviour of the anti-epileptic drug. PHT-release from ECC resulted in faster elution which was hallmarked by a high burst release. The study suggests that the electrochemical fabrication process of ECC matrices has a crucial influence on the release behaviour of drug-loaded PLGA microspheres. For the field to progress, it is essential to get an in-depth understanding about the parameters which cause the change in the release pattern of microsphere formulations. Beside this, future experiments need to consider *in-vivo* studies, to evaluate the biocompatibility and efficiency of drug-loaded ECC matrices.

6. References

1. Prockop, D.J. and A. Fertala, *The collagen fibril: the almost crystalline structure.* Journal of structural biology, 1998. **122**(1-2): p. 111-118.
2. Kucharz, E.J., *The collagens: biochemistry and pathophysiology*. 2012: Springer Science & Business Media.
3. Friess, W., *Collagen–biomaterial for drug delivery.* European Journal of Pharmaceutics and Biopharmaceutics, 1998. **45**(2): p. 113-136.
4. Nimni, M. and R. Harkness, *Molecular structures and functions of collagen.* Collagen, 1988. **1**: p. 1-77.
5. Printerest. 2017; Available from: https://www.pinterest.dk/pin/499125571175830231/.
6. Reiser, K., R. McCormick, and R. Rucker, *Enzymatic and nonenzymatic cross-linking of collagen and elastin.* The FASEB Journal, 1992. **6**(7): p. 2439-2449.
7. Lee, C.H., A. Singla, and Y. Lee, *Biomedical applications of collagen.* International journal of pharmaceutics, 2001. **221**(1-2): p. 1-22.
8. Reddy, M., et al., *A clinical study of a fibrinogen-based collagen fleece for dural repair in neurosurgery.* Acta neurochirurgica, 2002. **144**(3): p. 265-269.
9. Biom'up. 2017; Available from: http://www.biomup.com/en/cova-plus/cova-plus-abdo/3/.
10. Berjano, R., F.C. Vinas, and M. Dujovny, *A review of dural substitutes used in neurosurgery.* Critical Reviews in Neurosurgery, 1999. **9**(4): p. 217-222.
11. Kuschel, T.J., et al., *Prevention of postoperative pericardial adhesions with TachoSil.* The Annals of thoracic surgery, 2013. **95**(1): p. 183-188.
12. Narotam, P.K., et al., *Collagen matrix (DuraGen) in dural repair: analysis of a new modified technique.* Spine, 2004. **29**(24): p. 2861-2867.
13. Kato, Y.P., et al., *Mechanical properties of collagen fibres: a comparison of reconstituted and rat tail tendon fibres.* Biomaterials, 1989. **10**(1): p. 38-42.
14. Mosser, G., et al., *Dense tissue-like collagen matrices formed in cell-free conditions.* Matrix Biology, 2006. **25**(1): p. 3-13.
15. Matthews, J.A., et al., *Electrospinning of collagen nanofibers.* Biomacromolecules, 2002. **3**(2): p. 232-238.
16. Denis, F.A., et al., *Alignment and assembly of adsorbed collagen molecules induced by anisotropic chemical nanopatterns.* Small, 2005. **1**(10): p. 984-991.
17. Cheng, X., et al., *An electrochemical fabrication process for the assembly of anisotropically oriented collagen bundles.* Biomaterials, 2008. **29**(22): p. 3278-3288.
18. Younesi, M., *Heparinized collagen sutures for sustained delivery of PDGF-BB: Delivery profile and effects on tendon-derived cells In-Vitro.* Acta biomaterialia. **41**: p. 100-109.
19. Kishore, V., et al., *In vitro characterization of electrochemically compacted collagen matrices for corneal applications.* Biomedical Materials, 2016. **11**(5): p. 055008.
20. Younesi, M., et al., *Fabrication of compositionally and topographically complex robust tissue forms by 3D-electrochemical compaction of collagen.* Biofabrication, 2015. **7**(3): p. 035001.
21. Nguyen, T.-U., C.A. Bashur, and V. Kishore, *Impact of elastin incorporation into electrochemically aligned collagen fibers on mechanical properties and smooth muscle cell phenotype.* Biomedical Materials, 2016. **11**(2): p. 025008.
22. Islam, A., et al., *Computer aided biomanufacturing of mechanically robust pure collagen meshes with controlled macroporosity.* Biofabrication, 2015. **7**(3): p. 035005.
23. Schmidt, D., *Evidence-based review on the natural history of the epilepsies.* Current opinion in neurology. **25**(2): p. 159-163.
24. Goldberg, E.M., *Mechanisms of epileptogenesis: a convergence on neural circuit dysfunction.* Nature reviews. Neuroscience. **14**(5): p. 337-349.
25. Baum, L., *Antiepileptic drug delivery.* Advanced drug delivery reviews. **64**(10): p. 885-886.
26. Fisher, R.S., *ILAE official report: a practical clinical definition of epilepsy.* Epilepsia (Copenhagen). **55**(4): p. 475-482.

27. Berg, A.T., *Revised terminology and concepts for organization of seizures and epilepsies: Report of the ILAE Commission on Classification and Terminology, 2005-2009.* Epilepsia (Copenhagen). **51**(4): p. 676-685.
28. Fisher, R.S. and J. Ho, *Potential new methods for antiepileptic drug delivery.* CNS drugs, 2002. **16**(9): p. 579-593.
29. Scheffer, I.E., *ILAE classification of the epilepsies: Position paper of the ILAE Commission for Classification and Terminology.* Epilepsia (Copenhagen). **58**(4): p. 512-521.
30. Ure, J.A., *Update on the pathophysiology of the epilepsies.* Journal of the neurological sciences. **177**(1): p. 1-17.
31. Davies, J.A., *Mechanisms of action of antiepileptic drugs.* Seizure (London, England). **4**(4): p. 267-271.
32. Catterall, W.A., *Structure and function of voltage-sensitive ion channels.* Science (New York, N.Y.). **242**(4875): p. 50.
33. Llinás, R.R., *The intrinsic electrophysiological properties of mammalian neurons: insights into central nervous system function.* Science, 1988. **242**(4886): p. 1654-1664.
34. Kandel, E.R., et al., *Principles of neural science*. Vol. 4. 2000: McGraw-hill New York.
35. Context, U. 2017; Available from: http://understandingcontext.com/2014/01/ei-electric-potential-curve/.
36. Rojas, R., *Neural networks: a systematic introduction*. 2013: Springer Science & Business Media.
37. Rho, J.M., *The Pharmacologic Basis of Antiepileptic Drug Action.* Epilepsia (Copenhagen). **40**(11): p. 1471-1483.
38. Temkin, N.R., *Preventing and treating posttraumatic seizures: the human experience.* Epilepsia, 2009. **50**(s2): p. 10-13.
39. Schmidt, D., *Is antiepileptogenesis a realistic goal in clinical trials? Concerns and new horizons.* Epileptic disorders, 2012. **14**(2): p. 105-113.
40. Meldrum, B.S., *Update on the mechanism of action of antiepileptic drugs.* Epilepsia, 1996. **37**(s6).
41. new?, W.i. 2017; Available from: http://www.mjmsr.net/viewimage.asp?img=MullerJMedSciRes_2014_5_2_195_135796_f2.jpg.
42. Mantegazza, *Voltage-gated sodium channels as therapeutic targets in epilepsy and other neurological disorders.* Lancet neurology, 2010. **9**(4): p. 413.
43. Stefani, *Voltage-Activated Calcium Channels: Targets of Antiepileptic Drug Therapy?* Epilepsia (Copenhagen), 1997. **38**(9): p. 959.
44. Kwan, P., *The mechanisms of action of commonly used antiepileptic drugs.* Pharmacology & therapeutics (Oxford). **90**(1): p. 21-34.
45. Pongs, *Voltage-gated potassium channels: from hyperexcitability to excitement.* FEBS letters, 1999. **452**(1-2): p. 31.
46. Porter, R.J. and M.A. Rogawski, *New antiepileptic drugs: from serendipity to rational discovery.* Epilepsia, 1992. **33**(s1).
47. Rundfeldt, C. and R. Netzer, *The novel anticonvulsant retigabine activates M-currents in Chinese hamster ovary-cells tranfected with human KCNQ2/3 subunits.* Neuroscience letters, 2000. **282**(1): p. 73-76.
48. ouml and W. scher, *New visions in the pharmacology of anticonvulsion.* European journal of pharmacology. **342**(1): p. 1-13.
49. Olsen, R.W., *GABA and Epileptogenesis.* Epilepsia (Copenhagen). **38**(4): p. 399-407.
50. Rabow, L.E., S.J. Russek, and D.H. Farb, *From ion currents to genomic analysis: recent advances in GABAA receptor research.* Synapse, 1995. **21**(3): p. 189-274.
51. Granger, P., et al., *Modulation of the gamma-aminobutyric acid type A receptor by the antiepileptic drugs carbamazepine and phenytoin.* Molecular pharmacology, 1995. **47**(6): p. 1189-1196.

52. Shank, R.P., et al., *Topiramate: preclinical evaluation of a structurally novel anticonvulsant.* Epilepsia, 1994. **35**(2): p. 450-460.
53. Leach, J.P., *Effects of tiagabine and vigabatrin on GABA uptake into primary cultures of rat cortical astrocytes.* Seizure (London, England). **5**(3): p. 229-234.
54. Sills, G.J., *Vigabatrin and tiagabine are pharmacologically different drugs. A pre-clinical study.* Seizure (London, England). **8**(7): p. 404-411.
55. Meldrum, B.S., *Glutamate as a neurotransmitter in the brain: review of physiology and pathology.* The Journal of nutrition. **130**(4s suppl): p. 1007S.
56. Trist, D., *Excitatory amino acid agonists and antagonists: pharmacology and therapeutic applications.* Pharmaceutica Acta Helvetiae, 2000. **74**(2): p. 221-229.
57. Macdonald, R.L. and K.M. Kelly, *Antiepileptic drug mechanisms of action.* Epilepsia, 1995. **36**(s2).
58. Franco, V., *Novel treatment options for epilepsy: Focus on perampanel.* Pharmacological research. **70**(1): p. 35-40.
59. Pardridge, W.M., *Drug Delivery to the Brain.* Journal of cerebral blood flow and metabolism. **17**(7): p. 713-731.
60. Cook, M.J., et al., *Prediction of seizure likelihood with a long-term, implanted seizure advisory system in patients with drug-resistant epilepsy: a first-in-man study.* The Lancet Neurology, 2013. **12**(6): p. 563-571.
61. Kwan, P. and M.J. Brodie, *Early identification of refractory epilepsy.* New England Journal of Medicine, 2000. **342**(5): p. 314-319.
62. Oby, E. and D. Janigro, *The blood–brain barrier and epilepsy.* Epilepsia, 2006. **47**(11): p. 1761-1774.
63. Buxton, R.B. and L.R. Frank, *A model for the coupling between cerebral blood flow and oxygen metabolism during neural stimulation.* Journal of Cerebral Blood Flow & Metabolism, 1997. **17**(1): p. 64-72.
64. Abbott, N.J., L. Rönnbäck, and E. Hansson, *Astrocyte-endothelial interactions at the blood-brain barrier.* Nature reviews. Neuroscience, 2006. **7**(1): p. 41.
65. Dombrowski, S.M., et al., *Overexpression of multiple drug resistance genes in endothelial cells from patients with refractory epilepsy.* Epilepsia, 2001. **42**(12): p. 1501-1506.
66. Schmidt, D. and W. Löscher, *Drug resistance in epilepsy: putative neurobiologic and clinical mechanisms.* Epilepsia, 2005. **46**(6): p. 858-877.
67. Halliday, A.J., et al., *Novel methods of antiepileptic drug delivery—polymer-based implants.* Advanced drug delivery reviews, 2012. **64**(10): p. 953-964.
68. Bennewitz, M.F. and W.M. Saltzman, *Nanotechnology for delivery of drugs to the brain for epilepsy.* Neurotherapeutics, 2009. **6**(2): p. 323-336.
69. Rautio, J., et al., *Prodrugs: design and clinical applications.* Nature reviews. Drug discovery, 2008. **7**(3): p. 255.
70. Summers, M.A., J.L. Moore, and J.W. McAuley, *Use of verapamil as a potential P-glycoprotein inhibitor in a patient with refractory epilepsy.* Annals of Pharmacotherapy, 2004. **38**(10): p. 1631-1634.
71. Marchi, N., et al., *Seizure-Promoting Effect of Blood–Brain Barrier Disruption.* Epilepsia, 2007. **48**(4): p. 732-742.
72. Kokaia, M., et al., *Seizure suppression in kindling epilepsy by intracerebral implants of GABA- but not by noradrenaline-releasing polymer matrices.* Experimental brain research, 1994. **79**(2): p. 385-394.
73. Serralta, A., et al., *Effect of intracerebroventricular continuous infusion of valproic acid versus single ip and icv injections in the amygdala kindling epilepsy model.* Epilepsy research, 2006. **70**(1): p. 15-26.
74. Oommen, J., A.C. Kraus, and R.S. Fisher, *Intraventricular administration of gabapentin in the rat increases flurothyl seizure threshold.* Neuroscience letters, 2007. **417**(3): p. 308-311.

75. Tao, A., L. Tao, and C. Nicholson, *Cell cavities increase tortuosity in brain extracellular space.* Journal of Theoretical Biology, 2005. **234**(4): p. 525-536.
76. Pardridge, W.M., *Transport of small molecules through the blood-brain barrier: biology and methodology.* Advanced drug delivery reviews, 1995. **15**(1-3): p. 5-36.
77. Halliday, A. and M. Cook, *Polymer-based drug delivery devices for neurological disorders.* CNS & Neurological Disorders-Drug Targets (Formerly Current Drug Targets-CNS & Neurological Disorders), 2009. **8**(3): p. 205-221.
78. Lloyd, A.W., *Interfacial bioengineering to enhance surface biocompatibility.* Medical device technology, 2001. **13**(1): p. 18-21.
79. Szybala, C., et al., *Antiepileptic effects of silk-polymer based adenosine release in kindled rats.* Experimental neurology, 2009. **219**(1): p. 126-135.
80. Wilz, A., et al., *Silk polymer-based adenosine release: therapeutic potential for epilepsy.* Biomaterials, 2008. **29**(26): p. 3609-3616.
81. Arifin, D.Y., L.Y. Lee, and C.-H. Wang, *Mathematical modeling and simulation of drug release from microspheres: implications to drug delivery systems.* Advanced drug delivery reviews, 2006. **58**(12): p. 1274-1325.
82. Jyothi, N.V.N., et al., *Microencapsulation techniques, factors influencing encapsulation efficiency.* Journal of microencapsulation, 2010. **27**(3): p. 187-197.
83. Ghosh, S.K., *1 Functional Coatings and Microencapsulation: A General Perspective.* 2006.
84. Iqbal, M., et al., *Double emulsion solvent evaporation techniques used for drug encapsulation.* International journal of pharmaceutics, 2015. **496**(2): p. 173-190.
85. Gabor, F., *Ketoprofen-poly (D, L-lactic-co-glycolic acid) microspheres: influence of manufacturing parameters and type of polymer on the release characteristics.* Journal of microencapsulation, 1999. **16**(1): p. 1-12.
86. Meng, F.T., et al., *W/O/W double emulsion technique using ethyl acetate as organic solvent: effects of its diffusion rate on the characteristics of microparticles.* Journal of controlled release, 2003. **91**(3): p. 407-416.
87. Rosca, I.D., F. Watari, and M. Uo, *Microparticle formation and its mechanism in single and double emulsion solvent evaporation.* Journal of Controlled Release, 2004. **99**(2): p. 271-280.
88. Yeo, Y. and K. Park, *Control of encapsulation efficiency and initial burst in polymeric microparticle systems.* Archives of pharmacal research, 2004. **27**(1): p. 1.
89. Bodmeier, R. and J. McGinity, *Solvent selection in the preparation of poly (DL-lactide) microspheres prepared by the solvent evaporation method.* International journal of pharmaceutics, 1988. **43**(1-2): p. 179-186.
90. Mehta, R.C., B. Thanoo, and P.P. Deluca, *Peptide containing microspheres from low molecular weight and hydrophilic poly (d, l-lactide-co-glycolide).* Journal of Controlled Release, 1996. **41**(3): p. 249-257.
91. Rafati, H., et al., *Protein-loaded poly (DL-lactide-co-glycolide) microparticles for oral administration: formulation, structural and release characteristics.* Journal of Controlled Release, 1997. **43**(1): p. 89-102.
92. Li, X., et al., *Investigation on process parameters involved in preparation of poly-DL-lactide-poly (ethylene glycol) microspheres containing Leptospira Interrogans antigens.* International journal of pharmaceutics, 1999. **178**(2): p. 245-255.
93. Wu, J., et al., *Microspheres made by w/o/o emulsion method with reduced initial burst for long-term delivery of endostar, a novel recombinant human endostatin.* Journal of pharmaceutical sciences, 2009. **98**(6): p. 2051-2058.
94. Jiang, J.L., et al., *Injectable phenytoin loaded polymeric microspheres for the control of temporal lobe epilepsy in rats.* Restorative neurology and neuroscience, 2015. **33**(6): p. 823-834.
95. Berchane, N., et al., *Effect of mean diameter and polydispersity of PLG microspheres on drug release: Experiment and theory.* International journal of pharmaceutics, 2007. **337**(1-2): p. 118-126.

96. Viry, L., et al., *Emulsion-coaxial electrospinning: designing novel architectures for sustained release of highly soluble low molecular weight drugs.* Journal of Materials Chemistry, 2012. **22**(22): p. 11347-11353.
97. Sah, H., *Microencapsulation techniques using ethyl acetate as a dispersed solvent: effects of its extraction rate on the characteristics of PLGA microspheres.* Journal of Controlled Release, 1997. **47**(3): p. 233-245.
98. Viswanathan, N.B., et al., *Preparation of non-porous microspheres with high entrapment efficiency of proteins by a (water-in-oil)-in-oil emulsion technique.* Journal of controlled release, 1999. **58**(1): p. 9-20.
99. Balaiah, A., et al., *Formulation Development and in-vitro Characterization of oral Levetiracetam Microspheres.* Int. Res J Pharm App Sci, 2012. **2**: p. 13-21.
100. Mithani, S.D., et al., *Estimation of the increase in solubility of drugs as a function of bile salt concentration.* Pharmaceutical research, 1996. **13**(1): p. 163-167.
101. Jain, R.A., et al., *Controlled release of drugs from injectable in situ formed biodegradable PLGA microspheres: effect of various formulation variables.* European journal of pharmaceutics and biopharmaceutics, 2000. **50**(2): p. 257-262.
102. Park, T.G., *Degradation of poly (lactic-co-glycolic acid) microspheres: effect of copolymer composition.* Biomaterials, 1995. **16**(15): p. 1123-1130.
103. Lopez-Garcia, M., D. Beebe, and W. Crone, *Young's modulus of collagen at slow displacement rates.* Bio-medical materials and engineering, 2010. **20**(6): p. 361-369.
104. Huang, X. and C.S. Brazel, *On the importance and mechanisms of burst release in matrix-controlled drug delivery systems.* Journal of controlled release, 2001. **73**(2-3): p. 121-136.
105. Lee, P.I., *Effect of non-uniform initial drug concentration distribution on the kinetics of drug release from glassy hydrogel matrices.* Polymer, 1984. **25**(7): p. 973-978.
106. Chen, Y., et al., *A simple and versatile method for microencapsulation of anti-epileptic drugs for focal therapy of epilepsy.* Journal of Materials Chemistry B, 2015. **3**(36): p. 7255-7261.

Poster: 9th World Congress of Biomimetics, Artificial Muscles and Nano-Biotechnology

Dual Drug-eluting Collagen Matrix for Epilepsy Treatment

Marius Berthel[1,2], Xiao Liu[1], Zhilian Yue[1] and Gordon G. Wallace[1]

[1] ARC Centre of Excellence for Electromaterials Science, AIIM Facility, Innovation Campus, University of Wollongong, Wollongong, New South Wales 2522, Australia

[2] Department of Functional Materials in Medicine and Dentistry, University of Würzburg, Würzburg, Germany

mb141@uowmail.edu.au

Refractory Epilepsy

Epilepsy is the most prevalent chronic brain disease affecting approximately 1% of the worldwide population. It is characterised by recurrent and unpredictable seizures, which can cause loss of consciousness, falls and injury, psychosocial disability, and even mortality [1,2]. First approach for Epilepsy treatment is an oral application of anti-convulsive drugs (AEDs), but only leads to a satisfactory control up to 70% of patients while the rest of patients are unable to become sufficient seizure alleviation [3].

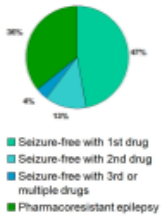

Figure 1. Pharmacoresistant in Epilepsy [3].

Due to the drug resistance, an increasing concentration of the antiepileptic drug is formed in the circulation instead of the brain as the desired target. The high level of AEDs in circulation leads to intolerable systemic side effects which decreases massively patients' wellbeing.

The Aim

The goal of our project is the development of a biodegradable collagen-based brain implant with sustained drug release properties of anti-Inflammatory Dexamethasone and anti-convulsive Levetiracetam to provide a novel medical device for the treatment of refractory Epilepsy.

Materials and Methods

Application of an electrical field (5V, 20 min) triggers the electrolysis of water which induces a pH gradient between the two electrodes. The amphoteric nature of collagen molecules leads to a negative net charge next to the cathode and contrary to a positive net charge next to the anode. Repulsion from the same charged electrodes towards the isoelectric point triggers a highly dense compaction of collagen molecules [4] .

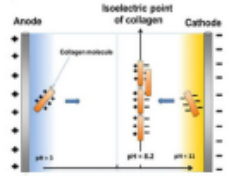

Figure 2. Principle of electrochemical process for preparing collagen sheets [5].

Our project investigates the loading efficiency of these methode to incorporate drug-loaded microparticles into compacted collagen matrices. For this aim microparticles were mixed to the collagen solution before applying an electric field.

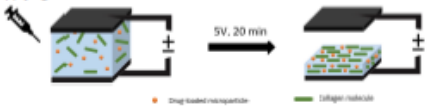

Figure 3. Process of microparticle incorporation into collagen matrices.

Results & Discussion

The presents of microparticles in the electrochemical fabrication process does not influence the compaction capability of collagen molecules. SEM-Images of fabricated collagen matrices could demonstrate a high microparticle entrapment and a 3-dimensional arrangement into the collagen films.

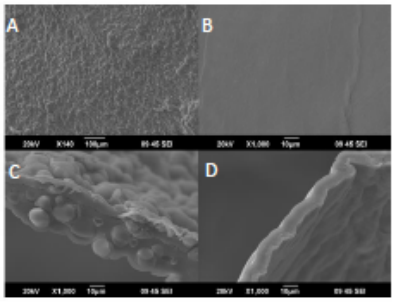

Figure 4. SEM analysis of the microscopic morphology of (A) microparticle-loaded collagen matrix, (B) compacted collagen without particles, (C) cross-section of microparticle-loaded collagen matrix and (D) cross-section of unloaded collagen sheet.

Conclusion

The present results indicate a great potential of electrochemical compacted collagen matrices as a novel drug delivery system with high microparticle entrapment. Increased mechanical stiffness of the collagen device compared to uncompacted collagen highly expands its application possibilities as a biomaterial in clinical use.

Future Work

Next steps in this project aims to characterize the drug release properties *in vitro* from the microparticle loaded collagen matrices. Adjustment of the desired release profile through optimizing of structure geometry will be performed. Finally the anti-convulsive efficacy of fabricated collagen sheets will be tested *in vivo* to evaluate its potential in clinical use.

Acknowledgement

The authors wish to acknowledge funding from the Australian Research Council (ARC) Centre of Excellence Scheme (CE140100012), the use of facilities at the University of Wollongong Electron Microscopy Centre, support of the Australian National Fabrication Facility (ANFF) – Materials Node. Funding from the Australian Government through the International Education and Training program in relation to project BIOFABrication for Future Manufacturing and the EU ICI ECP International joint program biofabrication mobility grant are gratefully acknowledged.

References

1. Goldberg, E.M., Mechanisms of epileptogenesis: a convergence on neural circuit dysfunction. Nature reviews. Neuroscience. 14(5): p. 337-349.
2. Schmidt, D., Evidence-based review on the natural history of the epilepsies. Current opinion in neurology. 25(2): p. 159-163.
3. Kwan, P., Early Identification of Refractory Epilepsy. The New England journal of medicine. 342(5): p. 314-319.
4. Kishore, V., characterization of electrochemically compacted collagen matrices for corneal applications. Biomedical materials (Bristol). 11(5): p. 055006.
5. Youssef, M., Heparinized collagen sutures for sustained delivery of PDGF-BB: Delivery profile and effects on tendon-derived cells in vitro. Acta biomaterialia. 41: p. 100-109.

ARC Centre of Excellence for Electromaterials Science

UNIVERSITY OF WOLLONGONG AUSTRALIA

Poster: International Conference on Nanoscience and Nanotechnology 2017

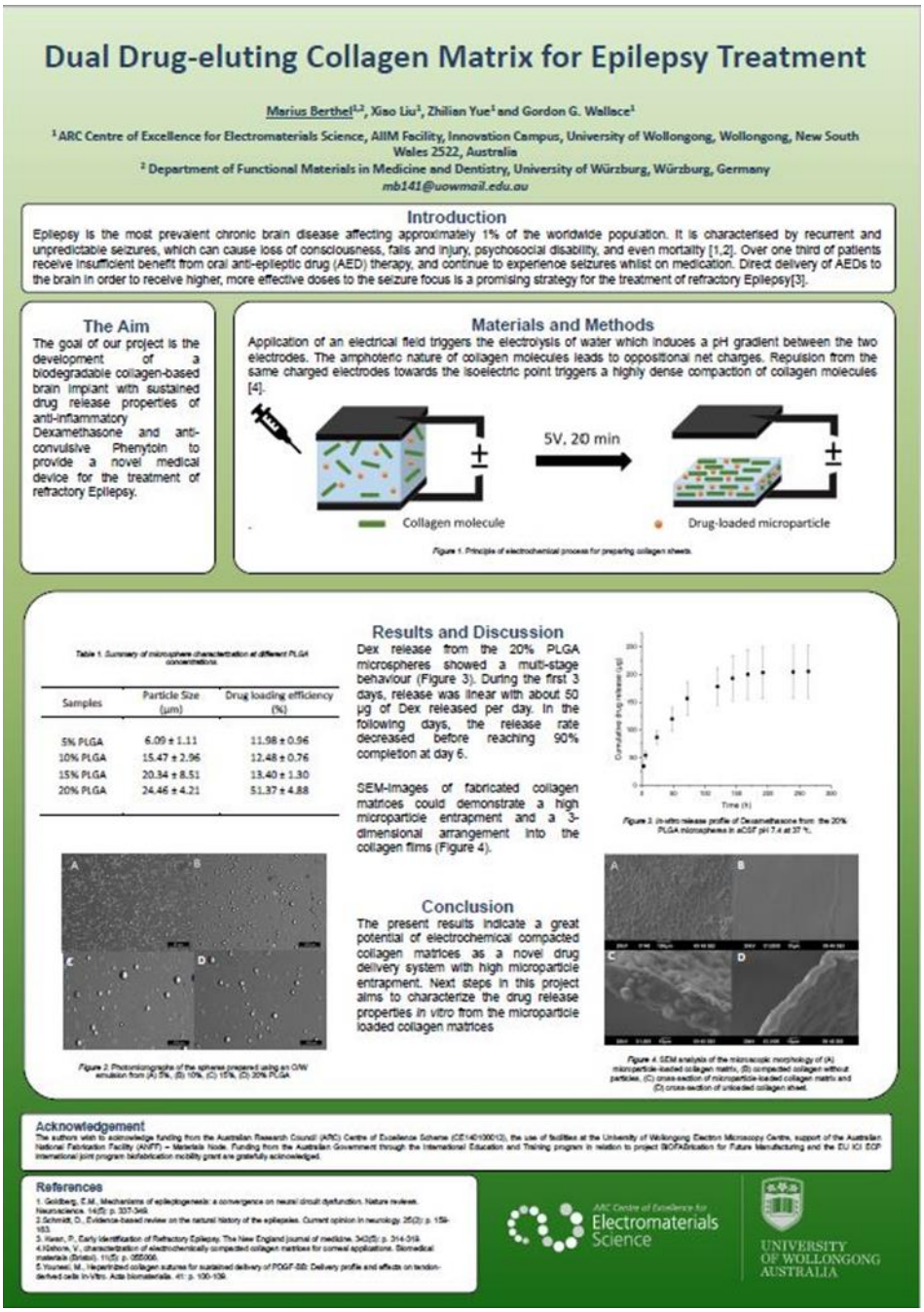

Dual Drug-eluting Collagen Matrix for Epilepsy Treatment

Marius Berthel[1,2], Xiao Liu[1], Zhilian Yue[1] and Gordon G. Wallace[1]

[1] ARC Centre of Excellence for Electromaterials Science, AIIM Facility, Innovation Campus, University of Wollongong, Wollongong, New South Wales 2522, Australia

[2] Department of Functional Materials in Medicine and Dentistry, University of Würzburg, Würzburg, Germany

mb141@uowmail.edu.au

Introduction

Epilepsy is the most prevalent chronic brain disease affecting approximately 1% of the worldwide population. It is characterised by recurrent and unpredictable seizures, which can cause loss of consciousness, falls and injury, psychosocial disability, and even mortality [1,2]. Over one third of patients receive insufficient benefit from oral anti-epileptic drug (AED) therapy, and continue to experience seizures whilst on medication. Direct delivery of AEDs to the brain in order to receive higher, more effective doses to the seizure focus is a promising strategy for the treatment of refractory Epilepsy[3].

The Aim

The goal of our project is the development of a biodegradable collagen-based brain implant with sustained drug release properties of anti-inflammatory Dexamethasone and anti-convulsive Phenytoin to provide a novel medical device for the treatment of refractory Epilepsy.

Materials and Methods

Application of an electrical field triggers the electrolysis of water which induces a pH gradient between the two electrodes. The amphoteric nature of collagen molecules leads to oppositional net charges. Repulsion from the same charged electrodes towards the isoelectric point triggers a highly dense compaction of collagen molecules [4].

Figure 1. Principle of electrochemical process for preparing collagen sheets.

Table 1. Summary of microsphere characterization at different PLGA concentrations.

Samples	Particle Size (µm)	Drug loading efficiency (%)
5% PLGA	6.09 ± 1.11	11.98 ± 0.96
10% PLGA	15.47 ± 2.96	12.48 ± 0.76
15% PLGA	20.34 ± 8.51	13.40 ± 1.30
20% PLGA	24.46 ± 4.21	51.37 ± 4.88

Figure 2. Photomicrographs of the spheres prepared using an O/W emulsion from (A) 5%, (B) 10%, (C) 15%, (D) 20% PLGA

Results and Discussion

Dex release from the 20% PLGA microspheres showed a multi-stage behaviour (Figure 3). During the first 3 days, release was linear with about 50 µg of Dex released per day. In the following days, the release rate decreased before reaching 90% completion at day 6.

SEM-images of fabricated collagen matrices could demonstrate a high microparticle entrapment and a 3-dimensional arrangement into the collagen films (Figure 4).

Figure 3. In-vitro release profile of Dexamethasone from the 20% PLGA microspheres in aCSF pH 7.4 at 37 °c.

Figure 4. SEM analysis of the microscopic morphology of (A) microparticle-loaded collagen matrix, (B) compacted collagen without particles, (C) cross-section of microparticle-loaded collagen matrix and (D) cross-section of unloaded collagen sheet.

Conclusion

The present results indicate a great potential of electrochemical compacted collagen matrices as a novel drug delivery system with high microparticle entrapment. Next steps in this project aims to characterize the drug release properties *in vitro* from the microparticle loaded collagen matrices

Acknowledgement

The authors wish to acknowledge funding from the Australian Research Council (ARC) Centre of Excellence Scheme (CE140100012), the use of facilities at the University of Wollongong Electron Microscopy Centre, support of the Australian National Fabrication Facility (ANFF) – Materials Node. Funding from the Australian Government through the International Education and Training program in relation to project BIOFABrication for Future Manufacturing and the EU ICI ECP international joint program biofabrication mobility grant are gratefully acknowledged.

References

1. Goldberg, E.M., Mechanisms of epileptogenesis: a convergence on neural circuit dysfunction. Nature reviews. Neuroscience. 14(5): p. 337-349.
2. Schmidt, D., Evidence-based review on the natural history of the epilepsies. Current opinion in neurology. 25(2): p. 159-163.
3. Kwan, P., Early identification of Refractory Epilepsy. The New England journal of medicine. 342(5): p. 314-319.
4. Kishore, V., characterization of electrochemically compacted collagen matrices for corneal applications. Biomedical materials (Bristol). 11(5): p. 055006.
5. Younesi, M., Hexamthiol collagen sutures for sustained delivery of PDGF-BB: Delivery profile and effects on tendon-derived cells in vitro. Acta biomaterialia. 41: p. 100-109.

ARC Centre of Excellence for Electromaterials Science

UNIVERSITY OF WOLLONGONG AUSTRALIA

Review Article

Expert Opinion on Drug Delivery

ISSN: 1742-5247 (Print) 1744-7593 (Online) Journal homepage: http://www.tandfonline.com/loi/iedd20

Advanced fabrication approaches to controlled delivery systems for epilepsy treatment

Gilles Sebastiaan van Tienderen, Marius Berthel, Zhilian Yue, Mark Cook, Xiao Liu, Stephen Beirne & Gordon G. Wallace

To cite this article: Gilles Sebastiaan van Tienderen, Marius Berthel, Zhilian Yue, Mark Cook, Xiao Liu, Stephen Beirne & Gordon G. Wallace (2018): Advanced fabrication approaches to controlled delivery systems for epilepsy treatment, Expert Opinion on Drug Delivery, DOI: 10.1080/17425247.2018.1517745

To link to this article: https://doi.org/10.1080/17425247.2018.1517745

ABSTRACT

Introduction: Epilepsy is a chronic brain disease characterized by unprovoked seizures, which can have severe consequences including loss of awareness and death. Currently, 30% of epileptic patients do not receive adequate seizure alleviation from oral routes of medication. Over the last decade, local drug delivery to the focal area of the brain where the seizure originates has emerged as a potential alternative and may be achieved through the fabrication of drug-loaded polymeric implants for controlled on-site delivery.

Areas covered: This review presents an overview of the latest advanced fabrication techniques for controlled drug delivery systems for refractory epilepsy treatment. Recent advances in the different techniques are highlighted and the limitations of the respective techniques are discussed.

Expert opinion: Advances in biofabrication technologies are expected to enable a new paradigm of local drug delivery systems through offering high versatility in controlling drug release profiles, personalized customization and multi-drug incorporation. Tackling some of the current issues with advanced fabrication methods, including adhering to GMP-standards and industrial scale-up, together with innovative solutions for complex designs will see to the maturation of these techniques and result in increased clinical research into implant-based epilepsy treatment.

Abbreviations: GMP: Good manufacturing process; DDS(s): Drug delivery system(s); 3D: Three-dimensional; AEDs: Anti-epileptic drugs; BBB: Blood brain barrier; PLA: Polylactic acid; PLGA: Poly(lactic-co-glycolic acid); PCL: poly(ε-caprolactone); ESE: Emulsification solvent evaporation; O/W: Oil-in-water; W/O/W: Water-in-oil-in-water; DZP: Diazepam; PHT: Phenytoin; PHBV: Poly(hydroxybutyrate-hydroxyvalerate); PEG: Polyethylene glycol; SWD: Spike-and-wave discharges; CAD: Computer aided design; FDM: Fused deposition modeling; ABS: Acrylonitrile butadiene styren; eEVA: Ethylene-vinyl acetate; GelMA: Gelatin methacrylate; PVA: Poly-vinyl alcohol; PDMS: Polydimethylsiloxane; SLA: Stereolithography; SLS: Selective laser sintering.

ARTICLE HISTORY
Received 23 April 2018
Accepted 24 August 2018

KEYWORDS
Advanced fabrication; controlled drug delivery systems; epilepsy; implant drug delivery; three-dimensional printing

Annex: Master thesis at the University of Wuerzburg

Julius-Maximilians-Universität Würzburg

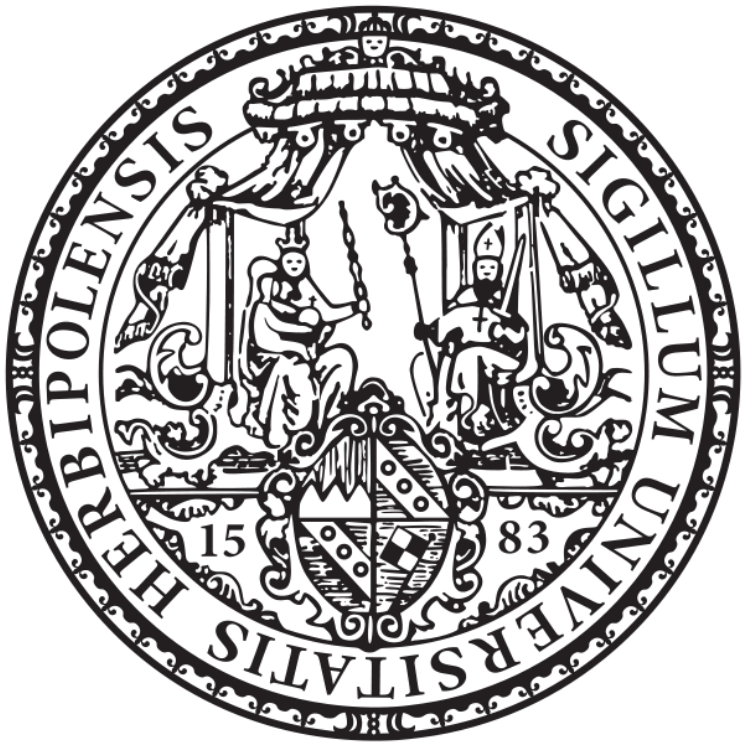

Combining melt electrowriting and electrospinning

Master's thesis

Faculty of Chemistry and Pharmacy

Department of Functional Materials in Medicine and Dentistry

Subject: Biofabrication

Marius Berthel

Würzburg, 25.09.2018

Supervisor: Prof. Paul D. Dalton

I, Marius Berthel, declare that this thesis is wholly my own work unless otherwise referenced or acknowledged. This document has not been submitted for any qualifications at any other academic institution.

_____

Marius Berthel

German Abstract – Zusammenfassung

Mundschleimhautdefekte mit freiliegendem Kieferknochen im Rahmen von Osteonekrosen, welche oftmals durch Langzeittherapien mit Bisphosphonaten hervorgerufen werden, erweisen sich als ernstzunehmendes Problem im Bereich der Mund-, Kiefer- und Gesichtschirurgie. Bei fortgeschrittener Nekrose ist eine Behandlung mit antibakteriellen Wirkstoffen oftmals nicht zielführend und eine Teilresektion des betroffenen Knochens ist notwendig. Um die mechanische Integrität des betroffenen Knochens zu gewährleisten, kommen Knochentransplantate zum Einsatz, welche jedoch oftmals ein unzureichendes Ausheilen der Wunde aufzeigen. Durch die Verwendung von Membranen, die das Implantat vor einer bakteriellen Infektion schützen und die Regeneration des Wundgewebes begünstigen könnte die Erfolgsrate der Behandlung gesteigert werden. In den letzten Jahrzehnten führte das Prinzip der *Guided Tissue Regeneration* (GTR) zu einem Paradigmenwechsel in der Chirurgie. Durch die räumliche Trennung langsam proliferierender Knochenzellen und schnell teilenden Weichgewebszellen der Mundschleimhaut, in Form einer Barrieremembran kann eine geführte Ausheilung der Wunde erfolgen.

Neue Forschungsansätze bedienen sich dabei sogenannten Elektrospinn-Verfahren und Additiven Fertigungsprozessen um Faserstrukturen im (Sub)-Mikrometer-Bereich herzustellen. Vor allem das sogenannte Melt Electrospinning (MES) und das daraus resultierende Melt Electrowriting (MEW) zeigen ein hohes Applikationspotential. Letzteres ermöglicht die exakte Positionierung solcher Fasern und somit die Produktion komplexer 3D-Strukturen.

Die Zielsetzung dieser Masterarbeit ist die 3D-Fertigung einer funktionsfähigen Membran mittels MES und MEW für die Zwecke der GTR im Bereich der Mund- Kiefer- und Gesichtschirurgie. Die entstehende Membran soll dabei im Wesentlichen aus zwei Teilen kombiniert werden. Zum einen soll mit dem Elektrospinn-Verfahren eine bakteriendichte Schicht hergestellt werden; im zweiten Schritt soll das Aufdrucken definierter Faserstrukturen im Sinne der GTR erfolgen.

Im ersten Schritt der Arbeit wurde die Herstellung der bakteriendichten Membran fokussiert, wobei verschiedene Prozessparameter (Temperatur, Düse, Kollektordistanz und -geschwindigkeit) erforscht wurden um ein dichtes Netzwerk von Submikron-Fasern zu generieren. Mit den optimierten Prozessparametern und einem neu-entwickelten

Düsensystem, indem eine Akupunkturnadel verarbeitet wurde, konnten Nanofasern von 193 nm ± 146 nm erzielt werden. Gemäß unserm besten Wissen sind dies die kleinsten Fasern, die bisher mittels MES-Verfahren produziert wurden. Eine erfolgreiche Untersuchung auf die Bakteriendichtigkeit konnte aufgrund limitierter Ressourcen und dem verfügbaren Zeitraum nicht umgesetzt werden. Desweitern konnte die Verbindung der elektrogesponnenen Komponente mit definierten Faserstrukturen anhand eines benutzerdefinierten Doppel-Druckkopf-Systems durchgeführt werden. Dabei wurden Unterschiede bei der Reihenfolge des Druckverfahrens der einzelnen Komponenten deutlich gemacht.

In der vorliegenden Arbeit konnte die Herstellung einer Membran mittels 3D-Druckverfahren demonstriert werden, die hohes Potential für weiterführende Studien aufweist.

Table of contents

Acknowledgments 6

List of abbreviations 7

1. Introduction 8

1.1 Challenges in operative dentistry - osteonecrosis of the jaw 8

1.2 Membrane technology for guided tissue regeneration 9

1.2.1 The principle of guided tissue regeneration 9

1.2.2 Membranes for guided tissue and bone regeneration 10

1.2.3 Anti-bacterial approaches in membrane technology 13

1.3 Additive manufacturing 14

1.3.1 Melt electrowriting 14

1.3.2 Multiphasic scaffolds 17

2. Aims and objectives 19

3. Materials and methods 21

3.1 Materials 21

3.2 MEW device 21

3.3 Processing 22

3.4 Scanning electron microscopy (SEM) and light microscopy 22

3.5 Bacterial test 23

4. Results & discussion 24

4.1 Investigations on the electrospun membrane 24

4.1.1 Establishing electrospinning on the double-headed MEW device 24

4.1.2 Membrane design 25

4.1.3 Effect of temperature on the fibre diameter 27

4.1.4 MES using an AP needle 32

4.1.5 Bacteria test on the electrospun membrane 37

4.1.6 Summary 39
4.2 Combining MEW and MES 40
4.2.1 Fabrication of MEW scaffolds 40
4.2.2 Fabrication of biphasic scaffolds 42
4.2.3 Summary 44
6. Conclusion 45
7. Future perspective 46
8. References 48
Appendix A 55

Acknowledgments

First, I wish to express my sincere gratitude to my supervisor Prof. Paul Dalton for giving me the opportunity to work within the research group. Furthermore, I want to thank you for all your guidance during the past two years. Moreover, I specifically thank you for allowing me to work independently, while making sure to guide me in the right direction when needed.

I would like to extend my gratitude to Andrei for his help during the project, especially for all the work at the REM. Furthermore, I want to thank Christoph and Carina for all your advice during the project.

I also must thank Maria, who shared her knowledge of microbiology with me and guided me through the bacteria experiments.

I also want to thank all members of the FMZ, I really appreciated the six months that I spent with you.

Finally, I want to thank my colleagues Angelina, Juliane, Maxim and Nick for all the adventures during our stay in Australia.

List of abbreviations

AP	acupuncture
AM	additive manufacturing
cm	centimetre
CPCs	cardiac progenitor cells
GTR	guided tissue regeneration
h	hour
HV	high voltage
kV	kilovolt
LB	lysogeny broth
MES	melt electrospinning
MEW	melt electrowriting
min	minute
mL	millilitre
mm	millimetre
ONJ	osteonecrosis of the jaw
PBS	phosphate-buffered saline
PCL	poly(ε-lactone)
PEVA	poly(ethylene-vinyl acetate)
PLA	poly(lactic acid)
PTFE	poly(tetrafluoroethylene)
S. aureus	Staphylococcus aureus
SD	standard deviation
sec	second
SEM	scanning electron microscopy
TE	tissue engineering
µL	microlitre

1. Introduction

1.1 Challenges in operative dentistry - osteonecrosis of the jaw

The treatment of several bone defects such as osteoporosis, bone metastasis and multiple myeloma, often involve the therapeutic use of bisphosphonates [1, 2]. Despite the efficacy to successfully treat bone disorders, studies of the past decades revealed the impact of bisphosphonates therapies to cause exposed and necrotic bones in the mandible and maxilla [3]. Osteonecrosis of the jaw (ONJ) is a severe condition hallmarked by the death of bone material (Figure 1).

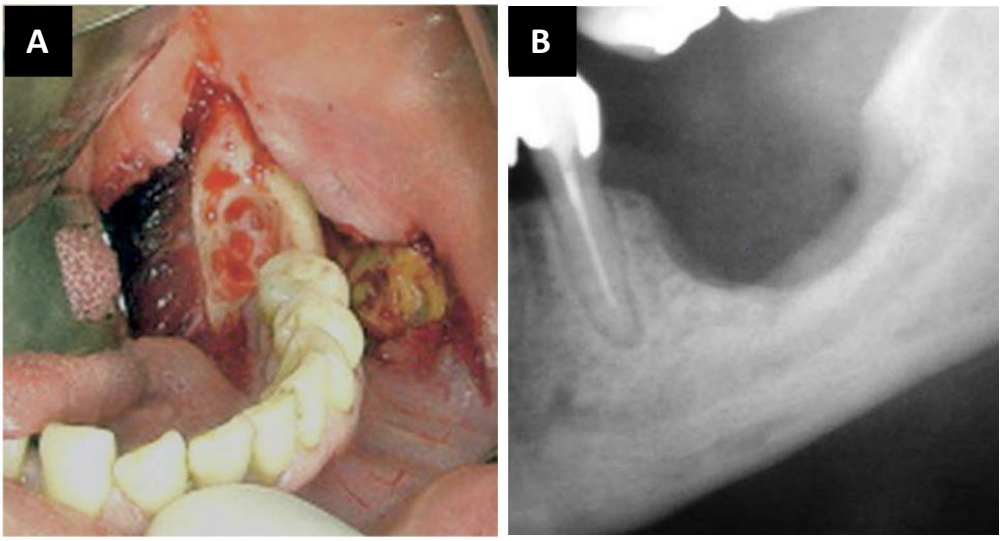

Figure 1. Appearance of necrotic bone and the surgical treatment. (A) Marginal resection of the necrotic bone in the mandible. (B) Radiograph of the mandible after bone resection [1].

Disruption of the hierarchical structure of the bone leads to joint pain and loss of function [4]. The adequate treatment strategy of bisphosphonate-related ONJ still remains controversy. First approaches are focused on the use of antibiotic agents and anti-bacterial mouth rinse [5]. If the disease persists despite long-term drug treatment, the resection of the necrotic bone is favourable. To guarantee the mobility of the patient, implants are used to ensure the mechanical stiffness of the jaw. Unfortunately, in some cases implant failures occur due to insufficient tissue regeneration or bacterial infections. To overcome this drawback, membranes are investigated which are able to enhance tissue regeneration and prevent bacteria infiltration towards the implant.

Box 1. A glance on bone remodelling

The term bone remodelling includes the removal and repair of damaged bone to guarantee its mechanical integrity and mineral homeostasis. Coordination of this accurately clocked mechanism is given by molecular mechanisms and several cellular participants, such as osteoclasts, osteoblasts and osteocytes [6]. While the exact mechanism of bone remodelling is still unknown, it is well established that in the beginning osteoclastic precursors become activated and undergo differentiation into osteoclasts. This cell type is capable of resorbing a discrete area of mineralised bone matrix, which is directly followed by a reversal phase in which osteoblasts, derived from osteoprogenitor cells, migrate into the resorption lacuna [7]. In the so-called formative phase, osteoblasts start to place unmineralised bone material (osteoid) into the resorption lacuna. If an adequate amount of osteoid is deposited, mature osteoblasts will undergo cell death or will be embedded into the mineralised matrix in which differentiation into osteocytes takes place. If new circles of bone remodelling are necessary, osteocytes will start the recruitment of osteoclasts to dispose damaged bone material.

1.2 Membrane technology for guided tissue regeneration

1.2.1 The principle of guided tissue regeneration

While in the early beginnings of clinical dentistry, surgery procedures were focussed on the repair instead of the full reconstitution of the lost tissue, over the last four decades, important steps have been made to initiate tissue regeneration. The origin of guided tissue regeneration (GTR) goes back to a series of studies starting from the early 1970s which were able to demonstrate the regenerative capability of periodontal tissue components [8]. Following these findings, it was hypothesised that by consequently separating fast proliferating soft tissue cells from slowly separating bone cells, superior tissue regeneration could be achieved [9]. First proof-of-concept studies presented by Nyman *et al.* and Gottlow *et al.* revealed the formation of new connective tissue using GTR technology [10, 11]. Periodontal defects were created in an animal-model and membranes were inserted over the denuded root surfaces of the teeth. By implantation of the physical barrier into the defect, the oral epithelium and the gingival

connective tissue were prevented to interrupt the healing process by cells deriving from the periodontal ligament (Figure 2).

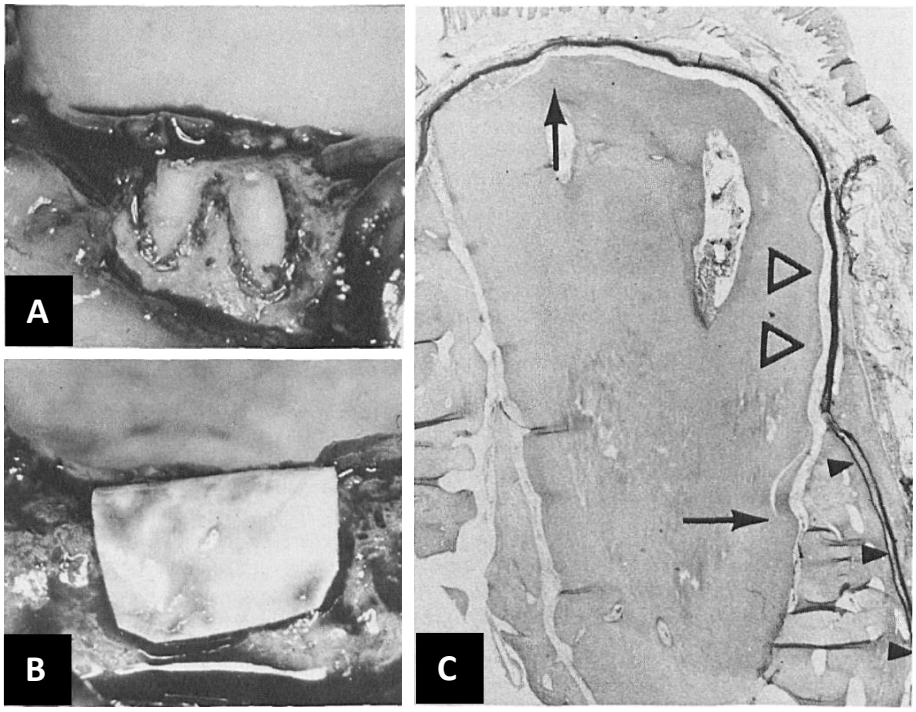

Figure 2. Design and outcome of the periodontal GTR study. (A) Resection of the crown of the tooth after root instrumentation. (B) Membrane insertion prior to flap replacement. (C) Incorporation of the membrane (arrowheads) within newly formed bone tissue (adapted from Gottlow *et al.* [10]).

As a result of this study, test surfaces exhibited significantly more new attachment than the control surface, providing evidence that the use of an occlusive membrane favoured repopulation of the wound area from cells of the periodontal ligament. These outcomes paved the way for a paradigm changes in clinical surgery.

1.2.2 Membranes for guided tissue and bone regeneration

Since the first GTR technology was applied to humans based on a cellulose acetate laboratory filter, the range of processable materials suitable for medical application constantly expanded ending in a great variety of membranes each offering clear advantages and disadvantages. As described by Scantlebury *et al.*, barrier membranes need to fulfil a range of essential requirements to be used in medical application. As already mentioned previously, membranes for GTR should provide space-making capabilities to ensure cell migration into the wound area for a certain time duration. Furthermore, biocompatibility, which means that the membrane does not trigger any adverse effect when interacting with the host tissue, is another crucial factor. Another important aspect is the mechanical strength of the barrier to prevent

interruption of the healing process due to underlying blood clots. To avoid removal surgeries of the implant, an adequate degradability of the membrane which matches the regeneration rate of the tissue is also highly favourable [12].

In general barrier membranes, which have been used in clinical applications can be grouped as resorbable or non-resorbable membranes (Table 1). Poly(tetrafluoroethylene) (PTFE) were the first non-resorbable membranes [13]. Today commercially available PTFE membranes are divided in high-density PTFE and titanium-reinforced high-density PTFE. PTFE membranes are hallmarked by these excellent stability characteristics providing space for tissue regeneration and integration and this good biocompatibility. The main drawback of non-resorbable membranes is the need for removal surgeries which is attended by pain for the patients, but also seen from an economic perspective, additional procedure costs. To address this limitation, first resorbable membranes were developed in the late 1980s, consisting of commercially available polyesters (e.g., poly(glycolic acid), poly(lactic acid) (PLA) and poly(ε-lactone) (PCL)). These synthetic biomaterials undergo polymer erosion through the cleavage of hydrolytically sensitive bonds and demonstrate degradation rates ranging from some month to several years. Early investigations of these biomaterials also proofed their superior biocompatibility [14, 15]. Despite the resorbable properties, an important concern for the use of resorbable membranes is the unpredictable resorption time and the degradation rate, which correlates with decreased mechanical strength by time [9].

Over the decades, nature-derived polymers are highly recognised alternatives to synthetic polymers due to their superior cell affinity [16, 17]. Most studies were undertaken on membranes consisting of collagen, derived from human skin, bovine tendon or porcine skin [9]. Despite their superior biocompatibility, collagen membranes present several limitations. It has been shown that these membranes are prone to bacteria colonisation which results in rapid degradation of the membrane by proteolytic enzymes and the loss of its mechanical strength [18]. Furthermore, there is a certain risk to transmit diseases to the patient by using animal-derived collagen [19].

Table 1. Currently commercially available barrier membranes for GTR (modified from Bottino *et al.* [13]).

Resorbability	Commercial Name	Composition	Degradation rate
Non-resorbable	Cytoplast TXT-200	high-density PTFE	Non-degradable
	Cytoplast Ti-250	Titanium-reinforced high-density PTFE	Non-degradable
Resorbable synthetic	Resolut LT	Poly-DL-lactic/co-glycolic acid	5 – 6 months
	Vicryl	Polyglactin 910	ca. 9 months
Resorbable collagen-based	AlloDerm	Collagen Type-I derived from cadaveric human skin	ca.16 weeks
	BioMend Extend	Collagen Type-I derived from bovine tendon	18 weeks

To date, a new strategy emerged in the field of GTR, investigating the incorporation of growth factors and bioactive molecules into barrier membranes [20-22]. For instance, Miron *et al.* demonstrated increased osteoblast proliferation and differentiation on a collagen barrier membrane soak-loaded in bone morphogenetic protein 2 and transforming growth factor ß1 [23]. Moreover, a commercially available enamel matrix derivative has provided increased periodontal regeneration by stimulating the formation of periodontal tissues [24].

1.2.3 Anti-bacterial approaches in membrane technology

Besides material considerations, studies of the last decades revealed the impact of pathogenic microorganism on the success of GTR strategies. It has been shown that adequate tissue regeneration cannot be achieved for barrier membranes which were implanted into bacterial infected areas [25, 26]. Furthermore, unresisted bacteria colonisation of the barrier membrane implies a high risk for the infection of underlying tissue. Due to bacteria infiltration, implant failures can occur which require the need for removal surgeries [27, 28]. As hallmarked by Selvig *et al.*, to ensure patients safety and to guarantee treatment success, it is essential to control the pathogenic microorganism in the implantation site [29].

To address this issue, research over the last years aimed to create anti-bacterial properties into the membranes [30-32]. For instance, Kenawy *et al.* reported the incorporation of tetracycline into poly(ethylene-vinyl acetate) (PEVA) and 50/50 PLA/PEVA fibrous mats by blending. *In vitro* release of these membranes demonstrated smooth release of the drug over about 5 days [30]. The efficacy of membranes blended with bactericidal metronidazole to successfully reduce bacteria growth and biofilm formation has been quantitatively assessed by Bottino *et al.* [33]. Another approach has been focussed on the surface modification of commercially available biodegradable membranes to create anti-bacterial properties. Membranes were mineralised with zinc phosphate, which resulted in significant decrease of Actinobacillus actinomycetemcomitans activity compared to non-mineralised control groups [34]. Another approach investigated ultrafine PLA fibres consisting of silver nanoparticles [35]. These fibres demonstrated the reduction of microorganism of about 98% and 94% against Staphylococcus aureus (S. aureus) and Escherichia coli, respectively.

Despite promising results in terms of anti-bacterial capabilities of GTR membranes, these studies have failed to provide sustained long-term release of anti-bacterial agents. Besides optimisation and development of biomaterials, recent advancements of fabrication technologies that enable the processing of complex polymer structures through more controlled and precise deposition of polymeric material could lead to a new paradigm of local drug delivery systems through offering high versatility in controlling drug release profiles, personalised customisation and multi-drug incorporation.

1.3 Additive manufacturing

Additive manufacturing (AM), also known as rapid manufacturing or rapid prototyping, is defined as the process of layer by layer deposition of material to make 3D objects according to a computer aided design model. This direct transformation offers the possibility of producing structures with complex geometry, which cannot be accessed by conventional material removal fabrication techniques. Furthermore, AM is highly suitable for small scale production, especially personalised manufacturing. Additionally, 3D printing approaches offer the possibility to process in a solvent-free fabrication mode, which implicates advantages for approval by regulatory agencies. These benefits have allowed the steady growth of AM techniques in biomedical application, especially in terms of tissue engineering (TE) and customised implants [36, 37].

1.3.1 Melt electrowriting

Recently, a novel electrohydrodynamic direct writing approach, defined as melt electrowriting (MEW) emerged in the field of AM [38]. Technically MEW evolved from the well-established electrospinning process, which has been intensively studied to produce micro/nanofibrous structures for a broad range of biomedical applications (Figure 3) [39-41].

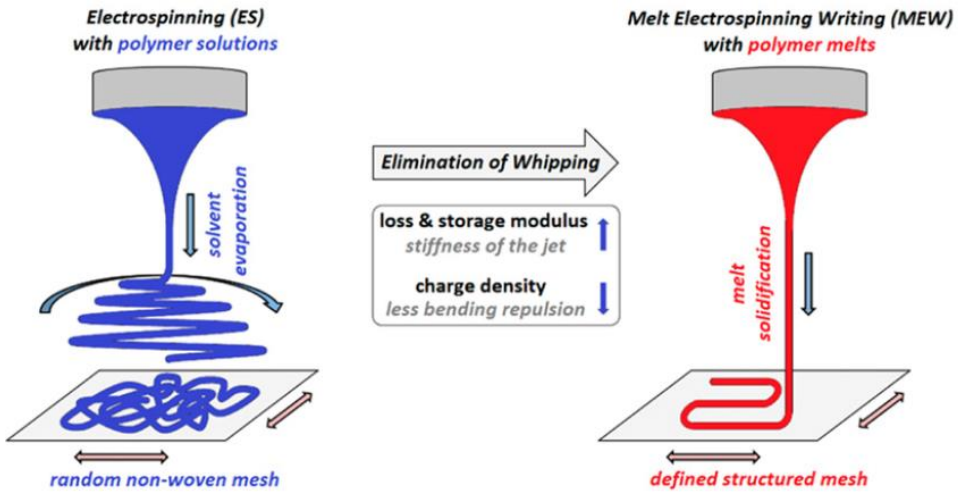

Figure 3. Fabrication modes to produce random non-woven polymer fibres (electrospinning) and accurate layer-by-layer deposition of polymeric fibres (MEW) [42].

In general, electrospinning involves the injection of a polymer solution or melt through a nozzle under high electrical field. The polymeric material at the tip of the spinneret forms a droplet. When the viscosity of the polymer solution is above a threshold, the ejected polymer will not break down as microdroplets due to Raleigh instabilities, resulting in continuous non-woven fibre deposition on the collector substrate [43, 44]. Due to the high viscosity, melt electrospinning (MES) typically provides fibres ranging from 5 to 40 µm whereas solution electrospinning typically results in submicron fibres. However, as reported by Dalton *et al.*, MES also offers the possibility to produce submicron fibres [45]. Despite clear advantages, compared to solution electrospinning, MES has only recently been investigated [46]. For instance, MES allows processing in a solvent-free mode, thus samples do not need to degas but also solvent accumulation during processing can be avoided [47]. Moreover, fibre diameters can be easily adjusted by the flow rate [48]. To date, it has been shown that a great variety of polymers with a long history of clinical use can be processed by MES [49-51].

Several studies have demonstrated the potential of electrospun (nano-)fibres in the field of TE to provide scaffolds which mimic the fibrinous structure of the extracellular matrix resulting in increased cell adhesion and proliferation [52-54]. However, the low pore sizes occurring due to the random deposition of fibres prevent cells to penetrate the mesh. As highlighted by Mikos *et al.*, scaffolds need to provide pore sizes of at least 20 µm to initiate cell invasion and growth [55]. Over the last decades several techniques, such as electro-conductive collectors, fibre deposition onto liquid, electric field manipulation and rotating devices were investigated to increase the control of fibre placement during electrospinning [56-59]. However, despite these approaches, accurate fibre deposition, as provided by AM has not been reached. In terms of MEW, the predictable deposition of fibres has been achieved by introducing a laterally translating collector system into MES (Figure 4).

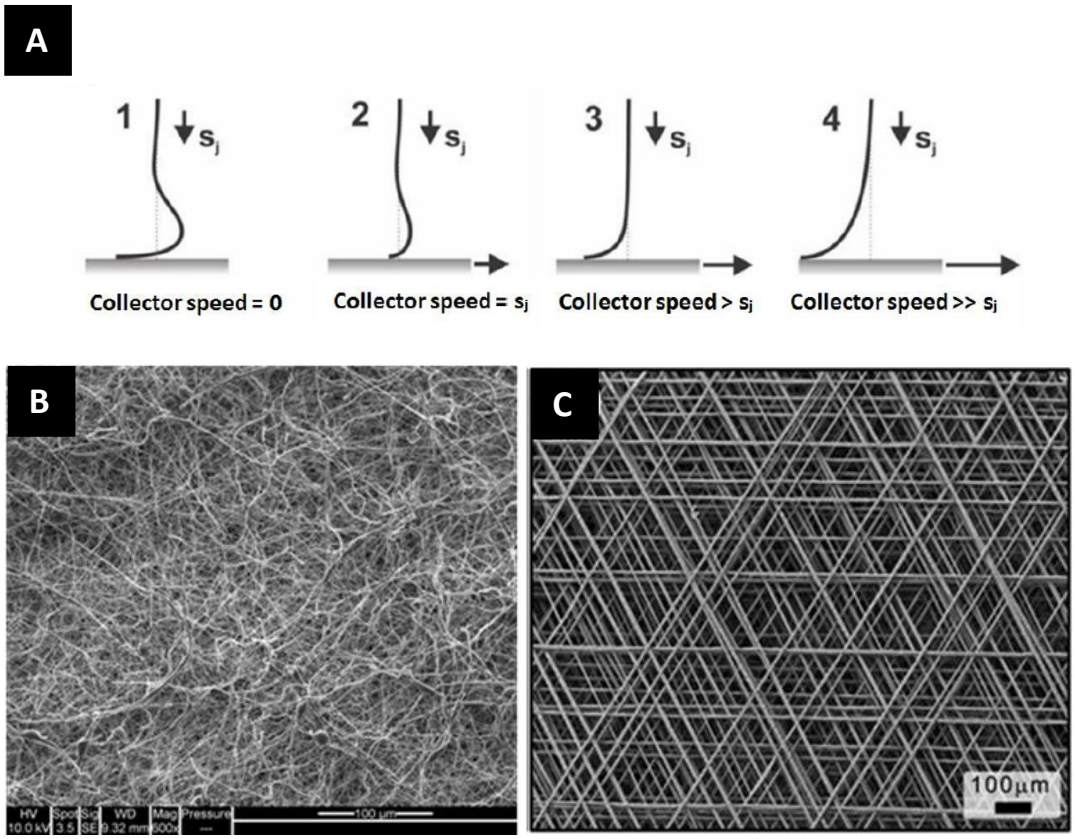

Figure 4. Fabrication mode of MES and the resulting fibre morphology. (A) Schematic showing of the MES jet depending on the speed of the collector. (B) Random deposition of electrospun fibres. (C) Accurate deposited fibres via MEW [60].

If the collector speed exceeds the speed of the jet (s_j), fibres are deposited from the region of the jet where the flight path is straight. The control of fibre deposition enables the layer-by-layer fabrication of scaffolds with complex geometry and patterns [60-63]. Over the last years, multiple studies have demonstrated the potential of MEW to provide scaffolds with pore sizes suitable for TE applications [47, 64, 65]. For instance, Farrugia *et al.* were able to fabricate melt-electrowritten porous PCL scaffolds with an interfibre distance (46 ± 22 µm) suitable for cell infiltration. Due to the high porosity of these scaffolds dermal fibroblast were able to penetrate and a 3D fibroblast scaffold with full cellular penetration has been achieved after 14 days *in vitro* [66]. More recently, Castilho *et al.* investigated the potential of MEW scaffold in cardiac TE. It has been demonstrated that cardiac progenitor cells (CPCs) showed improved alignment and growth along these highly ordered microfibre scaffolds (Figure 5) [67].

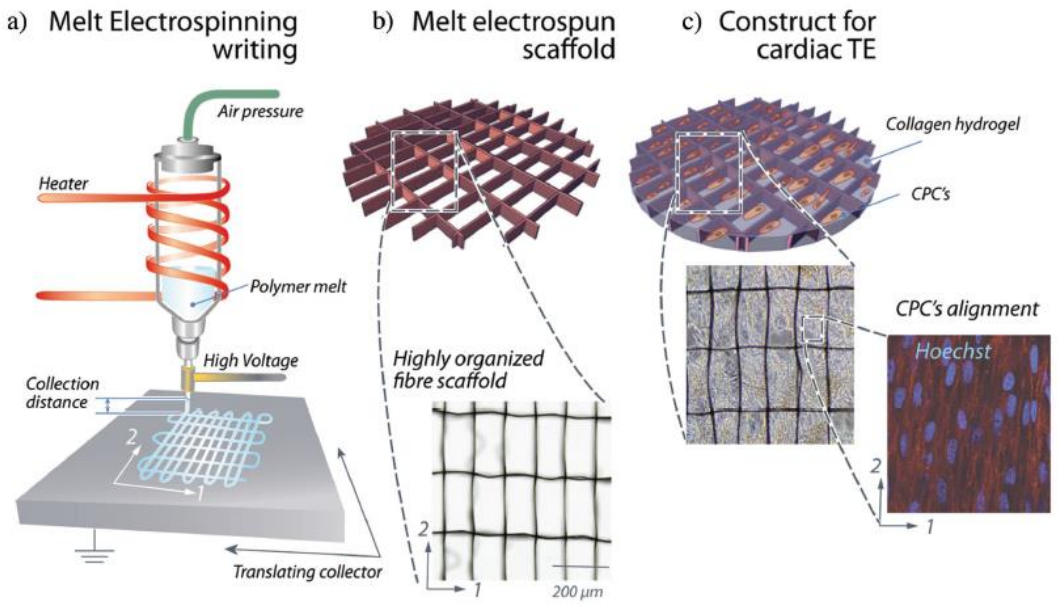

Figure 5. Fabrication of MEW scaffolds for cardiac TE. (A) MEW device set-up. (B) Well-organised MEW scaffolds. (C) Fibre scaffold infiltrated with CPCs/collagen hydrogel [67].

1.3.2 Multiphasic scaffolds

As highlighted by Dalton *et al.*, the combination of AM and electrospinning technologies can have a significant effect on future scaffold designs [68]. While AM provides scaffolds with high mechanical stability and offers the fabrication of higher constructs, it also includes lower resolution limits. In contrast, solution electrospinning results in fibres ranging in the nanometre scale, however this technology is unable to accurately deposit fibres. Early efforts to combine AM and electrospinning were reported in 2008 by three different groups [69-71]. For instance, Park *et al.* developed a nano- and microhybrid process consisting of direct polymer melt deposition and electrospinning [71]. The resulting 3D scaffold demonstrated an open porous network and a biocompatible ultrafine inner architecture (Figure 6).

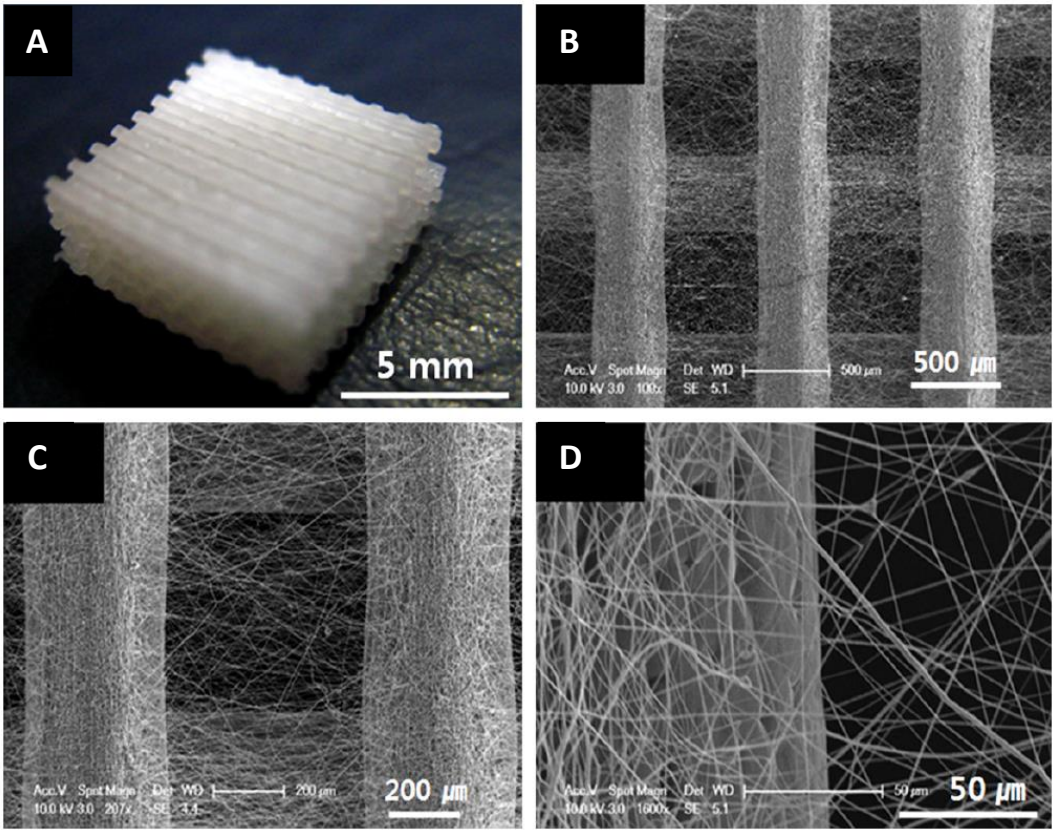

Figure 6. Bimodal scaffold. (A) Photograph of the resulting 3D structure. (B) Hybrid basic unit layer comprising of microfibres and the electrospun submicron fibres. (C and D) Magnified images of (B) [71].

This scaffold morphology allowed cell invasion while cell adhesion and proliferation were improved by the incorporated ultrafine fibres. In contrast to bimodal scaffold in which microfibrous and nanofibrous components are distributed throughout the 3D design, multiphasic scaffolds usually consist of different regions of pore size and porosity [68]. Due to the different morphology, scientists aimed to provide an adequate environment for different cell types, which are needed to build new functional tissue interfaces. As an example of this strategy, Vaquette *et al.* evaluated the potential of a biphasic scaffold to simultaneously regenerate alveolar bone and periodontal ligament complex [72]. In this study, an electrospun component was used as a support material for the adhesion of periodontal ligament cell sheets, whereas a fused deposition modelling scaffold was fabricated to provide space maintenance for the bone component.

2. Aims and objectives

As can been seen from the preceding literature investigations, despite of a broad spectrum of different materials and fabrication methods investigated, there remains the need for advanced GTR membranes to fulfil the essential aspects of oral and maxillofacial surgery:

I, Sufficient handling for the use in surgery

II, Appropriate biodegradability

III, Good mechanical stiffness to ensure placeholder-capacities

IV, High biocompatibility

V, Bacteria-tightness and anti-bacterial efficacy

VI, Surface modification with GTR capacities

The objective of this work was to investigate the combination of MES and MEW to fabricate a biphasic scaffold in a one-step process using a custom-build double-headed MEW device. By combining the power of these techniques, we assume that defined features of GTR could be addressed (Figure 7). MES parameters, especially the influence of temperature, will be investigated in order to produce a highly dense network of small fibres which could have the potential to prevent bacteria infiltration. To achieve this, we will further investigate a modified nozzle system, consisting of an acupuncture (AP) needle which is mounted within a nozzle. Building on this, melt electrowritten box structures, offering pore sizes suitable for cell infiltration will be investigated. Finally, the combination of both components will be explored using the optimised processing conditions. Surface morphology of the resulting biphasic scaffold will be analysed and evaluated.

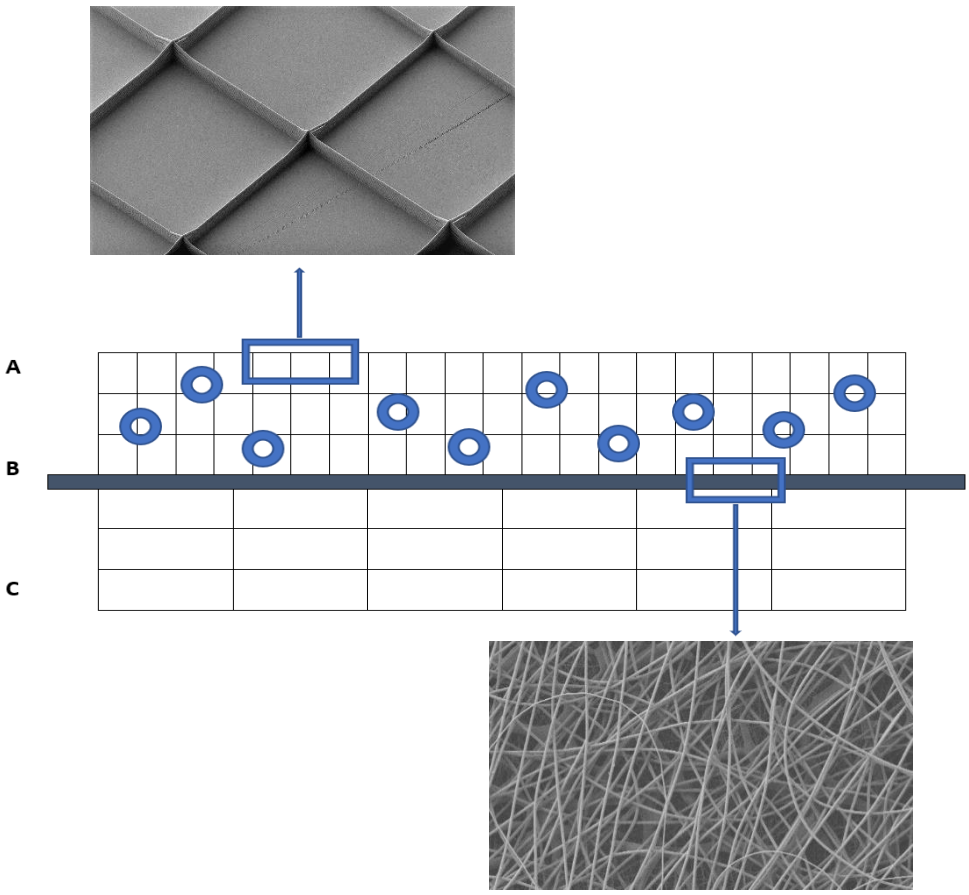

Figure 7. Concept of the multiphasic scaffold. B represents the melt electrospun component, which could prevent bacteria (blue circles) penetration towards the implant. A and C represent melt electrowritten box scaffolds with adjusted box width suitable for cell infiltration.

3. Materials and methods

3.1 Materials

All samples were produced with a good-manufacturing-practice-manufactured PCL, which has been purchased from Corbion, Inc. (PURASORB PC 12, Lot#1412000249, 03/2015, Gorinchem, Netherlands) and has been stored as described elsewhere [73]. AP needles and the 30G and 22G flat-tipped nozzles were cut to the appropriate length (Leonidov, Mainz, Germany) and (Carl Roth GmbH and Co. KG, Karlsruhe, Germany) respectively. The AP needle was then embedded within the nozzle by slightly crimping the uppermost part of the nozzle, so that the end of the AP needle is level (protrudes 3 to 1 mm) from the end of the nozzle.

3.2 MEW device

All studies were performed with a custom-built double-headed MEW device (Figure 8). An x-y slide system (Bosch Rexroth AG, Lohr am Main, Germany) was attached on an aluminium plate with connection to programmable logic controllers (Bosch Rexroth AG, Lohr am Main, Germany).

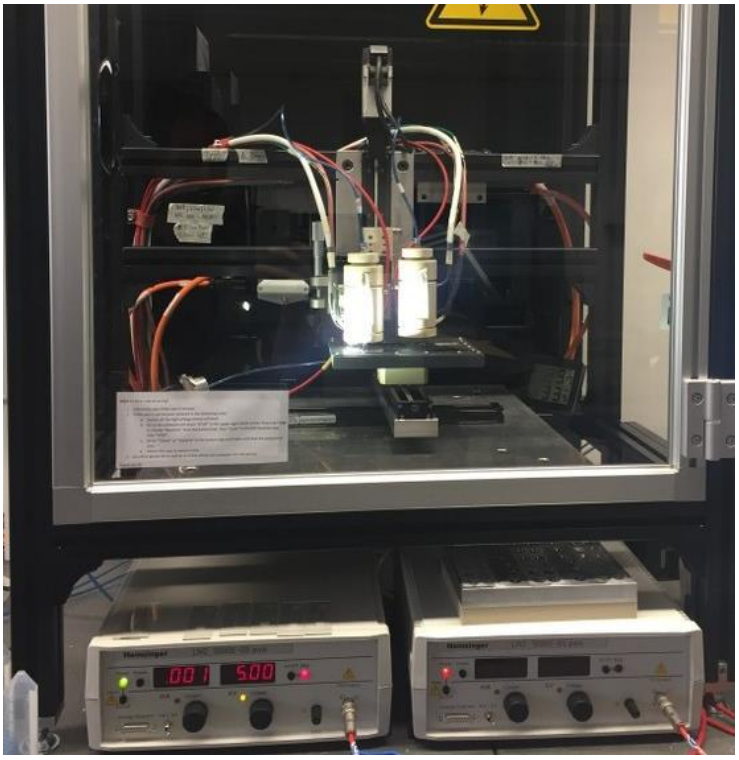

Figure 8. The double-headed MEW device used in this study.

This system was embedded within an aluminium frame box (68x60x80 cm) with polycarbonate windows. Material for processing was filled into glass syringes (Sigma-Aldrich, St. Louis, USA) and placed within an electrical heater and connected to a controllable air pressure system (Bosch Rexroth AG, Lohr am Main, Germany). A positive high voltage (HV) source (LNC 10000-5 pos, Heinzinger Electronic GmbH, Rosenheim, Germany) was linked to the HV electrode at the spinnerets and the negative HV source (LNC 10000-5 neg, Heinzinger Electronic GmbH, Rosenheim, Germany) was connected to a 200x175 mm stainless steel platform on which the collector was mounted [73].

3.3 Processing

MES was investigated at 22 ±2 °C and a relative humidity of 40 ±10 %. The temperature of the PCL melt for standardised conditions was set to 80 °C unless mentioned otherwise. In general, polymeric material was used within 7 days. The acceleration voltage (composed of the difference between negative voltage on the collector and the positive spinneret) was kept at 12 kV for electrospinning conditions and 6 kV for MEW, if not specifically stated otherwise. Patterning of the deposited material was generated using G-codes. Glass slides (26x50 mm) were used as collector material.

3.4 Scanning electron microscopy (SEM) and light microscopy

Samples were imaged using a stereomicroscope (Discovery V20, Carl Zeiss Microscopy GmbH, Göttingen, Germany). SEM of the membranes and scaffolds was investigated using a Crossbeam 340 SEM (Carl Zeiss Microscopy, Göttingen, Germany) equipped with GEMINI e-Beam column. Prior to SEM imaging, samples were sputter coated with a 3 nm layer of platinum (Leica EM ACE600, Wetzlar, Germany). ImageJ software was utilised to determine fibre diameters of the electrospun and melt electrowritten samples. In case of the electrospun membrane, for each varied parameter three samples were analysed by imaging a random region of each sample. To quantify electrospun fibre diameters, SEM images were overlaid with a grid and all overlapping fibres were counted manual (Figure 9). For the MEW scaffolds, measurements were taken at 20 random regions of the microscopic image. Mean diameter, median and standard deviation (SD) was calculated.

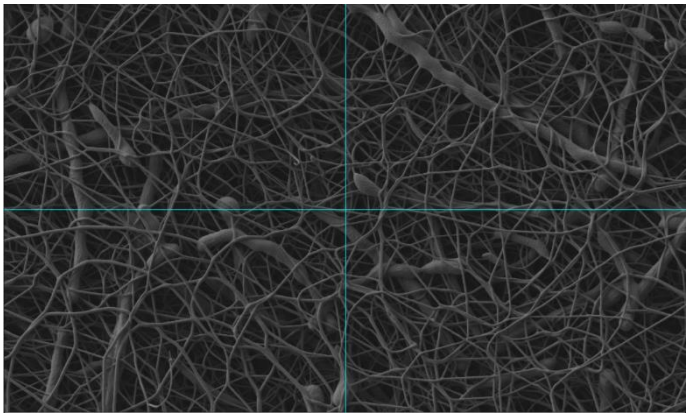

Figure 9. Determination of fibre diameters by overlaying a grid.

3.5 Bacterial test

Bacteria-tightness of membranes were tested against gram-positive bacteria (S. aureus) using a self-designed diffusion assay. The tryptone agar solution was prepared by weighting 2 g yeast extract (AppliChem, Darmstadt, Germany), 4 g tryptone (AppliChem, Darmstadt, Germany), 2 g NaCl (Sigma Aldrich, St. Louis, USA) and 6 g agar (AppliChem, Darmstadt, Germany) into 400 mL of double distilled water and sterilised at 120 °C in the autoclave for 20 min followed by casting onto disposable sterilised petri dishes (90 mm) for solidification. S. aureus was cultured at 37 °C for 24 h in a sterilised lysogeny broth (LB)-medium and then diluted with LB-medium to a concentration of around 1 x 10^5 colony forming units/mL. Three membranes were inserted into custom-built steel rings and the edges were fixed using a glue (Adchem, Wendelstein, Germany). These constructs were set into 6-well plates. 1 mL of the bacteria solution was injected on top of the membrane while 3 mL of LB-medium was added into the outer plate. Plates were incubated at 37 °C for 24 h. On the following day 100 µL were taken from the bacteria solution and from the outer LB-medium and spread onto agar plates using sterilised glass marbles. Plates were than incubated for another 24 h and bacteria growth on the plates were examined to evaluate diffusion of S. aureus through the membrane.

To investigate cytotoxicity of the different materials used in this study, S. aureus solution was spread onto agar plates. Membranes + 20 µL LB-medium, membranes + 20 µL phosphate-buffered saline (PBS), membranes + glue, pure glue and steel rings were gently pressed onto the agar plates. Samples were incubated at 37 °C for 24 h and the zone of inhibition of S. aureus growth was macroscopic evaluated.

4. Results & discussion

4.1 Investigations on the electrospun membrane

In this chapter initial experiments are described and discussed with focus on the preparation of the electrospun membrane of the biphasic scaffold. Different fabrication parameters are investigated with the aim to fabricate high quality fibres with minimum fibre diameter.

4.1.1 Establishing electrospinning on the double-headed MEW device

The literature investigating MES reveals a broad variation in the fabrication parameters, specifically in terms of the collector distance and the applied voltage. To assess a standardised electrospinning setup on the custom-built MEW device, first studies were performed to investigate the influence of the applied voltage regarding the collector distance. For this aim a 30G needle was used and the polymer temperature was kept at 80 °C while a minimal pressure of 0.1 bar was adjusted. Collector distances of 10 mm, 15 mm and 20 mm were investigated. When applying a voltage of at least 9 kV to a collector distance of 10 mm, formation of a Taylor cone was observed, and electrospinning occurred within 2 min onto glass microscope slides (Figure 10). By increasing the collector distance to 15 mm, higher voltages (12 kV) were necessary to initiate fibre deposition. However, MES at a collector distance of 15 mm was unstable and resulted in jet breakup. By increasing the collector distance to 20 mm, even with maximum voltage (17 kV), no Taylor cone formation was observed.

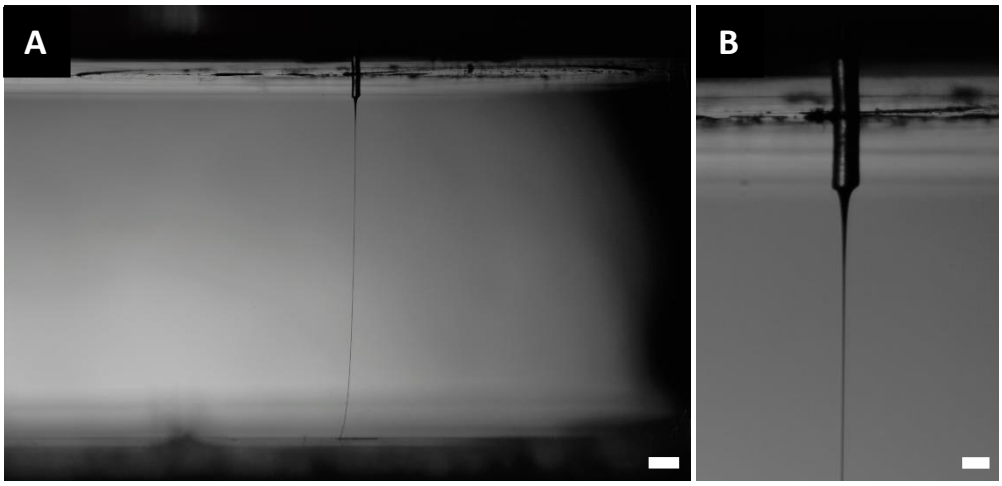

Figure 10. Electrospinning setup. (A) Fibre deposition onto glass microscope slides at a collector distance of 10 mm. (B) Taylor cone formation at the top of the nozzle. Scalebars: A: 1 mm; B: 300 µm.

Overall, these results indicate that for our work, a collector distance of 10 mm is most suitable for MES as no jet breakup was observed. Furthermore, this collector distance allows decent voltages with no need to apply maximum voltage (17 kV). It has been shown that at high voltages arcing occurs, especially when moving the spinneret between two microscope slides. Consequently, continuous arcing can result in lower fibre uniformity but also can lead to severe instrument damage. However, it also has been demonstrated that a high electrical field provides higher uniformity of the deposited fibres [73]. Taken these considerations into account, it has been chosen to continue following experiments with an applied voltage of 12 kV. This was the maximum value which was able to be used at a collector distance of 10 mm without arcing.

As illustrated in Figure 10, compared to solution electrospinning which typically shows whipping of the jet, jet from the polymer melt showed almost linear deposition characteristics. This finding is in line with observations from different studies. As declared by Dalton *et al.*, bending of molten polymer jets might be occur next to the collector, but is not regarded as an absolute phenomenon of MES [45, 74]. Furthermore, it is important to notice that the jet flow was inconsistent within the first 10 min. To ensure the production of high quality fibres we thus used a sacrificial pattern prior to the desired pattern which has been described previously by Hrynevich *et al.* [75].

4.1.2 Membrane design

By moving the collector during MES, a circular membrane was designed using G-code. As illustrated in Figure 11, the first step of the pattern is a clockwise full movement by a certain radius. After completion of the circle, the jet moves towards the centre. At this point, the next circular movement is performed.

The efficacy to fabricate uniform membranes with the above described pattern mostly relies on the spacing between two circular movements and the adjusted collector speed. In our study the distance between the circular patterns was set to 50 µm. This distance seemed to be the maximum resolution of the system. Furthermore, by using spacings smaller than 50 µm electrostatic repulsion could occur between the fibres leading to uncontrolled fibre deposition. However, to ensure overlapping of the circles we mainly focussed on the optimisation of the

applied collector speed. For this aim, three different speeds (1000, 100 and 10 mm/min) were investigated (Figure 12).

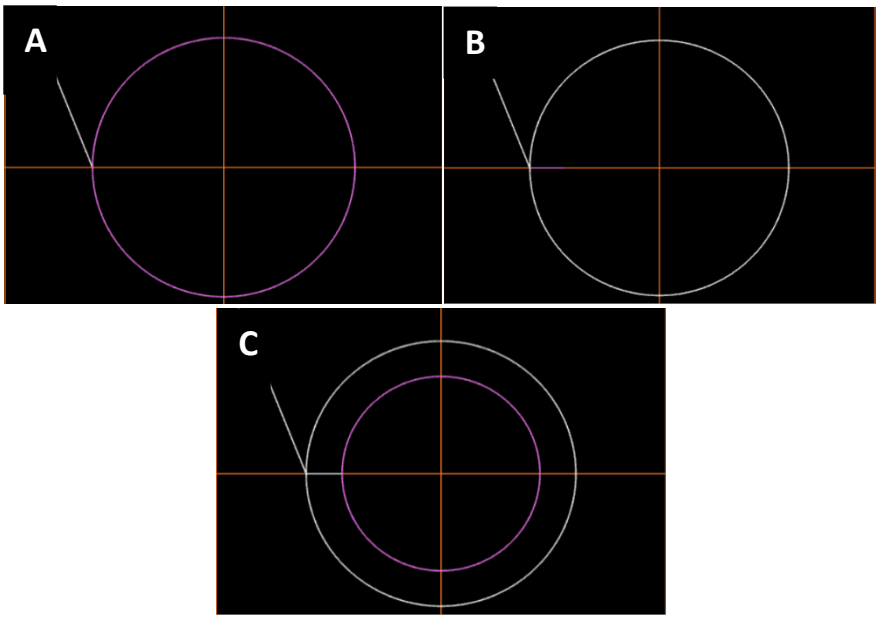

Figure 11. G-code pattern for the electrospun membrane. (A) Clockwise circular full movement. (B) Spacing line towards the centre. (C) Repeated clockwise circular full movement.

Samples prepared with a collector speed of 1000 mm/min resulted in an almost transparent monolayered membrane with a strand width of around 25 µm (Figure 12). Due to the lack of overlaps between the circles, it was not possible to detach the sample from the glass slide.

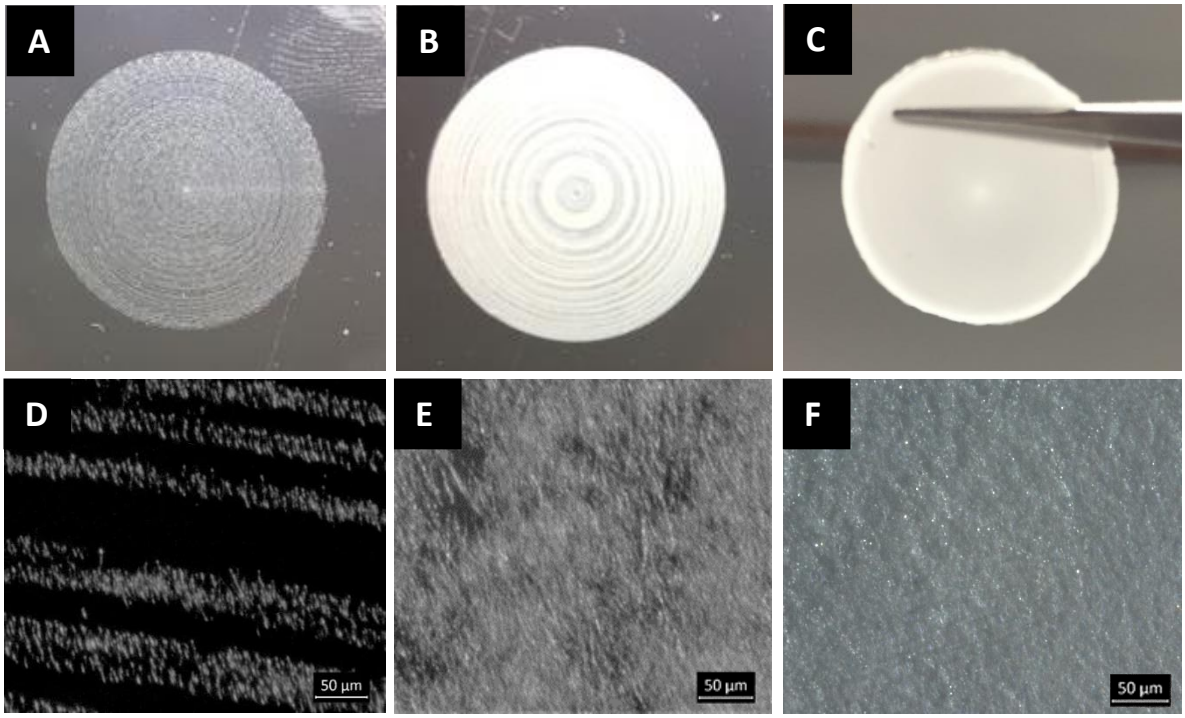

Figure 12. Membranes fabricated at different collector speeds. (A and D) 1000 mm/min. (B and E) 100 mm/min. (C and F) 10 mm/min.

By decreasing the collector speed to 100 mm/min, more material was deposited on the microscope slide, which lead to a non-transparent membrane. Compared to the fibre strands prepared by 1000 mm/min, deposited fibres at 100 mm/min resulted in a 4 to 5-fold increase of the strand width and overlapping of the circles. Nevertheless, these membranes also revealed gaps, where no polymeric material was deposited. When slowing down the collector movement to 10 mm/min, a membrane was obtained in which no gaps between the fibre strands have been observed. The connection of the single fibrous layers resulted in a uniform membrane which was able to detach with tweezers without damage. Interestingly, these samples have shown a brighter spot in the centre of the membrane, indicating that less material was deposited at this point. To address this issue, an additional G-code has been inserted into the pattern which provided pausing of the collector movement for 60 s when the jet was standing above the centre point to increase material deposition (Appendix A).

Ultimately, this study has demonstrated that with adequate deposition times (10 mm/min) overlapping and fusion of the single fibre strength can be achieved which has resulted in a macroscopic uniform membrane. Nevertheless, these primary observations need to be followed up by more detailed characterisation of the membrane morphology.

4.1.3 Effect of temperature on the fibre diameter

Keeping the end-goal in mind, one of the most essential requirements of the electrospun membrane is the formation of a dense network of submicron fibres. The electrospinning temperature has a profound effect on the fibre diameter due to the change in the viscosity of the fluid. To determine the optimal processing temperature which results in the smallest fibre diameters, five different values were investigated (80, 100, 120, 140 and 160 °C) while the nozzle size and the applied pressure were kept constant (30G and 0.1 bar, respectively). The surface morphology and the fibre diameter were determined by SEM micrographs.

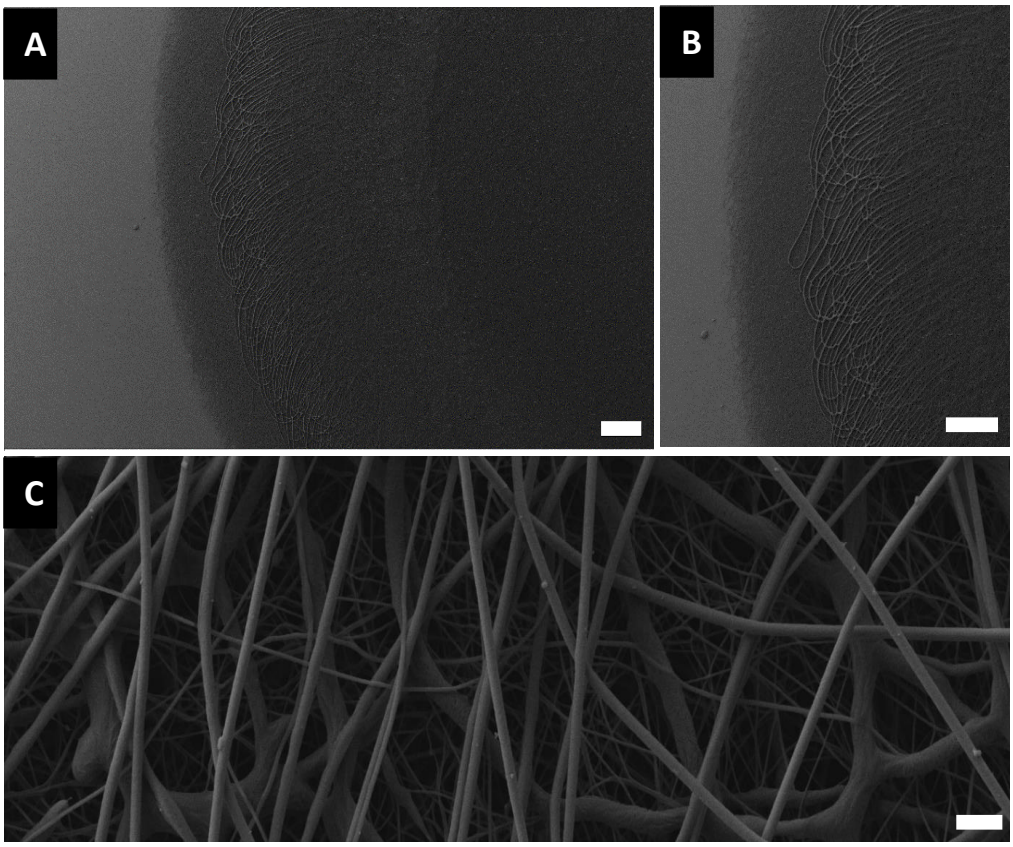

Figure 13. Representative SEM image of the melt electropun membranes prepared at 80 °C. (A) Time-dependent fibre pulsing. (B) Magnified image of (A). (C) Fibre morphology. Scalebars: A and B: 200 µm; C: 2 µm.

As illustrated in Figure 13, samples fabricated at a processing temperature of 80 °C demonstrated constant fibre deposition. However, it has been noticed that at decent time intervals fibres were deposited with significant higher fibre diameters (Figure 13 B). This finding is in line with the work of Hochleitner and colleagues, who found a time-dependent fluctuation of the mass flow, referred to as pulsing [73]. As has been demonstrated, these flow instabilities can be caused by changes in the feeding pressure or the acceleration voltage. As the applied pressure was kept constant during the experiment, it can be assumed that in our study fibre pulsing has been occurred by changes in the strength of the electric field. It is likely that through the excess of deposited material, shielding effects have been occurred, resulting in a decrease of the acceleration voltage. Analysing the SEM micrographs revealed fibre diameters of 339 ± 191 nm (average ± SD) with relatively large deviation due to the instabilities described above.

When increasing the temperature to 100 °C, significant changes of the membrane morphology have been observed. Membranes prepared at 100 °C were characterised by an inconsistent jet flow resulting in jet breakup at random spots (Figure 14). It is also important to notice, that the increased temperature resulted in some regions where molten fibres have been deposited.

Furthermore, increasing the temperature correlated with more pulsing. As a result, the measurement of the fibre diameter provided a higher mean diameter (493 nm) with dramatic increase of the SD (842 nm) (Figure 15). These observations can be explained by the decrease of the viscosity resulting in higher flow rates of the polymer melt. As has been noted earlier by Dalton *et al.*, MES typically results in the most consistent fibres when the flow rate is relatively low [76].

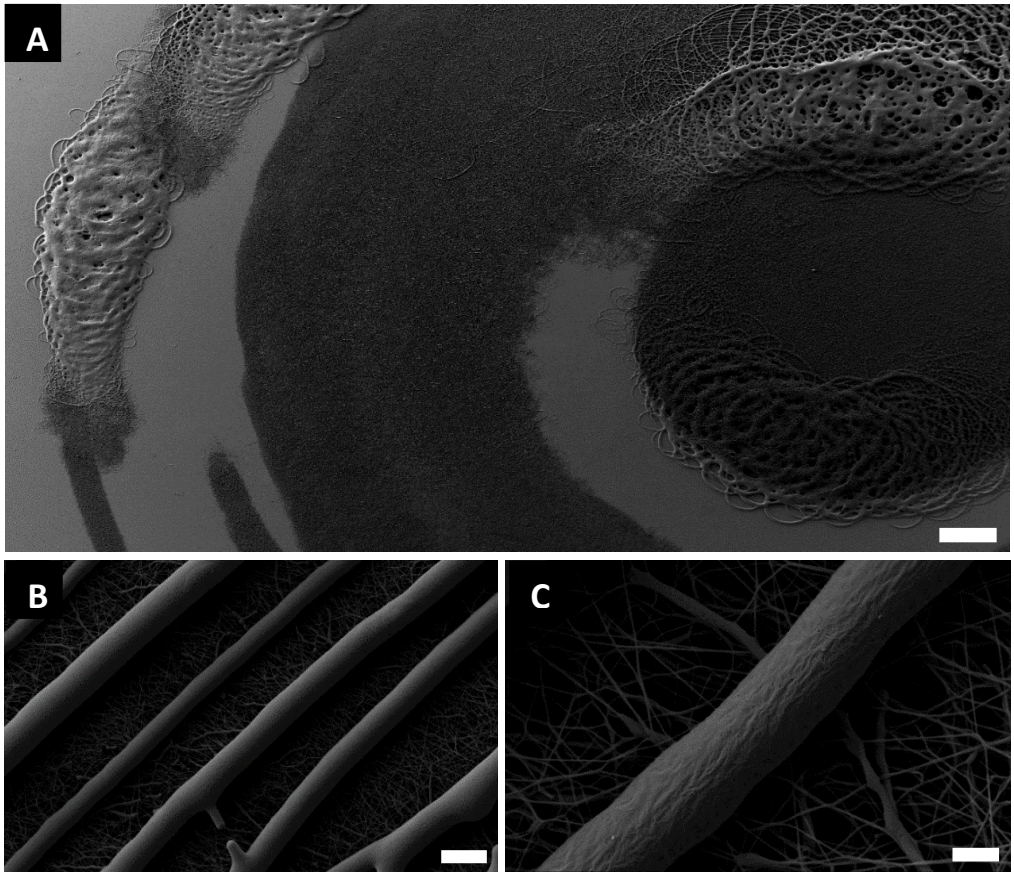

Figure 14. Representative SEM image of the melt electrospun membranes prepared at 100 °C. (A) Unstable fibre deposition on the microscope slide. (B) Pulsing phenomena. (C) Magnified image of (B). Scalebars: A: 200 µm; B: 10 µm; C: 2 µm.

In general, a good tool to evaluate the strength of the fluctuation of the jet flow is the median/average ratio. As described by Hochleitner *et al.*, a homogenous jet diameter results in a narrow and symmetrical distribution function with values close to 1.0. If pulsing phenomena occur the distribution functions gets more asymmetrical [73].

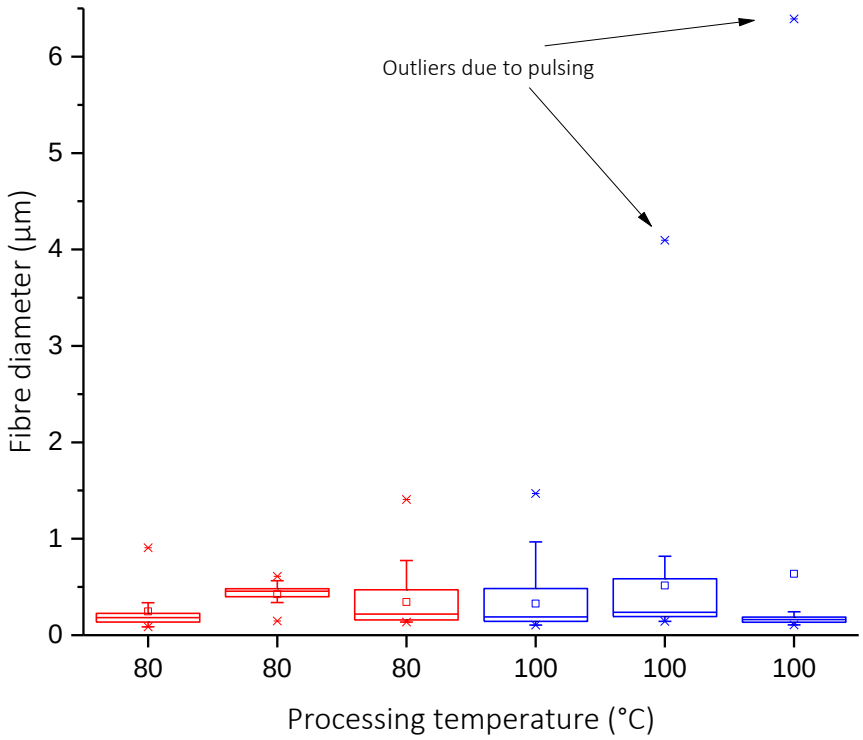

Processing temperature (°C)	80	100
Average, nm	339	493
Median, nm	285	196
SD, nm	191	842
Ratio, median/average	0.84	0.40

Figure 15. Fibre diameters at different processing temperatures.

Dramatic changes of the morphology of the melt electrospun fibres were reported by increasing the temperature to 120 °C (Figure 16). As can be seen from Figure 16, samples have lost the circular G-code pattern and fibres haven been deposited randomly on the microscope slide. Moreover, the collected fibres had a very low quality with a diameter range from several microns to some nanometres. The decrease of the viscosity also resulted in molten fibres onto the glass slide (Figure 16 B). In comparison to solution electrospinning which relies on solvent evaporation to solidify polymeric material, MES is determined by cooling of the polymer jet. The results described above indicate that a processing temperature of 120°C by a given

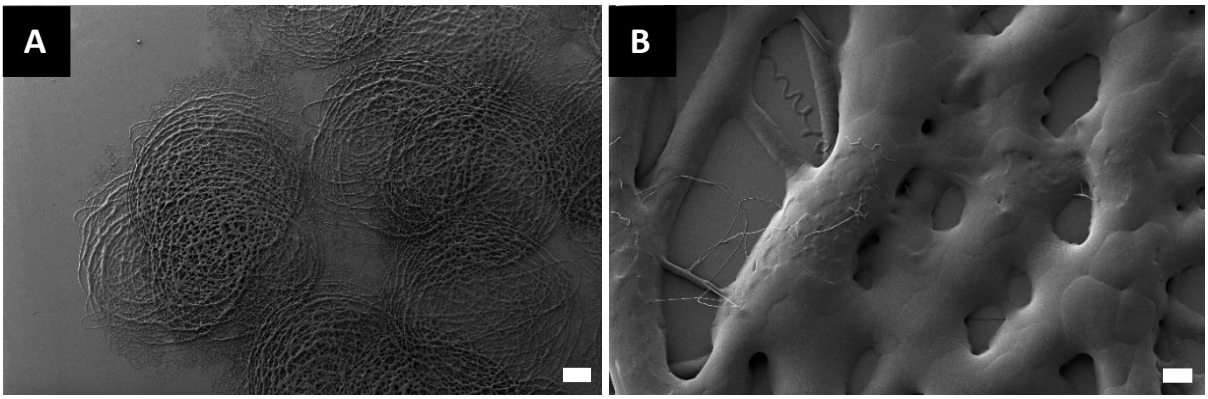

Figure 16. Representative SEM image of the melt electrospun membranes prepared at 120 °C. (A) Unstable fibre deposition on the microscope slide. (B) Magnified image of (A). Scalebars: A: 200 µm; B: 2 µm.

collector distance of 10 mm does not provide enough time for adequate cooling before reaching the collector surface. In line with this finding, further increase of the processing temperature to 140°C and 160 °C, respectively, also resulted in unstable flow rates which were hallmarked by random fibre deposition and pulsing (Figure 17).

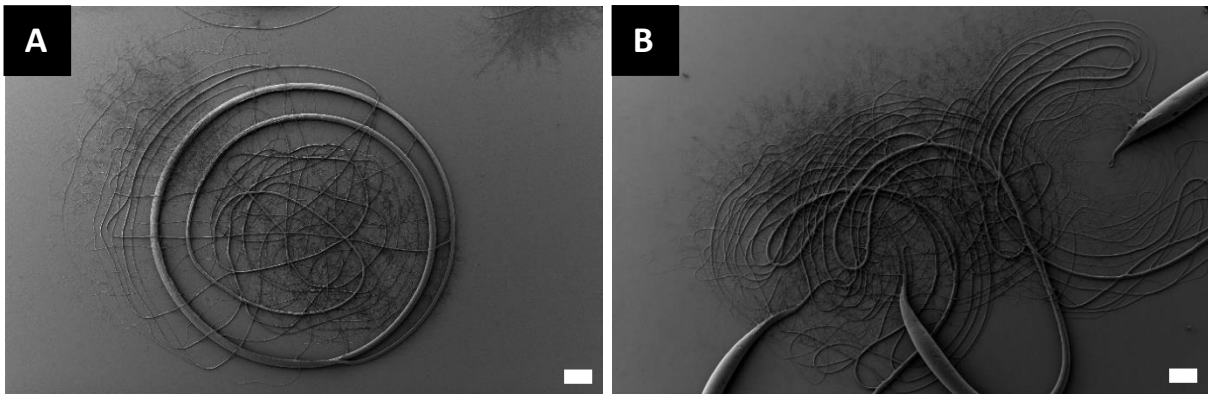

Figure 17. Representative SEM image of the melt electrospun membranes at different process temperatures. (A) 140 °C. (B) 160 °C. Scalebars: 200 µm.

These findings ultimately demonstrate that the processing temperature has a crucial influence on the surface morphology of the deposited fibres. While a processing temperature of 80 °C provided constant jet flow with some fluctuation of the flow rate, increasing the temperature lead to more pulsing phenomena and as a consequence ended up in a complete loss of the control of the fibre diameter.

4.1.4 MES using an AP needle

As reported by Hochleitner *et al*., the fabrication of ultrafine fibres by MES depends on three key parameters: a high electrical field, a low flow rate and a small spinneret size [42]. As described in chapter 4.1.3, electrospinning using the smallest nozzle size (30G) available provided fibres in the nanometre range. However, fibre diameters showed relatively high SD. In order to achieve even smaller fibre diameters with higher quality we further investigated a modified nozzle system, in which an AP needle (ø 300 µm) has been mounted into a nozzle (ø 700 µm) (Figure 18).

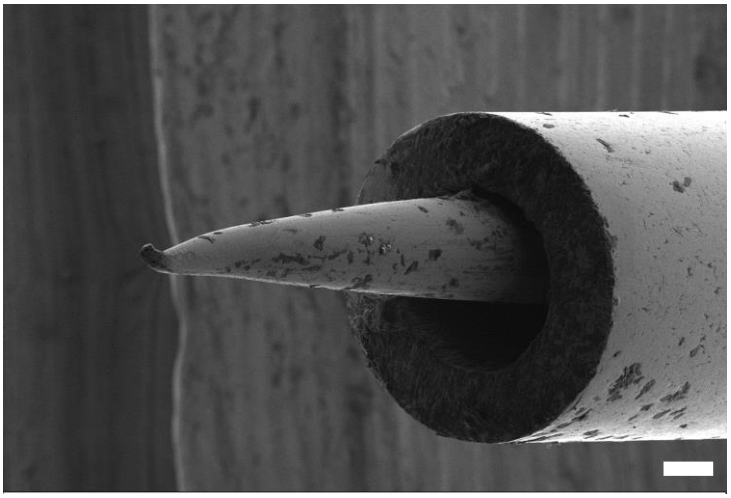

Figure 18. SEM images of the AP modified nozzle. Scalebar: 100 µm.

As illustrated in Figure 18, the AP needle is not centred in the middle of the nozzle. Furthermore, the tip of the AP needle is bent. It is likely that bending of the needle has occurred by inserting the nozzle into the heating system of the MEW device.

Due to the novelty of this nozzle system, initial experiments investigated the optimal overlap of the AP needle for MES. By macroscopic analysis of the polymer melt flow using a 3 mm overlap of the AP needle, it has been found that higher processing temperatures of 120 °C are required to initialise fibre deposition. It can be assumed that this phenomenon relies on significant cooling of the polymer jet at the AP needle. As can be seen from Figure 19, when applying pressure to the system, a polymer droplet occurs at the nozzle tip. Due to the electric field, the polymer melt is drawn along the AP needle. When reaching the tip of the needle, initialisation of the polymer jet onto the collector can be recorded.

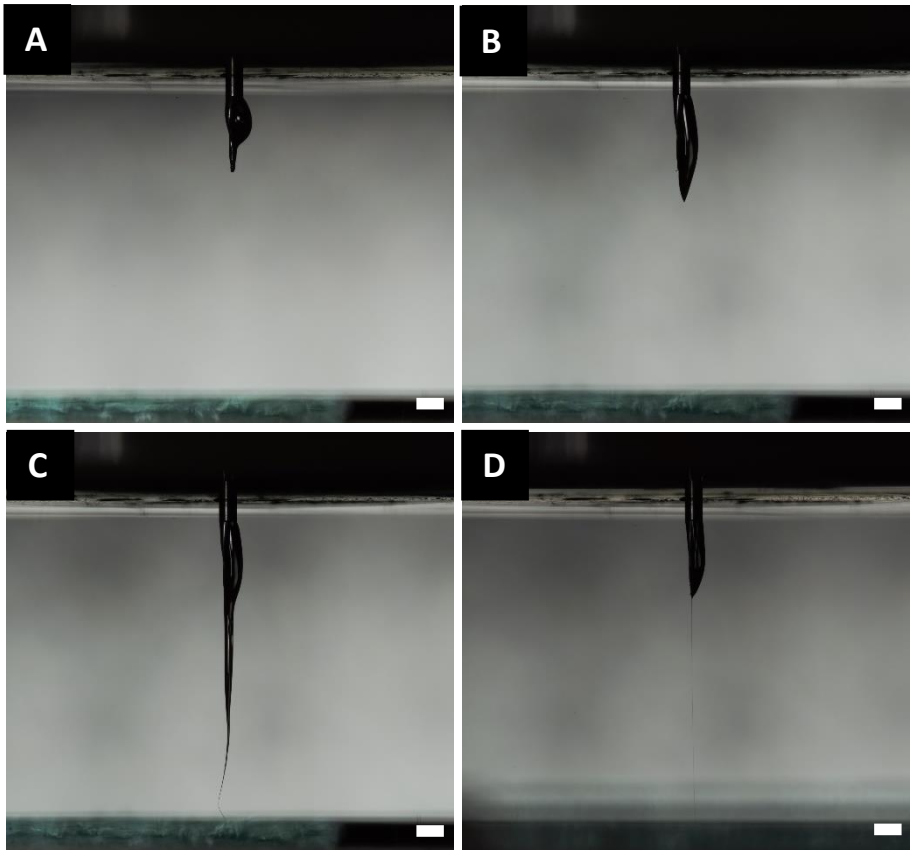

Figure 19. MES using a 3 mm AP needle. (A) Formation of polymer droplet next to the nozzle. (B) Polymer melt draws down the AP needle. (C) Initial polymer deposition starts at the needle tip. (D) Polymer jet after stabilisation. Scalebars: 1 mm.

Analysing the morphology of the deposited material revealed the fabrication of very poor-quality fibres, similar to previous observations described in chapter 4.1.3 (Figure 20).

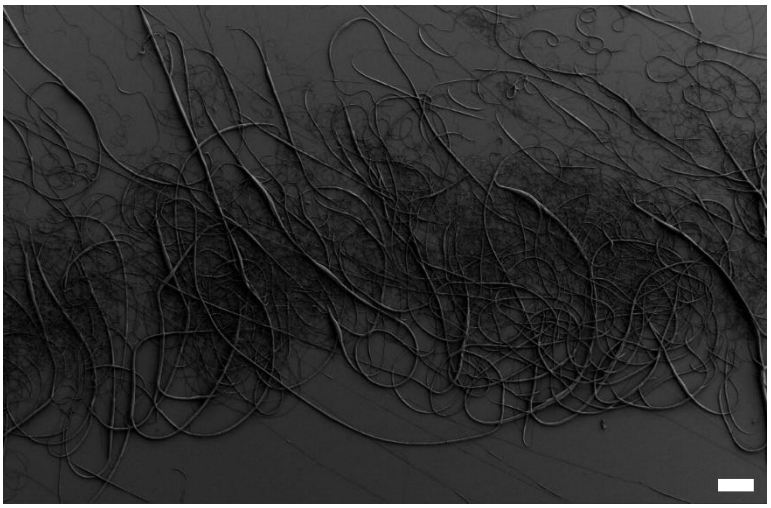

Figure 20. SEM image of deposited fibres using a modified 3 mm AP nozzle system. Scalebar: 200 µm.

To address the limitation of the processing temperature due to cooling effects at the AP needle, an AP nozzle with reduced overlap (1 mm) was adjusted and investigated on its potential to fabricate fibres at lower temperature (80 °C). Macroscopic observation of this novel system showed smoother melt flow along the AP needle, compared to the 3 mm overlap and permitted MES at 80 °C (Figure 21).

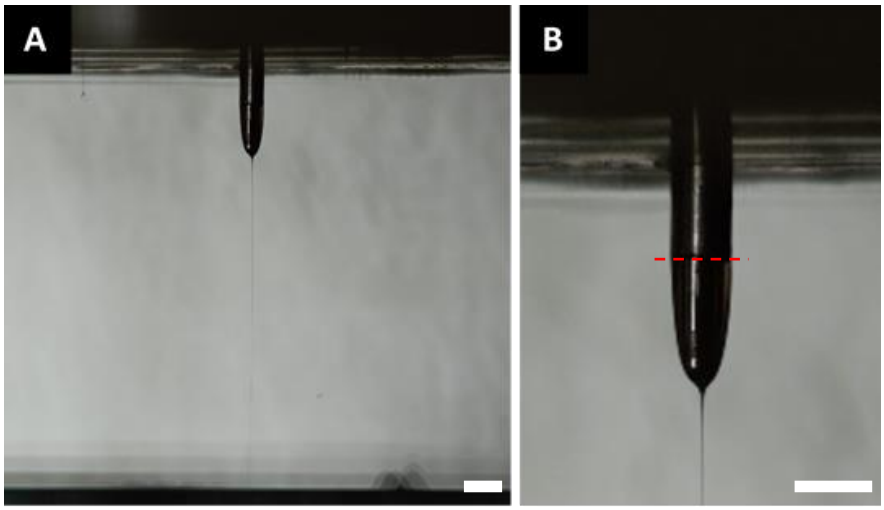

Figure 21. MES with a 1 mm AP nozzle system. (A) Fibre deposition onto the microscope slide. (B) Magnified image of (A) (dashed line indicates start of the AP needle). Scalebars: 1 mm.

To assess which processing temperature would be most suitable to fabricate uniform fibres using the improved AP nozzle system, similar to chapter 4.1.3, five different temperatures were evaluated, and the surface morphology was analysed by SEM (Figure 22).

MES at 80 °C provided submicron fibres which had diameters of 834 nm ± 320 nm. When increasing the processing temperature to 100 °C, the fibre diameter decreased to 707 nm ± 257 nm and provided higher uniformity (Figure 23). Electrospun fibres fabricated at 120 °C, showed a significant reduction of the fibre diameter to 193 nm ± 151 nm. By further increase of the temperature, the collected fibres revealed an increase of the fibre diameter to 519 nm ± 389 nm and demonstrated significantly more irregularities. Given the high processing temperature, 140 °C-fibres resulted in significant fusion of the fibres. These observations are even more distinct on fibres prepared at 160 °C. Deposited fibres were molten and completely fused together. These results indicate that cooling of the polymer jet by a given collector distance of 10 mm is not sufficient to provide fibres when using processing temperatures above 140 °C.

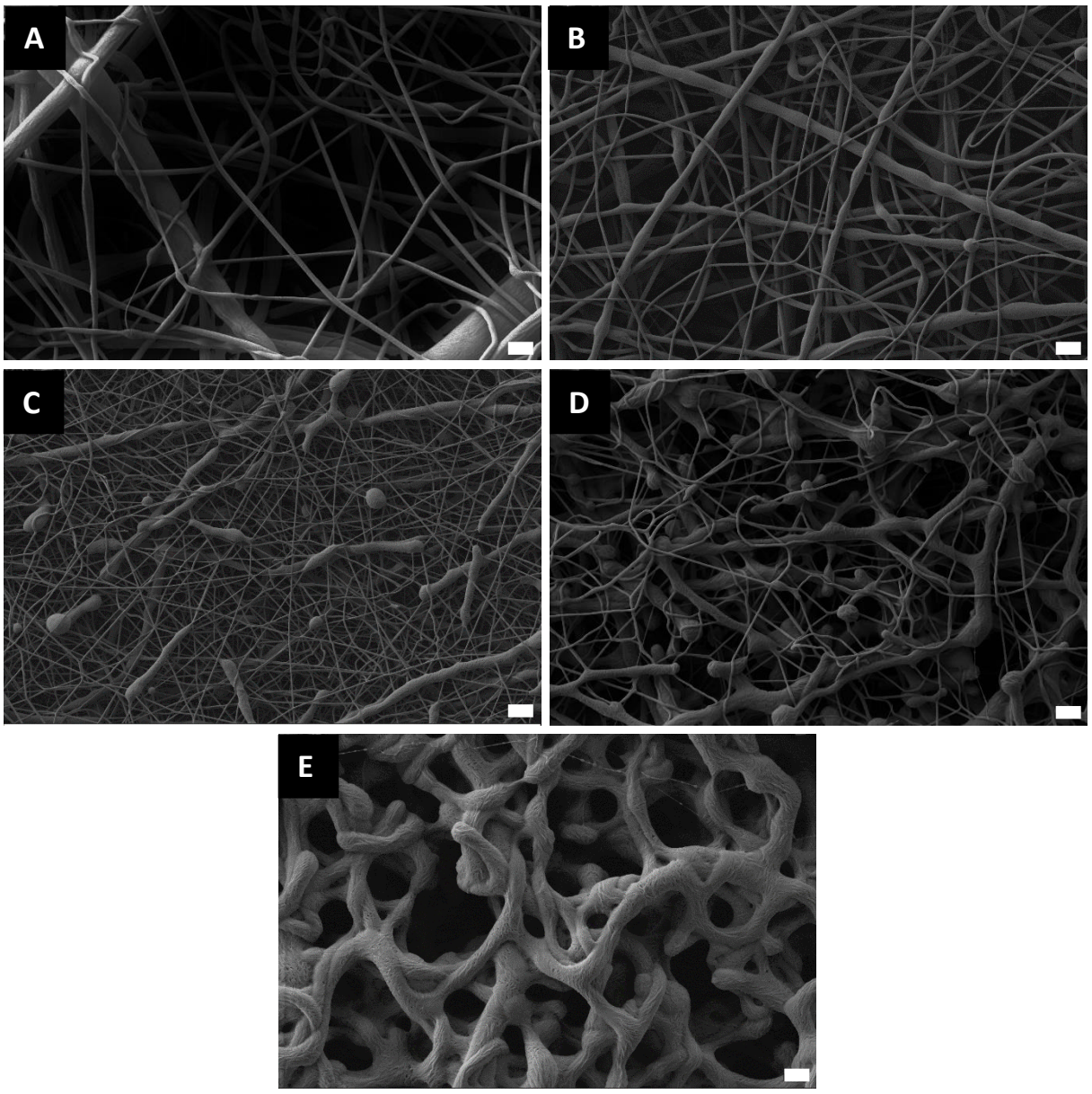

Figure 22. Representative SEM images of electrospun membranes prepared at different temperatures. (A) 80 °C. (B) 100 °C. (C) 120 °C. (D) 140 °C. (E) 160 °C. Scalebars: 2 µm.

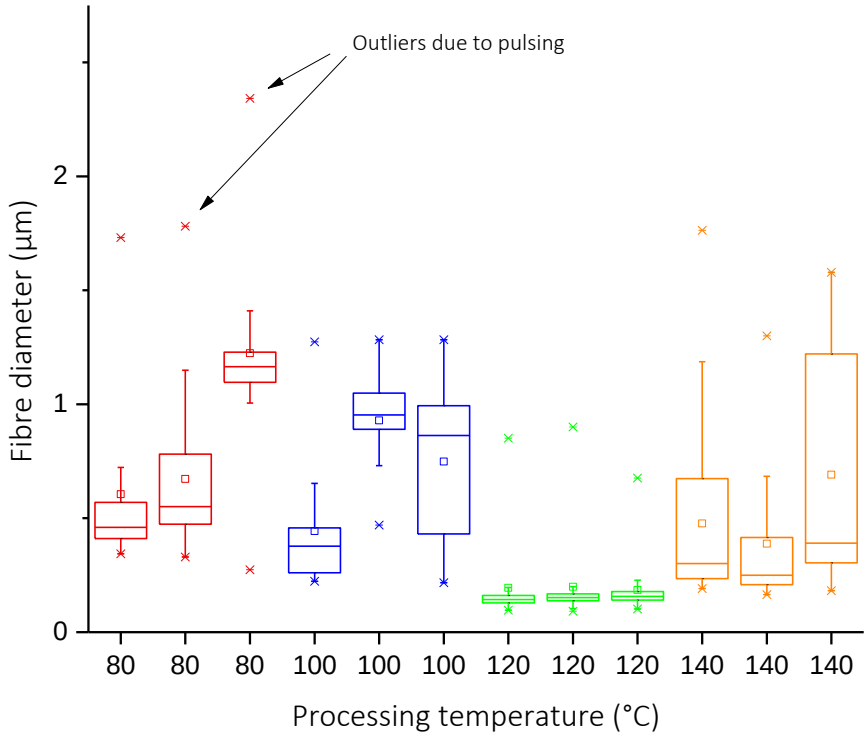

Processing temperature (°C)	80	100	120	140
Average, nm	834	707	193	519
Median, nm	725	731	151	314
SD, nm	320	257	146	389
Ratio, median/average	0.87	1.03	0.78	0.61

Figure 23. Fibre diameters at different processing temperatures using the improved AP modified nozzle.

Overall, these pilot experiments showed for the first time that submicron fibres can be easily fabricated using an AP modified nozzle. Compared to submicron fibres prepared with a 30G needle (80 °C and 100 °C), these fibres demonstrated increased uniformity. It has been noticed that the decrease in viscosity has a dramatic influence on the fibre diameter ending up to 193 nm ± 146 nm at a processing temperature of 120 °C. To the best of our knowledge these fibres are the smallest fibres reported for MES to date.

4.1.5 Bacteria test on the electrospun membrane

For a successful adoption of the biphasic scaffold in oral and maxillofacial surgery, it is important to evaluate the efficacy to prevent bacteria penetration towards the implant. To address this issue, a diffusion test was designed using gram-positive S. aureus strains as a model bacterium (Figure 24). S. aureus represents a typical bacterium in humans, which can be found on the oral mucosa. The bacteria solution was injected above the electrospun membrane, which was glued on the wall of the steel ring and the bacteria penetration into the LB-medium was investigated over a period of 24 h. On the following day samples were taken from the bacteria solution above and from the LB-medium and were plated onto agar plates to evaluate bacteria colonisation.

Figure 24. Bacteria diffusion test through the electrospun membrane.

Analysis of the first experiments showed that neither on the LB medium nor on the bacterial solution plates a bacterial colonisation took place. As the positive control has shown the existence of S. aureus bacteria, we assumed that bacteria died after injection onto the membranes. Given that sterilisation of the membranes was performed using an ethanol solution which was followed by drying for 2 h, it is likely that residual ethanol on the membranes had caused the death of the bacteria. Thus, after sterilisation, membranes were washed three times with a PBS solution to remove the residual organic solvent. Repetition of the bacteria diffusion test including the PBS treatment, provided identical results as previously described, showing bacteria colonisation only on the positive control.

In order to define which part of the experiment is responsible for the bacteria death, we further started an agar diffusion test investigating five different systems: membrane + PBS, membrane + LB-medium, steel ring, membrane with glue and glue (Figure 25).

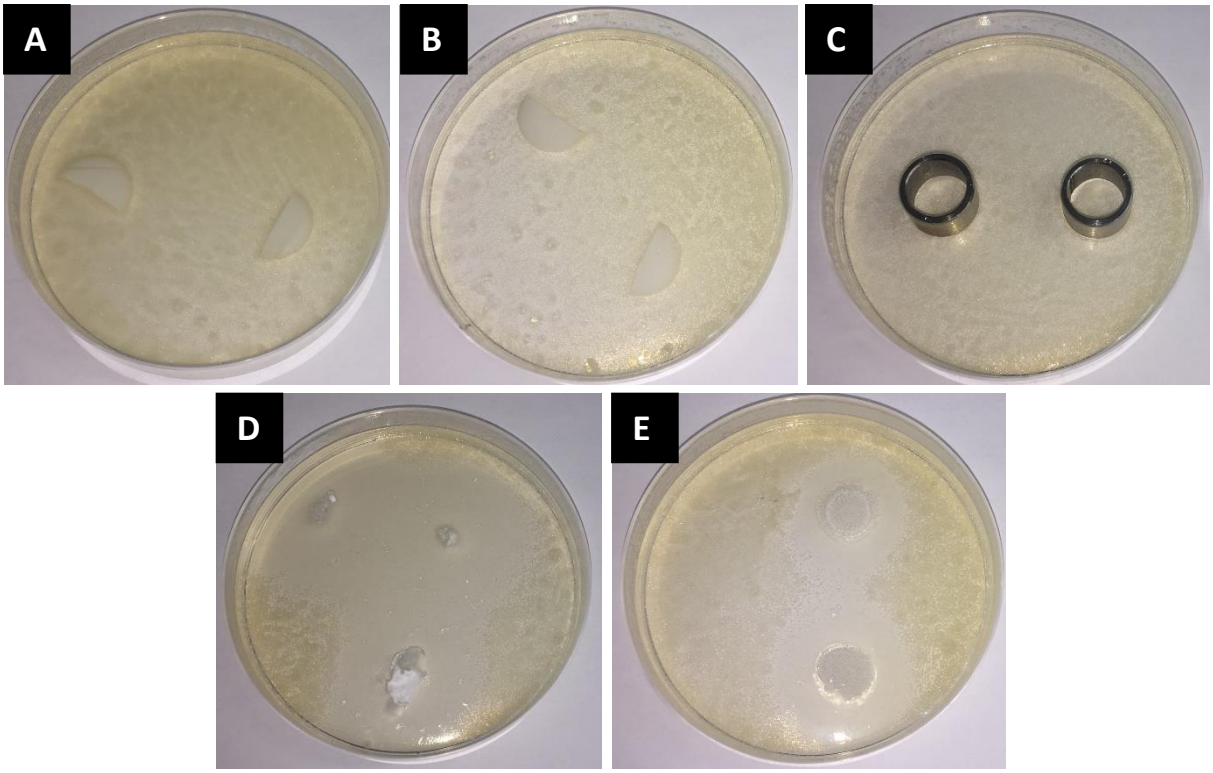

Figure 25. Results of the agar diffusion test. (A) membrane + PBS. (B) membrane + LB-medium. (C) steel ring. (D) membrane + glue. (E) glue.

In the case of membrane + PBS, membrane + LB-medium and steel ring, no inhibition of the bacteria colonisation has been observed (Fig. 25 A – C). In contrast, analysing the samples of membrane + glue and pure glue, a clear inhibition of the bacteria growth has occurred (Fig. 25 D and E). These findings ultimately demonstrate that the glue has cytotoxic properties and caused failure of the diffusion test.

As may be evident from the findings above, to ensure the success of the designed bacteria diffusion test an alternative glue needs to be considered which guarantees tightness between the membrane and the steel ring but also cytocompatibility. Due to the limited resources available and with regard on the time frame, future experiments need to follow up on the bacteria diffusion through the electrospun membrane.

4.1.6 Summary

In this chapter, we investigated the possibility of MES to create a dense network of submicron fibres. Summarised, the experimental outcome of this study demonstrates a crucial influence of the process conditions on the fibre morphology of the membrane. Especially, the processing temperature revealed to have a major effect on the fibre diameter as well as on the fibre uniformity. The most promising results were obtained using a novel nozzle system consisting of an AP needle embedded into a nozzle which was able to demonstrate the fabrication of submicron fibres. To the best of our knowledge, these are the smallest fibres prepared by MES to date. However, there still remains the need for further improvement regarding uniformity and standardisation of the AP nozzle system.

Despite these promising results, for a successful adoption of the membrane into clinical use these initial experiments need to be followed up with more detailed characterisation. For instance, an important factor is the tensile strength of the membrane to guarantee patients safety. Unfortunately, this issue could not be addressed during this master thesis due to the damage of the mechanical tester. Moreover, further studies need to investigate the bacteria-tightness of the membrane as the designed bacteria diffusion test failed.

4.2 Combining MEW and MES

This chapter illustrates and discusses the results from the fabrication of melt electrowritten scaffolds and the combination with the electrospun component of the biphasic scaffold. Melt electrowritten scaffolds are adjusted to offer suitable size for GTR and comparisons are made between MES on top of the MEW scaffold and vice versa.

4.2.1 Fabrication of MEW scaffolds

For the GTR-active component of the biphasic scaffold, microfibre scaffolds were melt electrowritten using G-code to produce box-shaped pores, as described elsewhere [42]. For our study we aimed for a box width of 200 µm for cell invasiveness and different amounts of layers were investigated, referred to 200_5L, 200_15L and 200_30L (Figure 26).

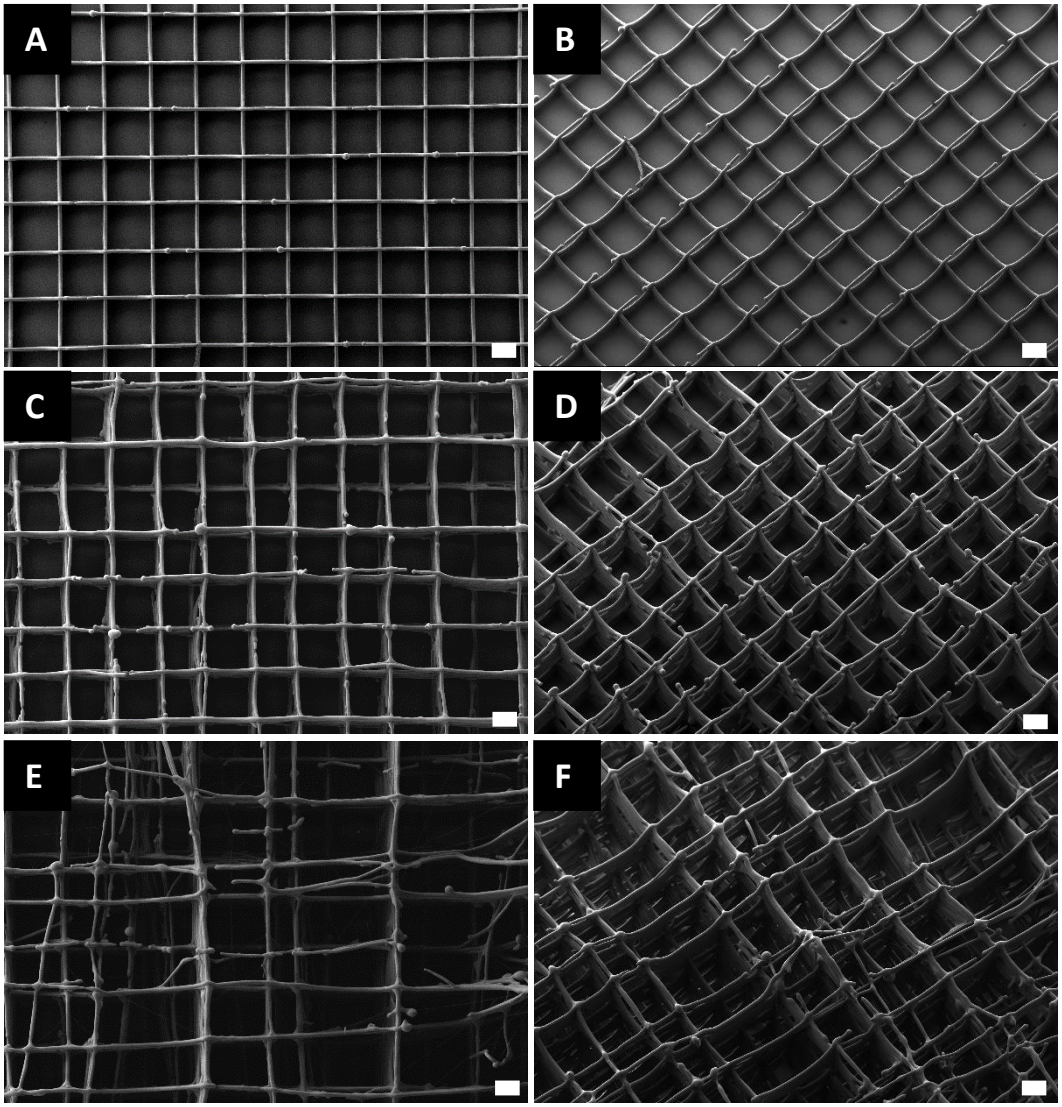

Figure 26. SEM images of melt electrowritten scaffolds. (A and B) 200_5L. (C and D) 200_15L. (E and F) 200_30L. Scalebars: A,C,E: 100 µm; B,D,F: 200 µm.

The dimension of the box-shaped pores and the fibre diameter were measured from SEM images. It has been noticed that the actual box width of the scaffold is smaller than the designed 200 µm. This is due to the fact that the G-code in general does not take the fibre thickness into account. 200_5L and 200_15L resulted in a mean box width of 177 µm ± 5.6 µm and 181 µm ± 19.1 µm, respectively and a mean fibre diameter of 14.7 µm ± 1.4 µm and 16.3 µm ± 2.2 µm (Table 2). While 200_5L offered regular box width, pores of the 200_15L revealed more variation of the size. When looking at the 200_30L sample, fibre deposition was even more uncontrolled resulting in the loss of defined box structures. This observation is in line with the work of Brown and colleagues, who found that increased height of fibres correlates with the loss of the deposition control due to charge accumulation on the fibres [60].

Table 2. Microfibre scaffold measurement determined from SEM images.

Scaffold	Box Width (µm)	Fibre Diameter (µm)
200_5L	177 ± 5.6	14.7 ± 1.4
200_15L	181 ± 19.1	16.3 ± 2.2
200_30L	-	18.7 ± 3.9

Overall, this study showed the ability to fabricate 3D box structures with defined box dimensions suitable for GTR application.

4.2.2 Fabrication of biphasic scaffolds

As may be evident from the above, to fabricate a multicomponent scaffold, different processing parameters are required to guarantee optimal output (Table 3). To achieve this, a custom-built double-headed MEW device was investigated. With this system, essential parameters such as collector distance, processing temperature, feeding pressure and the acceleration voltage can be adjusted separately for each nozzle.

Table 3. Set values for the fabrication of the multicomponent membrane.

Setting	Set value for MEW	Set value for MES
Nozzle	22G	AP nozzle system
Voltage (kV)	6	12
Feeding pressure (bar)	2	0.1
Temperature (°C)	80	120
Collector distance (mm)	4	10
Collector speed (mm/min)	500	10

A G-code pattern was designed which combined the box scaffold pattern and the circular electrospun membrane. To ensure coordinate stacking of the two components the designed G-code also did factor the distance between the two heads (65 mm).

Initial experiments investigated MES on top of the MEW scaffold. A box-shaped scaffold consisting of 10 layers with the dimension of 7x7 mm was printed and after completion, the AP nozzle system was moved to the middle of the left wall of the MEW scaffold starting clockwise circular movements with an initial radius of 3.5 mm.

SEM images were taken from the sample to evaluate the surface morphology of the biphasic scaffold (Figure 27 A and B). SEM images revealed the successful stacking of the electrospun membrane on top of the melt electrowritten scaffold. However, it is noteworthy that sagging of the electrospun component into the pores of the MEW scaffold can be observed. Furthermore, compared to the surface investigated in chapter 4.1.4, it seems that the density of the electrospun fibres is reduced. It is likely that this phenomenon is caused by the relatively

high pore size, which complicates the attachment of the electrospun part directly on top of the scaffold and leads to stretching of the fibres.

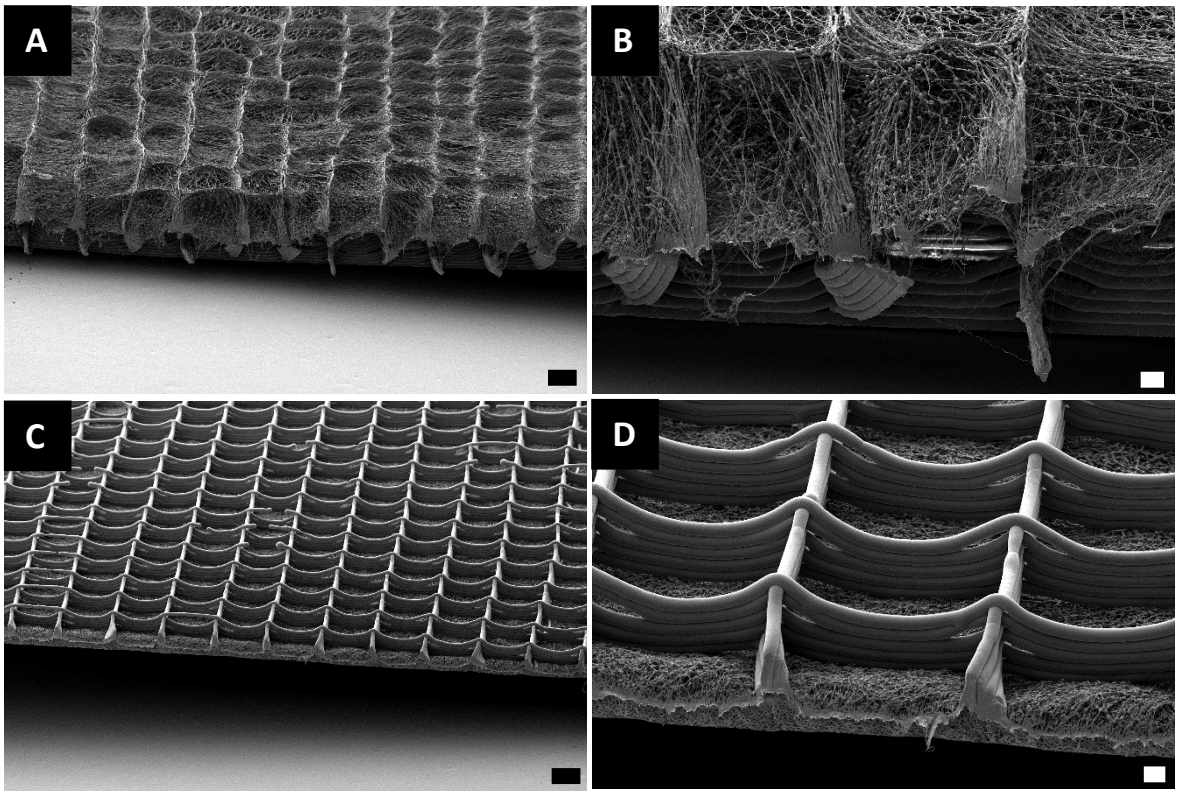

Figure 27. SEM images of the biphasic scaffolds. (A and B) MES on top of the MEW scaffold. (C and D) MEW scaffold on top of MES. Scalebars: A and C: 200 µm; B and D: 20 µm.

To address this issue, we further investigated the possibility to print a 5-layered MEW scaffold consisting of the same dimensions as previously described on top of the electrospun component. As illustrated in Figure 27 C and D, the surface of the electrospun membrane demonstrates higher density compared to Figure 27 A and B. Furthermore, the thickness of the electrospun component seems to be thicker when compared to the top-printed sample, even though the quantitative thickness is hard to access from the images due to bending effects. The MEW scaffold on top of the electrospun component demonstrates well-defined box-shaped pores. Interestingly, no shielding effects from the electrospun upper part can be noticed.

Ultimately, these pilot experiments demonstrated the fabrication of a biphasic scaffold by combining MES and MEW. As MES on top of the MEW scaffold resulted in a decrease of the fibre density and additionally showed sagging effects, it can be assumed that this printing order is unsuitable for the use as a barrier membrane against bacteria penetration. Conversely, MEW on top of the membrane provided the integrity of both component of the biphasic scaffold.

4.2.3 Summary

Experimental results highlight for the first time that a biphasic scaffold, comprising of melt electrospun submicron fibres and box-shaped MEW scaffolds, can be easily assessed in a one-step process using a double headed printer configuration. It has been noticed that MES on top of the MEW scaffold shows sagging effects which results in reduced fibre density. However, for a successful use of this biphasic scaffold in clinical surgeries, the fabrication process must guarantee the integrity of the single components. Even though MEW on top of the electrospun component had no macroscopic effects on the integrity of the electrospun fibres, this process order only enables MEW on one side of the electrospun component. Thus a 3-layered scaffold, which offers GTR structures on both side of the electrospun core cannot be achieved. To investigate a multiphasic scaffold, the deposition of the electrospun fibres on top of the MEW scaffold needs to be improved. An interesting study would be to start MES on top of the MEW scaffold at a higher collector speed and gradually slow down to the desired speed. This initial fibre deposition could act as a support structure, by partially reducing the pore size and facilitating fibre attachment on top of the scaffold.

6. Conclusion

In this project, the combination of two powerful technologies (MES and MEW) in a one-step process was investigated to fabricate a biphasic scaffold suitable for clinical application. MES parameters were assessed to provide high quality fibres with small fibre diameters. Initial experiments have demonstrated the ability to fabricate submicron fibres with a modified nozzle system including an AP needle. To the best of our knowledge, these are the smallest fibres produced via MES reported to date. However, there remains the need to evaluate the potential of the membrane to prevent bacteria infiltration. Moreover, box-structured scaffolds with pore sizes conductive to cell invasiveness were successfully prepared by MEW. By investigating a custom-built double-headed MEW device we were able to successfully combine MES and MEW to create a biphasic scaffold. These results indicate a promising base-material for further modification and optimisation.

7. Future perspective

At this stage the project is still in its infancy and needs to be followed up with more detailed characterisation. As already mentioned in previous chapters, some fundamental studies of the biphasic scaffold regarding its biocompatibility, mechanical strength and bacteria tightness needs to be completed. Nevertheless, this primary work indicates great potential for further development:

Incorporation of anti-bacterial properties

As may be evident from the preceding literature investigation, anti-bacterial properties of the biphasic scaffold are an important factor which needs to be considered in further investigations. An interesting approach would be the incorporation of anti-bacterial agents into the melt electrowritten/ -spun fibres, which could be easily assessed by blending. However, it is important to consider thermostability and sustained long-term release of the drug. As recently explored by Eberle during her master thesis in the research group, MEW provides the possibility for a coaxial printing-setup [77]. This opens the path to create core/shell fibre structures, in which the active component could be incorporated into the core material. The superior release behaviour from core/shell fibres has been demonstrated earlier by Zhang *et al.* [78].

Combination of the biphasic scaffold with bioactive molecules and growth factors

The incorporation of bioactive molecules or growth factors into the MEW scaffold would be another approach to improve the application of the biphasic scaffold. Studies of the last decade revealed that coating of electrospun fibres with biomimetic calcium phosphate results in increased bone formation [79, 80]. Thus, coating the melt electrowritten surface facing the bone implant would be an interesting approach which needs to be considered in following studies.

To improve the healing process of the device, coating of the scaffold facing the oral mucosa with collagen could be advantageous. A recently developed electrochemical alignment technique of collagen, referred to as electrochemical compaction, would be a simple method

to provide highly robust bundles of collagen [81]. In general, this process is based on the electrolysis of an aqueous monomeric collagen solution. Due to the amphoteric nature the generated pH triggers repulsion from the same charged electrodes and leads to compaction at the isoelectric point. This technique has been used in our previous work to incorporate drug-loaded microspheres in a mechanical robust collagen matrix. However, an interesting investigation would be the possibility to combine MEW scaffolds with the aligned collagen structures (Figure 28).

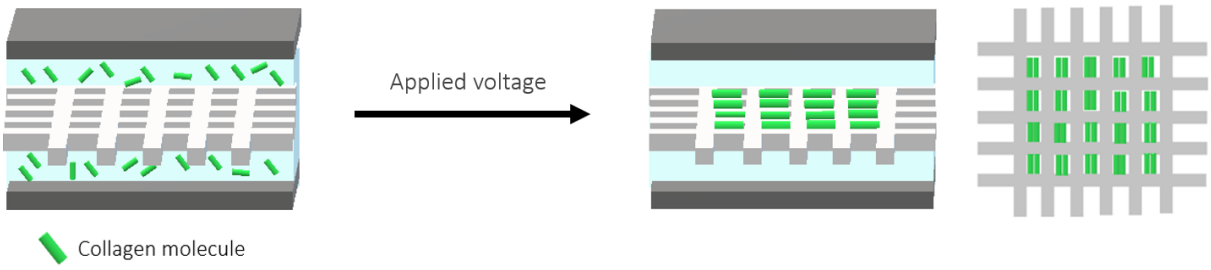

Figure 28. Schematic representation of the electrocompaction process combined with a MEW scaffold.

This composition could lead to superior mechanical properties and as well to an increase wound healing due to the excellent cell affinity of collagen. Furthermore, as already mentioned, there also remains the possibility to incorporate drug-loaded microspheres into the hybrid scaffold using electrochemical compaction. Especially this would be a suitable approach for thermosensitive drugs, which cannot be processed using the prolonged elevated temperatures required for MEW.

8. References

1. Curi, M.M., *et al.*, *Treatment of avascular osteonecrosis of the mandible in cancer patients with a history of bisphosphonate therapy by combining bone resection and autologous platelet-rich plasma: report of 3 cases.* Journal of Oral and Maxillofacial Surgery, 2007. **65**(2): p. 349-355.
2. Ruggiero, S.L., J. Fantasia, and E. Carlson, *Bisphosphonate-related osteonecrosis of the jaw: background and guidelines for diagnosis, staging and management.* Oral Surgery, Oral Medicine, Oral Pathology, Oral Radiology and Endodontics, 2006. **102**(4): p. 433-441.
3. Ruggiero, S.L., *et al.*, *Osteonecrosis of the jaws associated with the use of bisphosphonates: a review of 63 cases.* Journal of Oral and Maxillofacial Surgery, 2004. **62**(5): p. 527-534.
4. Assouline-Dayan, Y., *et al.*, *Pathogenesis and natural history of osteonecrosis*. *Seminars in Arthritis and Rheumatism*. 2002. Elsevier. **32**(2): p. 94 - 124.
5. Mücke, T., *et al.*, *Bisphosphonate related osteonecrosis of the jaws treated by surgical resection and immediate osseous microvascular reconstruction.* Journal of Cranio-Maxillofacial Surgery, 2009. **37**(5): p. 291-297.
6. Raggatt, L.J. and N.C. Partridge, *Cellular and molecular mechanisms of bone remodelling.* Journal of Biological Chemistry, 2010: p. jbc. R109. 041087.
7. Hill, P. and M. Orth, *Bone remodelling.* Journal of Orthodontics, 1998. **25**(2): p. 101-107.
8. Karring, T., *et al.*, *Development of the biological concept of guided tissue regeneration—animal and human studies.* Periodontology 2000, 1993. **1**(1): p. 26-35.
9. Zhang, Y., *et al.*, *Membranes for guided tissue and bone regeneration.* Annals of Oral & Maxillofacial Surgery, 2013. **1**(1): p. 10.
10. Gottlow, J., *et al.*, *New attachment formation as the result of controlled tissue regeneration.* Journal of Clinical Periodontology, 1984. **11**(8): p. 494-503.
11. Nyman, S., *et al.*, *The regenerative potential of the periodontal ligament: an experimental study in the monkey.* Journal of Clinical Periodontology, 1982. **9**(3): p. 257-265.
12. Scantlebury, T.V., *1982-1992: A decade of technology development for guided tissue regeneration.* Journal of Periodontology, 1993. **64**: p. 1129-1137.

13. Bottino, M.C., *et al.*, *Recent advances in the development of GTR/GBR membranes for periodontal regeneration—a materials perspective.* Dental Materials, 2012. **28**(7): p. 703-721.
14. Frazza, E. and E. Schmitt, *A new absorbable suture.* Journal of Biomedical Materials Research Part A, 1971. **5**(2): p. 43-58.
15. Nair, L.S. and C.T. Laurencin, *Biodegradable polymers as biomaterials.* Progress in Polymer Science, 2007. **32**(8-9): p. 762-798.
16. Felipe, M.E.M., *et al.*, *Comparison of two surgical procedures for use of the acellular dermal matrix graft in the treatment of gingival recessions: a randomized controlled clinical study.* Journal of Periodontology, 2007. **78**(7): p. 1209-1217.
17. Santos, A., G. Goumenos, and A. Pascual, *Management of gingival recession by the use of an acellular dermal graft material: A 12-case series.* Journal of Periodontology, 2005. **76**(11): p. 1982-1990.
18. Sela, M.N., *et al.*, *Adherence of periodontopathic bacteria to bioabsorbable and non-absorbable barrier membranes in vitro.* Clinical Oral Implants Research, 1999. **10**(6): p. 445-452.
19. Döri, F., *et al.*, *Effect of platelet-rich plasma on the healing of intra-bony defects treated with a natural bone mineral and a collagen membrane.* Journal of Clinical Periodontology, 2007. **34**(3): p. 254-261.
20. Nevins, M.L. and M.A. Reynolds, *Tissue engineering with recombinant human platelet-derived growth factor BB for implant site development.* Compend Contin Educ Dent, 2011. **32**(2): p. 18-20.
21. Christgau, M., *et al.*, *Growth factors and cytokines in autologous platelet concentrate and their correlation to periodontal regeneration outcomes.* Journal of Clinical Periodontology, 2006. **33**(11): p. 837-845.
22. Kaigler, D., *et al.*, *Platelet-derived growth factor applications in periodontal and peri-implant bone regeneration.* Expert Opinion on Biological Therapy, 2011. **11**(3): p. 375-385.
23. Miron, R.J., *et al.*, *Osteoblast proliferation and differentiation on a barrier membrane in combination with BMP2 and TGFβ1.* Clinical Oral Investigations, 2013. **17**(3): p. 981-988.

24. Sculean, A., *et al.*, *Enamel matrix proteins and periodontal wound healing and regeneration.* Clinical Advances in Periodontics, 2011. **1**(2): p. 101-117.
25. Nowzari, H., F. Matian, and J. Slots, *Periodontal pathogens on polytetrafluoroethylene membrane for guided tissue regeneration inhibit healing.* Journal of Clinical Periodontology, 1995. **22**(6): p. 469-474.
26. MacDonald, E.S., *et al.*, *Clinical and microbiological evaluation of a bioabsorbable and a nonresorbable barrier membrane in the treatment of periodontal intraosseous lesions.* Journal of Periodontology, 1998. **69**(4): p. 445-453.
27. Landsberg, C.J., A. Grosskopf, and M. Weinreb, *Clinical and Biologic Observations of Demineralized Freeze-Dried Bone Allografts in Augmentation Procedures Around Dental Implants.* International Journal of Oral & Maxillofacial Implants, 1994. **9**(5).
28. Jovanovic, S.A., H. Spiekermann, and E.J. Richter, *Bone regeneration around titanium dental implants in dehisced defect sites: a clinical study.* International Journal of Oral & Maxillofacial Implants, 1992. **7**(2).
29. Selvig, K.A., *et al.*, *Regenerative surgery of intrabony periodontal defects using ePTFE barrier membranes: scanning electron microscopic evaluation of retrieved membranes versus clinical healing.* Journal of Periodontology, 1992. **63**(12): p. 974-978.
30. Kenawy, E.-R., *et al.*, *Release of tetracycline hydrochloride from electrospun poly (ethylene-co-vinylacetate), poly (lactic acid), and a blend.* Journal of Controlled Release, 2002. **81**(1-2): p. 57-64.
31. Zamani, M., *et al.*, *Controlled release of metronidazole benzoate from poly ε-caprolactone electrospun nanofibers for periodontal diseases.* European Journal of Pharmaceutics and Biopharmaceutics, 2010. **75**(2): p. 179-185.
32. He, C.L., Z.M. Huang, and X.J. Han, *Fabrication of drug-loaded electrospun aligned fibrous threads for suture applications.* Journal of Biomedical Materials Research Part A: An Official Journal of The Society for Biomaterials, The Japanese Society for Biomaterials, and The Australian Society for Biomaterials and the Korean Society for Biomaterials, 2009. **89**(1): p. 80-95.
33. Bottino, M.C., V. Thomas, and G.M. Janowski, *A novel spatially designed and functionally graded electrospun membrane for periodontal regeneration.* Acta Biomaterialia, 2011. **7**(1): p. 216-224.

34. Chou, A.H., *et al.*, *Antibacterial effect of zinc phosphate mineralized guided bone regeneration membranes.* Implant Dentistry, 2007. **16**(1): p. 89-100.
35. Xu, X., *et al.*, *Biodegradable electrospun poly (L-lactide) fibers containing antibacterial silver nanoparticles.* European Polymer Journal, 2006. **42**(9): p. 2081-2087.
36. Chia, H.N. and B.M. Wu, *Recent advances in 3D printing of biomaterials.* Journal of Biological Engineering, 2015. **9**(1): p. 4.
37. Gross, B.C., *et al.*, *Evaluation of 3D printing and its potential impact on biotechnology and the chemical sciences*. 2014, ACS Publications.
38. Brown, T.D., P.D. Dalton, and D.W. Hutmacher, *Melt electrospinning today: An opportune time for an emerging polymer process.* Progress in Polymer Science, 2016. **56**: p. 116-166.
39. Hu, X., *et al.*, *Electrospinning of polymeric nanofibers for drug delivery applications.* Journal of Controlled Release, 2014. **185**: p. 12-21.
40. Arinstein, A. and E. Zussman, *Electrospun polymer nanofibers: mechanical and thermodynamic perspectives.* Journal of Polymer Science Part B: Polymer Physics, 2011. **49**(10): p. 691-707.
41. Agarwal, S., J.H. Wendorff, and A. Greiner, *Use of electrospinning technique for biomedical applications.* Polymer, 2008. **49**(26): p. 5603-5621.
42. Hochleitner, G., *et al.*, *Additive manufacturing of scaffolds with sub-micron filaments via melt electrospinning writing.* Biofabrication, 2015. **7**(3): p. 035002.
43. Cipitria, A., *et al.*, *Design, fabrication and characterization of PCL electrospun scaffolds—a review.* Journal of Materials Chemistry, 2011. **21**(26): p. 9419-9453.
44. Rayleigh, L., *XX. On the equilibrium of liquid conducting masses charged with electricity.* The London, Edinburgh, and Dublin Philosophical Magazine and Journal of Science, 1882. **14**(87): p. 184-186.
45. Dalton, P.D., *et al.*, *Electrospinning of polymer melts: Phenomenological observations.* Polymer, 2007. **48**(23): p. 6823-6833.
46. Hutmacher, D.W. and P.D. Dalton, *Melt electrospinning.* Chemistry–An Asian Journal, 2011. **6**(1): p. 44-56.
47. Muerza-Cascante, M.L., *et al.*, *Melt electrospinning and its technologization in tissue engineering.* Tissue Engineering Part B: Reviews, 2014. **21**(2): p. 187-202.

48. Brown, T.D., *et al.*, *Melt electrospinning of poly (ε-caprolactone) scaffolds: Phenomenological observations associated with collection and direct writing.* Materials Science and Engineering: C, 2014. **45**: p. 698-708.
49. Kim, S.J., *et al.*, *Fabrication and characterization of 3-dimensional PLGA nanofiber/microfiber composite scaffolds.* Polymer, 2010. **51**(6): p. 1320-1327.
50. Li, X., *et al.*, *Preparation and characterization of PLLA/nHA nonwoven mats via laser melt electrospinning.* Materials Letters, 2012. **73**: p. 103-106.
51. Detta, N., *et al.*, *Melt electrospinning of polycaprolactone and its blends with poly (ethylene glycol).* Polymer International, 2010. **59**(11): p. 1558-1562.
52. Ghasemi-Mobarakeh, L., *et al.*, *Electrospun poly (ε-caprolactone)/gelatin nanofibrous scaffolds for nerve tissue engineering.* Biomaterials, 2008. **29**(34): p. 4532-4539.
53. Shin, M., H. Yoshimoto, and J.P. Vacanti, *In vivo bone tissue engineering using mesenchymal stem cells on a novel electrospun nanofibrous scaffold.* Tissue Engineering, 2004. **10**(1-2): p. 33-41.
54. Li, W.J., *et al.*, *Electrospun nanofibrous structure: a novel scaffold for tissue engineering.* Journal of Biomedical Materials Research: An Official Journal of The Society for Biomaterials, The Japanese Society for Biomaterials, and The Australian Society for Biomaterials and the Korean Society for Biomaterials, 2002. **60**(4): p. 613-621.
55. Pham, Q.P., U. Sharma, and A.G. Mikos, *Electrospun poly (ε-caprolactone) microfiber and multilayer nanofiber/microfiber scaffolds: characterization of scaffolds and measurement of cellular infiltration.* Biomacromolecules, 2006. **7**(10): p. 2796-2805.
56. Zhang, D. and J. Chang, *Electrospinning of three-dimensional nanofibrous tubes with controllable architectures.* Nano Letters, 2008. **8**(10): p. 3283-3287.
57. Smit, E., U. Bűttner, and R.D. Sanderson, *Continuous yarns from electrospun fibers.* Polymer, 2005. **46**(8): p. 2419-2423.
58. Deitzel, J., *et al.*, *Controlled deposition of electrospun poly (ethylene oxide) fibers.* Polymer, 2001. **42**(19): p. 8163-8170.
59. Subramanian, A., *et al.*, *Preparation and evaluation of the electrospun chitosan/PEO fibers for potential applications in cartilage tissue engineering.* Journal of Biomaterials Science, Polymer Edition, 2005. **16**(7): p. 861-873.

60. Brown, T.D., P.D. Dalton, and D.W. Hutmacher, *Direct writing by way of melt electrospinning.* Advanced Materials, 2011. **23**(47): p. 5651-5657.
61. Wunner, F.M., *et al.*, *Melt Electrospinning Writing of Three-dimensional Poly (ε-caprolactone) Scaffolds with Controllable Morphologies for Tissue Engineering Applications.* Journal of Visualized Experiments: JoVE, 2017(130).
62. Brown, T.D., *et al.*, *Design and fabrication of tubular scaffolds via direct writing in a melt electrospinning mode.* Biointerphases, 2012. **7**(1): p. 13.
63. Ristovski, N., *et al.*, *Improved fabrication of melt electrospun tissue engineering scaffolds using direct writing and advanced electric field control.* Biointerphases, 2015. **10**(1): p. 011006.
64. Bas, O., *et al.*, *Enhancing structural integrity of hydrogels by using highly organised melt electrospun fibre constructs.* European Polymer Journal, 2015. **72**: p. 451-463.
65. Yang, G.-H., F. Mun, and G. Kim, *Direct electrospinning writing for producing 3D hybrid constructs consisting of microfibers and macro-struts for tissue engineering.* Chemical Engineering Journal, 2016. **288**: p. 648-658.
66. Farrugia, B.L., *et al.*, *Dermal fibroblast infiltration of poly (ε-caprolactone) scaffolds fabricated by melt electrospinning in a direct writing mode.* Biofabrication, 2013. **5**(2): p. 025001.
67. Castilho, M., *et al.*, *Melt Electrospinning Writing of Poly-Hydroxymethylglycolide-co-ε-Caprolactone-Based Scaffolds for Cardiac Tissue Engineering.* Advanced Healthcare Materials, 2017. **6**(18): p. 1700311.
68. Dalton, P.D., *et al.*, *Electrospinning and additive manufacturing: converging technologies.* Biomaterials Science, 2013. **1**(2): p. 171-185.
69. Kim, G., *et al.*, *Hybrid process for fabricating 3D hierarchical scaffolds combining rapid prototyping and electrospinning.* Macromolecular Rapid Communications, 2008. **29**(19): p. 1577-1581.
70. Moroni, L., J. De Wijn, and C. Van Blitterswijk, *Integrating novel technologies to fabricate smart scaffolds.* Journal of Biomaterials Science, Polymer Edition, 2008. **19**(5): p. 543-572.
71. Park, S.H., *et al.*, *Development of dual scale scaffolds via direct polymer melt deposition and electrospinning for applications in tissue regeneration.* Acta Biomaterialia, 2008. **4**(5): p. 1198-1207.

72. Vaquette, C., *et al.*, *A biphasic scaffold design combined with cell sheet technology for simultaneous regeneration of alveolar bone/periodontal ligament complex.* Biomaterials, 2012. **33**(22): p. 5560-5573.
73. Hochleitner, G., *et al.*, *Fibre pulsing during melt electrospinning writing.* BioNanoMaterials, 2016. **17**(3-4): p. 159-171.
74. Dalton, P.D., *et al.*, *Patterned melt electrospun substrates for tissue engineering.* Biomedical Materials, 2008. **3**(3): p. 034109.
75. Hrynevich, A., *et al.*, *Dimension-Based Design of Melt Electrowritten Scaffolds.* Small, 2018. **14**(22): p. 1800232.
76. Dalton, P.D., *et al.*, *Direct in vitro electrospinning with polymer melts.* Biomacromolecules, 2006. **7**(3): p. 686-690.
77. Eberle, F., Master Thesis, Universität Würzburg, 2018.
78. Zhang, Y., *et al.*, *Coaxial electrospinning of (fluorescein isothiocyanate-conjugated bovine serum albumin)-encapsulated poly (ε-caprolactone) nanofibers for sustained release.* Biomacromolecules, 2006. **7**(4): p. 1049-1057.
79. Yang, F., J. Wolke, and J. Jansen, *Biomimetic calcium phosphate coating on electrospun poly (ε-caprolactone) scaffolds for bone tissue engineering.* Chemical Engineering Journal, 2008. **137**(1): p. 154-161.
80. Mavis, B., *et al.*, *Synthesis, characterization and osteoblastic activity of polycaprolactone nanofibers coated with biomimetic calcium phosphate.* Acta Biomaterialia, 2009. **5**(8): p. 3098-3111.
81. Cheng, X., *et al.*, *An electrochemical fabrication process for the assembly of anisotropically oriented collagen bundles.* Biomaterials, 2008. **29**(22): p. 3278-3288.

Appendix A

```
(Start of part)
G91
G3 X0 Y0 I3.5 F10
G1 X0.05 Y0 F10
G3 X0 Y0 I3.45 F10
G1 X0.05 Y0 F10
.
.
.
G3 X0 Y0 I0.10 F10
G1 X0.05 Y0 F10
G3 X0 Y0 I0.05 F10
G1 X0.05 Y0 F10
G4 S60
(End of part)
```

Figure 29. G-code written to fabricate circular electrospun membranes with a diameter of 7 mm.